Politecnico di Milano
Space Propulsion Laboratory

University of California, Irvine
Mechanical and Aerospace Engineering

School of Industrial and Information Engineering
Department of Aerospace Science and Technology (DAER)
M.Sc. in Aeronautical Engineering

ENGINE-TYPE AND PROPULSION-CONFIGURATION SELECTIONS FOR LONG-DURATION UAV FLIGHTS

Supervisors:

Prof. William A.Sirignano PhD.
Prof. Feng Liu PhD.
University of California, Irvine

Prof. Filippo Maggi PhD.
Politecnico di Milano

M.Sc. Thesis of:

Daniele Cirigliano
Id. 838030

Academic Year 2016/2017

SUPERVISORS:
Prof. William A.Sirignano PhD.
Prof. Feng Liu PhD.
Prof. Filippo Maggi PhD.

LOCATIONS:
Irvine, California
Milano, Italia

That you are here — that life exists and identity,
That the powerful play goes on, and you may contribute a verse.

— Walt Whitman, 1867

to my family

ABSTRACT

The gas turbine engine efficiency deteriorates dramatically when its size is reduced. This fact limits its use for low-power and long duration applications, due to fuel weight. It is conceivable to replace a small scale gas turbine engine with a different power generating technology such as a Diesel engine providing higher efficiency. In this work, comparisons are made for propulsion systems for unmanned flights with several hundred kilowatts of propulsive power at moderate subsonic speeds up to fifty hours in duration. The weights of the propulsion system, required fuel, and total aircraft are considered. Gas-turbine engines, two- and four-stroke reciprocating (diesel and spark-ignition) engines, and electric motors (with battery storage and/or electric generation) are analyzed. Detailed MATLAB codes are developed to assess thermodynamic properties of the engines in the range of interest. Consideration is given to two types of missions: (i) a mission dominated by a constant-power requirement and (ii) a mission with intermittent demand for high thrust and/or substantial auxiliary power. The two surviving competitors are gas-turbine engines and turbo-charged four-stroke Diesel engines, each type driving propellers. It is shown that hybrid-electric schemes and one engine mechanically driving several propellers are less efficient. At the 500 kW level, one gas-turbine engine driving a larger propeller is more efficient for durations up to twenty-five hours, while several Diesel engines driving several propellers become more efficient at longer durations. The decreasing efficiency of the gas-turbine engine with decreasing size and increasing compression ratio is a key factor. The increasing efficiency of propellers with decreasing size is another key factor.

Key words: Gas-turbine, Diesel engine, Efficiency, Long-duration, UAV, Thermodynamic cycle, Matlab code.

ESTRATTO

L'efficienza di un motore turbogas diminuisce sensibilmente quando si riducono le sue dimensioni. Questo fatto limita il suo utilizzo in applicazioni dove basse potenze e lunghe durate sono necessarie, a causa dell'elevato peso del combustibile. È quindi lecito pensare di sostituire un piccolo motore turbogas con una diversa tecnologia, come per esempio un più efficiente motore Diesel. In questo lavoro sono stati effettuati confronti tra sistemi propulsivi adatti a voli a pilotaggio remoto dove sono richieste alcune centinaia di kilowatt di potenza propulsiva a velocità subsoniche fino a cinquanta ore di volo. Si è tenuto conto del peso del sistema propulsivo, del combustibile necessario e del velivolo completo. Sono stati analizzati motori turbogas, motori a combustione interna due e quattro tempi (Diesel e ad accensione comandata), e motori elettrici (con batterie e/o generatori elettrici). Sono stati sviluppati dettagliati codici MATLAB per il calcolo delle proprietà termodinamiche dei motori nei range di interesse. Si è data enfasi a due tipi di missioni: (i) una in cui è richiesta potenza costante e (ii) una con necessità intermittente di elevata spinta e/o potenza ausiliaria a bordo. I due candidati finali sono i motori turbogas e i motori Diesel quattro tempi turbo-aspirati, ciascuno azionante una o più eliche. Si dimostra che configurazioni ibride e disposizioni in cui un motore è collegato meccanicamente a più eliche sono scelte poco efficienti. Per potenze intorno ai 500 kW, un motore turbogas che azioni un'elica di grandi dimensioni è la scelta più efficiente per durate fino a venticinque ore, mentre un sistema comprendente più motori Diesel azionanti un'elica ciascuno diventa più conveniente per durate maggiori. Uno dei fattori chiave è il progressivo calo di efficienza dei motori turbogas al diminuire delle dimensioni e all'aumentare del rapporto di compressione. Un altro elemento fondamentale è l'aumento dell'efficienza propulsiva delle eliche al diminuire del diametro.

Parole chiave: Turbina a gas, Motore Diesel, Efficienza, Durata di volo, Drone, Ciclo termodinamico, codice Matlab.

PUBLICATIONS

This thesis work has been adapted into a paper according to AIAA standards[1] and submitted for publication to the *Journal of Propulsion and Power (AIAA)*, on November 16, 2016.

At the present date, the document is still under review.

March 20, 2017

1 See http://arc.aiaa.org/page/styleandformat for formatting details.

We are like dwarfs sitting on the shoulders of giants.
We see more, and things that are more distant, than they did,
not because our sight is superior or because we are taller than they,
but because they raise us up, and by their great stature add to ours.

— John of Salisbury, *Metalogicon* (1159)

ACKNOWLEDGEMENTS

I would first like to thank my thesis advisors, prof. William A. Sirignano and prof. Feng Liu of the School of Mechanical and Aerospace Engineering at University of California, Irvine. The door to their offices was always open whenever I ran into a trouble spot or had a question about my research or writing. They consistently allowed this paper to be my own work, but steered me in the right direction whenever they thought I needed it.

My gratitude also goes to prof. Filippo Maggi of the Department of Aerospace Science and Technology at Politecnico di Milano. Despite the distance, he always kept my research under his supervision. His insightful comments and encouragement were extremely important.

The authors were encouraged by the original suggestion from Dr. Kenneth M. Rosen (General Aero-Science Consultants, LLC) that the Diesel engine could compete with the gas-turbine engine at lower power levels. Valuable insights about the application of reciprocating engines were provided by Mr. Roy Primus (GE Global Research) and Mr. Patrick Pierz (Insitu, Inc.). Remarkable work was done on turbine engines by Aaron M. Frisch. Without their passionate participation and input, this thesis could not have been successfully conducted.

I must express my very profound gratitude to my family for providing me with unfailing support and continuous encouragement throughout my years of study. This accomplishment would not have been possible without them. Finally, I would like to thank all my friends from California, Japan, Hawaii, Belgium, El Salvador, Germany, Pakistan, Brazil, Iran, Mexico, Spain and Italy, which made my journey a worth-living experience. I will never forget you.

Thank you.

Daniele Cirigliano

March 20, 2017

CONTENTS

LIST OF FIGURES

LIST OF TABLES

NOMENCLATURE

$\bar{C}_D$	Average drag coefficient
$\bar{S}_p$	Average piston speed
$\dot{m}_{inj}$	Fuel flow through the injector
$\tilde{R}$	Average Boltzmann constant of cylinder content
A	Cylinder wall surface
a	Acceleration at take-off
A_C	Curtain area
A_E	Effective flow area
A_T	Throat area
A_{inj}	Injector cross sectional area
A_{wet}	Wetted wing area
B	Cylinder bore
b	Aircraft wing span
c	Reference chord length
C_D	Discharge coefficient
C_L	Lift coefficient
C_P	Power coefficient
C_T	Thrust coefficient
c_{pb}	Specific heat pressure-constant of burned gas
C_{Pi}	Induced power coefficient
c_{vb}	Specific heat volume-constant of burned gas
c_{vu}	Specific heat volume-constant of unburned gas
D	Propeller diameter
D_v	Valve diameter
F	Net accelerating force at take-off
h	Heat transfer coefficient
$h_{i,j}$	Sensible energy per unit mass flow
J	Advance ratio
k	Wall thermal conductivity
L	Cylinder stroke
L/D	Lift over drag ratio
L_v	Valve lift
M	Mach number
m	Cylinder content mass
M_b	Molecular mass of the burned gas
m_b	Burned zone mass
m_c	Chamber mass
m_f	Fuel mass
m_f	Mass of fuel
M_u	Molecular mass of the unburned gas
m_u	Unburned zone mass
m_{air}	Air mass
m_{cc}	Crankcase mass
m_{in}	Mass entering the system
m_{out}	Mass leaving the system
M_{TIP}	Tip Mach number
N	Engine rpm

n	Propeller rpm
n_r	Shaft revolutions per engine firing
p_c	Chamber pressure
p_i	Pressure at point i
p_T	Pressure upstream the turbocharger turbine
p_{amb}	Ambient pressure
p_{cc}	Crankcase pressure
Pr	Prandtl number
Q	Heat energy
Q_b	Fuel low heating value
Q_{ch}	Energy released by combustion
Q_{ht}	Energy lost by heat transfer to the walls
Q_{in}	Energy entering the system
Q_{out}	Energy leaving the system
Q_{sens}	Sensible energy
r/R	Radial coordinate over radius
R_b	Boltzmann constant of burned gas
R_u	Boltzmann constant of unburned gas
S	Entropy
T	Cylinder content temperature
T_b	Temperature of burned zone
T_c	Chamber temperature
T_i	Temperature at point i
T_m	Mean temperature
T_u	Temperature of unburned zone
T_w	Cylinder walls temperature
T_{amb}	Ambient temperature
T_{cc}	Crankcase temperature
U	Internal energy
V	Cylinder content volume
V_b	Burned zone volume
v_b	Specific volume of burned gas
V_c	Chamber volume
V_c	Clearance volume
V_i	Volume at point i
V_u	Unburned zone volume
v_u	Specific volume of unburned gas
V_{cc}	Crankcase volume
W	Work energy
w	Induced velocity
x_b	Mass fraction burned
z	Altitude

Greek Letters

α	Air–fuel ratio
α_{st}	Stoichiometric air–fuel ratio
η_b	Combustion efficiency
η_c	Compressor adiabatic efficiency
η_d	Diffuser adiabatic efficiency
η_m	Mechanical efficiency

η_{conv}	Energy conversion efficiency
η_{el}	Electric motor efficiency
η_{gear}	Gearbox efficiency
η_{id}	Ideal efficiency
η_{mech}	Mechanical efficiency
η_{prop}	Propeller efficiency
η_{th}	Thermal efficiency
γ	Specific heat ratio
γ_b	Specific heat ratio of burned zone
γ_c	Specific heat ratio of compression stroke
γ_e	Specific heat ratio of expansion stroke
μ	Dynamic viscosity
ω	Rotational speed
Φ	Equivalence ratio
ϕ	Flow coefficient
π_b	Combustion chamber pressure ratio
π_c	Turbocharger compression ratio
π_d	Diffuser pressure ratio
π_t	Turbine pressure ratio
Ψ	Stage loading coefficient
ρ	Density
σ	Blade solidity
τ_c	Compressor temperature ratio
τ_t	Turbine temperature ratio
Θ	Cycle temperature ratio
θ	Crank angle
ε	Cylinder compression ratio

Other Symbols

$\mathcal{A}$	Propeller disc area
$\mathcal{B}$	Propeller blade number
$\mathcal{L}$	Propeller blade length
$\mathcal{P}$	Power
$\mathcal{P}_c$	Compressor power
$\mathcal{P}_i$	Induced power
$\mathcal{P}_s$	Net shaft power
$\mathcal{P}_t$	Turbine power
$\mathcal{P}_u$	Useful power
$\mathcal{P}_{cruise}$	Engine power at cruise
$\mathcal{P}_{prop}$	Propeller input power
$\mathcal{R}$	Degree of reaction
$\mathcal{T}$	Thrust
$\mathcal{T}_{cruise}$	Aircraft thrust at cruise
$\mathcal{T}_{TO}$	Aircraft thrust at take-off
$\mathcal{V}$	True airspeed
$\mathcal{V}_{jet}$	Exhaust gases velocity
$\mathcal{V}_{TO}$	Aircraft speed at take-off
$\mathcal{W}$	Weight
$\mathcal{W}_0$	Take-off gross weight
$\mathcal{W}_{crew}$	Crew weight
$\mathcal{W}_e$	Empty structural weight
$\mathcal{W}_{fuel}$	Fuel weight
$\mathcal{W}_{payload}$	Payload weight

ACRONYMS

AF Activity Factor

BDC Bottom Dead Center

CA Crank Angle

CFD Computational Fluid Dynamics

CI Compression Ignition

EM Electric Motor

GB Gearbox

KE Kinetic Energy

LEAP Leading Edge Aviation Propulsion

LHV Low Heating Value

OPR Overall Pressure Ratio

PTO Power Take Off

SI Spark Ignition

ST Specific Thrust

TBO Time Between Overhaul

TBR Time Between Replacement

TDC Top Dead Center

TSFC Thrust Specific Fuel Consumption

UAV Unmanned Aerial Vehicle

WAR Wetted Aspect Ratio

Part I

CREATION OF THE MODELS

1 INTRODUCTION

1.1 ON POWER AND WEIGHT

The aeronautics and the automotive industries share some typical issues: both of them pursue a reduction of the general weight of the engines in order to, alternatively, reduce the specific fuel consumption or increase the payload. For an engine of a given power, reducing the fuel consumption means savings (generally desired in the automotive world), while more payload translates into more profits for passenger airlines, or more room to store weapons and loads in military applications. Unfortunately, the weight of an engine - of any kind - is generally tied to structural constraints, i.e. thermodynamic cycles, mechanical and thermal stresses, and so on.[1] Of course, technology can provide lighter (and more expensive) materials, but at least the order of magnitude of the weight for a given power turns out to be quite fixed.

A different approach consists in trying to increase the power supplied by the engine, theoretically keeping constant weight and size. This technique is called *turbocharging*; generally, a radical change in the engine architecture is needed in this scenario. It is worth to stress the fact that higher power levels generally mean higher pressures and temperatures. In this scenario a proper cooling system should be well integrated with the machine; for the need of pipes, holes, heat exchangers, pumps and sometimes the presence of a cooling fluid, this translates in a certain increase of weight (and costs).

All this being said, a typical trend in industrial engineering is to raise the *Power-to-Weight ratio*. The typically used metrical unit of the Power-to-Weight ratio is W/kg according to SI, or hp/lb in Imperial and US units. Please, note that "Weight" in this context is a colloquial term for "mass".

The scenario gets more complex if other parameters are taken into account. For instance, among different engines, the one with lower Power-to-Weight ratio might sometimes be preferable because of its

1 For instance, reciprocating Diesel engines require thick walls to sustain the high pressures involved. Moreover, reliability and safety regulations induce designers to "oversize" some parts to prevent fatigue failures. Finally, some design choice might be due to redundancy and should not be considered as a "waste weight".

higher *thermal efficiency*. In a general sense, the efficiency of a thermal engine relates the useful work with the energy available to perform it. Hence, one may want to maximize the first aspect (increase the output work/power) or minimize the second (decrease the fuel mass/-mass flow rate), depending on the mission profile. This type of analysis is essential for industries to be able to make informed decisions on the most efficient way to power their machines. A power-weight-efficiency analysis is the basis of this thesis.

1.2 BACKGROUND

It is well known that scaling down gas-turbine engines results in decreased efficiency because of the so-called scale effects: profile losses, endwall losses, Reynolds number effects, heat transfer and tip clearance losses. A brief explanation follows.

Scaling down the engine implies the reduction of the core size. Reducing the passage area, a lower mass flow rate is ingested by the engine, translating in a lower net power delivered by the machine. Moreover, due to manufacturing tolerances, the physical gap between the blades and the casing is basically constant, i.e. is independent on the engine's size; however, the blade heights scale with the engine. It follows that the relative tip clearance increases when the engine scales down, producing a strong efficiency drop. Decreasing the size of the core engine past an inlet diameter of 10 cm, results in efficiencies approaching 80% and below. The reduced efficiency is also the result of another source of loss: the low Reynolds number. The Reynolds number effects occur from an increase of viscous dissipation loss from boundary layers. The lower the Reynolds number, the larger the boundary layers and therefore more viscous dissipation and energy lost from the flow.

The master thesis of Aaron Frisch [1] finds that, at very low size and power (inlet diameter below 10 cm and 300 kW), the gas-turbine engine efficiency becomes too low. It is conceivable that at some point it can be replaced by another source of power, such as an internal combustion (IC) engine. The Diesel cycle is theoretically more efficient than the Otto cycle, given the higher compression ratios and lean-burn combustion. Hence, a Diesel engine may be the best candidate for this purpose, resulting in the same amount of power generation yet at a higher efficiency.

UAVs (Unmanned Aerial Vehicles) are often used in long military missions, like reconnaissance flights. Current technology allows these planes to fly at altitudes up to 25000 feet, but engineers are designing reconnaissance UAVs able to fly up to 50000 feet in the near future [2]. One of the most critical requirements is the time a reconnaissance UAV can fly continuously without refueling. Because UAVs are not burdened with the physiological limitations of human pilots, they

can be designed for maximized on-station times. The maximum flight duration of unmanned aerial vehicles varies widely, depending on the power source. Solar electric UAVs, for example, hold the potential for unlimited flight, a concept championed by the Helios Prototype [3] and accomplished by the Solar Impulse Project in 2016, the first solo solar flight circumnavigation of the globe. On the other hand, the full-solar propulsion is suitable only for those applications where high thrust and large payloads are not required.

Several studies aim to find alternative UAV power sources. For instance, [4] explains the potential of using laser power to extend UAV's flight duration. A clear example is the Stalker UAS, produced by Lockheed Martin, which can carry a payload of 2 lbs for a maximum of 2 hours (extended to 5.5 lbs and 8 hours in the XE version) [5]. By the use of a photovoltaic receiver and on-board power management hardware, the vehicle can be powered for over 48 hours.

For 40 hours missions and beyond, the fuel cell can be the best candidate if thrust and payload are not negligible, or for the production of electrical power on-board. Current technology is exploring the use of solid hydrogen rods instead of gaseous hydrogen in fuel cells; while the use of rods is suitable for 2-20 kW power plants, the excessive weight of large 100 kW cells may be justified only if very long missions are involved [6].

For mid-long mission durations, between 20 and 40 hours, the reciprocating engine is likely the best candidate to drive the aircraft, because of its higher efficiency (i.e. lower fuel consumption) compared to a turbine engine of the same power [7].

1.3 MOTIVATION AND OBJECTIVES

There exist pressures from policy-makers to move towards a common fuel which would be of the type used for jet or diesel engines. Thus, we are left with questions concerning the optimal selection of engine type and configuration for long-duration, lower-to-mid subsonic speed of lighter aircraft. Which engine type is optimal for a given duration? How many engines should be used for a given engine type to produce a certain required thrust? Might an hybrid electric-combustion power source be helpful? Can one engine power more than one propeller either by direct mechanical connection or electrical generation for electric motors? Is there a threshold flight duration when replacing the gas turbine engine with another power source results in less fuel needed? These are examples of the questions to be addressed here. A $300 - 500$ kW is considered as the power target in this work.

Although some practical knowledge is already part of the "know-how" of aircraft industries, as far as author knowledge no hints of a thorough and analytical selection guideline supported by solid theo-

Table 1: Engines and power sources investigated.

Turbine engines	Turbofan
	Turbojet
	Turboprop
	Cruise missiles
	Gas turbines for naval applications
Electric motors	*All types*
Reciprocating engines	Diesel and spark ignition
	2- and 4-strokes
	Turbocharged and naturally aspirated

retical basis is available in the literature. This work aims to answer the previous questions by means of selection criteria based on efficiency and weight.

1.3.1 Presentation Plan

At first, a review on the engines available nowadays is performed in Chapter 2. The propulsive technologies investigated are summarized in Table 1. Considerations on power, weight and size are outlined. By multiplying the fuel consumption by the flight duration, the weight of the fuel needed to accomplish that mission is obtained. Hence, both the *dry weight* and the *full weight*[2] are studied in this work. On so doing, the flight duration is the parameter used to compare the various engines' full weight. A deeper analysis on different engines configurations[3] developing $\simeq 500$ kW is made. The application of each engine technology in Table 1 to different mission durations is investigated.

Taken the results of Chapter 2, the most promising engines from Table 1 -*those ones requiring the lowest full weight per mission*- are selected, discarding the others. On these candidates, an analysis of the thermodynamic cycle is performed in Chapter 3: a numerical MATLAB code is developed for each one of them. These engines are compared for different levels of power, altitude and mission duration.

2 The dry weight is basically the weight of all the mechanical parts of the engine, including manifolds, cooling systems and casing. The full weight is the sum of the dry weight plus the fuel weight. The amount of fuel needed for a certain mission, in terms of mass, is given by (fuel consumption [kg/s]) $\times$ (mission duration [s]). For a more intuitive reading of the fuel consumption, from now on [liters/hour] will be used, and the mass of fuel will be given by (fuel density [kg/lt]) $\times$ (fuel consumption [lt/h]) $\times$ (mission duration [h]).

3 Configuration: assembly of a certain number of engines, propellers, power devices and mechanical joints mounted on an aircraft.

In the second part, a further selection is made and just few candidates are deeply analyzed in Chapter 4. Four configurations are investigated for propelling a long range reconnaissance drone, varying the number of engines and propellers. However, the influence of the propeller number, size, rpm and aerodynamics can clearly play a role in the choice. For this reason Chapter 5 focuses on the propeller efficiency evaluation. Finally, Chapter 6 shows the application of the coupled engine-propeller assembly, based on the analyses previously made. It will be shown that for a certain power requirement, there is a *best choice* on which engine to use, depending on cruise mission duration and altitude.

REFERENCES

[1] A. M. Frisch. "Scaling Effects on the Performance and Efficiency of Gas Turbine Engines." Master of Science Project. University of California, Irvine, 2014.

[2] M. Peck. "U.S. Air Force seeks ideas for de-icing Reapers." In: *Aerospace America* 54.3 (2016), p. 5.

[3] The UAVs. *A brief introduction to the UAV Endurance*. May 22, 2016. URL: http://www.theuav.com/.

[4] S. Frink. *Alternative UAV power sources becoming a reality*. 11 September 2012. Military & Aerospace Electronics. URL: http://www.militaryaerospace.com/articles/2012/09/alternative-uav-power.html.

[5] Lockheed Martin. *Stalker UAS*. Retrieved October 20, 2016. 2016. URL: http://www.lockheedmartin.com/us/products/stalker-uas.html.

[6] K. Button. "Powering Airlines with hydrogen." In: *Aerospace America* 54.2 (2016), p. 5.

[7] N. E. Daidzic, L. Piancastelli, and A. Cattini. "Diesel engines for light-to-medium helicopters and airplanes (Editorial)." In: *International Journal of Aviation, Aeronautics, and Aerospace* 1.3 (2014). URL: http://commons.erau.edu/ijaaa/vol1/iss3/2.

2 ENGINES REVIEW

2.1 POWER AND WEIGHT

In this study, many engine types have been investigated. Data on power, weight and size have been collected from technical sheets available in open literature. All the data are reported in Appendix A. A wide range of power sources are considered, including reciprocating engines, turbine-based engines, and electric motors. for a complete list of the technologies investigated, see Table 1.

Fig. 1 shows the relation between weight and power for the different engines investigated. The diagram is a log-log plot with six orders of magnitude in the abscissa and in the ordinate. The engines tend to be organized along a straight line, or *reference line*, suggesting a power law in the form $\mathcal{W} = a + b\mathcal{P}^c$. ($\mathcal{W}$=weight, $\mathcal{P}$=power). Fitting curves have been optimized with the coefficients in Table 2.

In Fig. 1, attention should be paid to the central part of the diagram. Around 100 kW commercial naturally aspirated engines distance dramatically from the straight line: these engines follow the reference line only in the first part of the plot, say between 0.1 and 30 kW, than they diverge. Formula 1 engines, however, seem to re-arrange the family along the straight line after 300 kW. This can be due to their large bore-to-stroke ratio (usually >1) and the use of cutting-edge light materials. Nevertheless, these engines work at very high rpm and are not very fuel efficient. For a given power, turbocharged engines are generally heavier than their naturally aspirated counterpart, mostly because of the turbocharger itself.

Table 2: Coefficients of the power-weight fitting curves in the form $\mathcal{W} = a + b\mathcal{P}^c$.

	a	b	c	Power range [kW]
IC engines	0.068	0.5608	1.2	$0.1 \div 1000$
Turbine engines	-303.9	15.54	0.5188	$300 \div 10^5$
Electric motors	-2.354	1.609	0.6693	$5 \div 300$

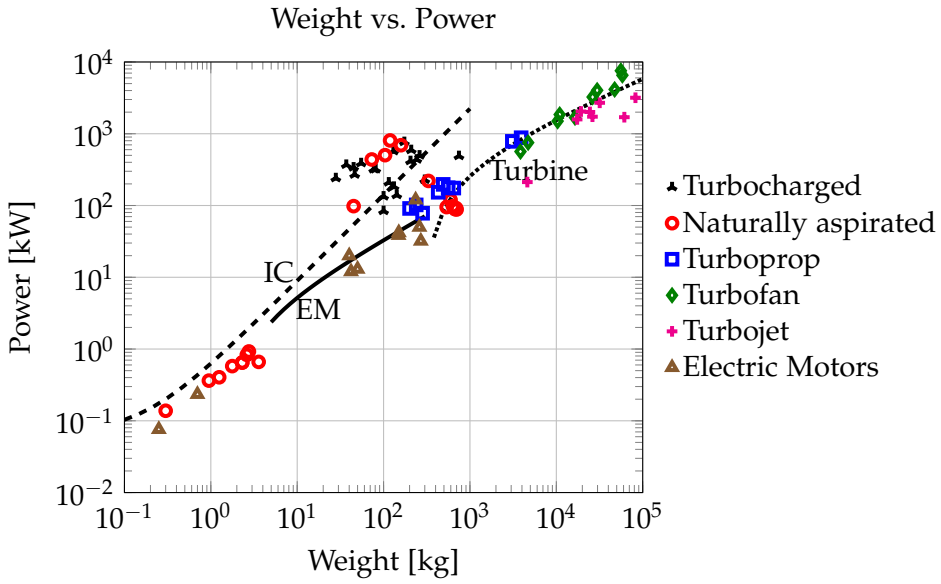

Figure 1: Weight and power of the power sources investigated.

Turbocharged engines range between 20 and 1000 kW. For a given power output, two opposite trends take place in these engines: on one side the additional weight of the turbocharger make them heavier than their naturally aspirated counterpart; on the other side, due to the larger amount of compressed air in the pistons and in the manifolds, they can be smaller (but also thicker to sustain the higher pressure). The first trend, however, is predominant, and they are almost always the heaviest between turbocharged and naturally aspirated engines, for a fixed power. The weights of turbocharged engines vary little over a wide power range. These engines are one order of magnitude heavier than what the average reference line would suggest.

Turboprop engines follow the straight line, but due to the architecture of the engine itself, they seem to be used only for applications over 100 kW. Turbofan and turbojet engines occupy the top-right part of the diagram. Both the categories are lower limited by 10^3 kW, and reach easily 10^5 kW when high by-pass turbofan and afterburning jet engines are involved. For the same power, however, turbojet engines are lighter; turbofan engines suffer from the additional weight of the outer bypass channel and the large fan. Cruise missiles are the most compact and light application among turbine engines; they fit the same linear trend (on a $log - log$ plot) of larger turbine-based engines. The use of one of these power sources on an aircraft could fit the purpose of this work; unfortunately, most of the data concerning these engines, like weight, power and fuel consumption, are confidential. The electric motors investigated are located on the reference line and can be manufactured in a large range of power: below 1 kW, e.g. for aircraft modeling, up to tens of kW.

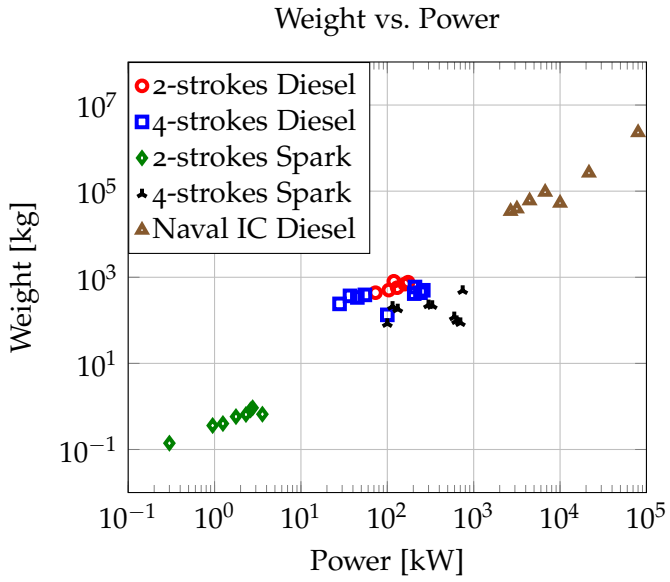

Figure 2: Focus on weight and power of the existing reciprocating engines.

From the previous discussion, turbofan and turbojet engines are discarded for the purpose of this work, both for their weight and because they largely exceed the power range of interest, 300 kW. Because of their lightness, electric motors might seem to be the most suitable for this mission. Reciprocating engines are available too, but attention should be paid to the engine architecture to determine the actual weight.

Figure 2 shows the reciprocating engines weight versus power in detail, focusing on the ignition technique. In the region of 10^2 kW, specifications of 2 and 4-stroke Diesel engines and also 4-stroke spark ignition engines are available. 2-stroke spark ignition engines are mostly used in small displacement motorcycles, hence their power output is limited to few horse power, say 15 hp (12 kW). In fact, 4-stroke spark-ignition engines are generally preferable for more powerful motorbikes.

Naval 2 strokes Diesel engines, instead, are extremely massive and heavy, and are reported here just for comparison. This family of engines is characterized by very low bore-to-stroke ratios (below 0.1) and rpm usually between 30 and 100. It is obvious that they are not suited for aeronautic purposes, because of the size, weight and power.

Finally, it can be noted that in the range between 100 and 300 kW, SI engines are lighter than CI engines. This is due to a general lighter architecture of the former, which don't need to withstand the high cylinder pressures typical of Diesel engines. Moreover, SI engines usually have more slender cylinders, allowing them to reach very high rpm.

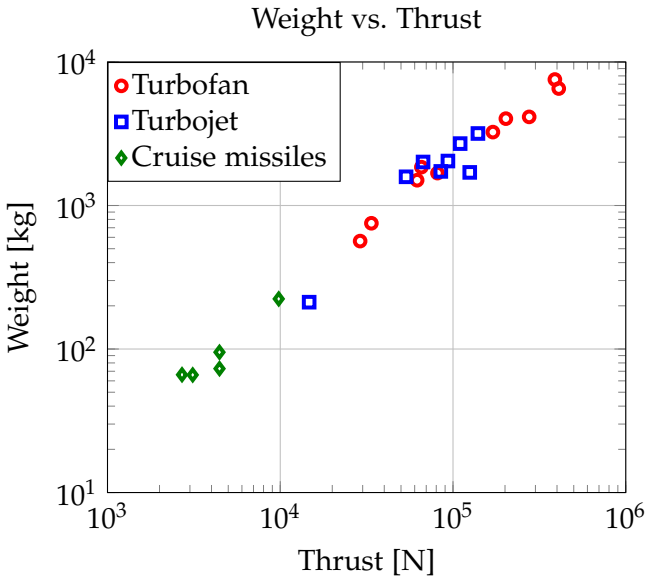

Figure 3: Focus on weight and thrust of the existing turbine-based engines.

In Fig. 3 a detail of turbine engines is presented. These engines are generally reported according to their thrust instead of power. Hence, for comparing this family with the other engines of Table 1, a conversion from thrust to power is needed. As a first computation, for a steady level flight, neglecting the lower order ram thrust:

$$\begin{cases} V_{jet} = \dfrac{\mathcal{T}}{(\dot{m}_{air} + \dot{m}_f)} \\ \mathcal{P} = \dfrac{1}{2}\left[(\dot{m}_{air} + \dot{m}_f) V_{jet}^2\right] \end{cases} \tag{1}$$

It follows that, in order to know the power of a turbine-based engine, the static thrust, the inlet air mass flow rate and the fuel mass flow rate must be known. If the thrust is given at a certain flight speed, ram thrust must be taken into account too.

To take into account the fuel needed for a given mission, the rate of fuel burning must be known. There exist two main definitions of fuel consumption:

THRUST SPECIFIC FUEL CONSUMPTION TSFC $= \dfrac{\dot{m}_f}{\mathcal{T}}$ is a measure of how much fuel is injected to produce a certain amount of thrust. It is generally used in aeronautical turbine engines and is measured in kg/N·s or lb/N·s.

BRAKE SPECIFIC FUEL CONSUMPTION BSFC $= \dfrac{\dot{m}_f}{\mathcal{P}}$ measures the amount of fuel burned to supply a certain power output. It is typically used for comparing the efficiency of internal combustion engines with a shaft output. Its units are kg/W·s or lb/hp·s.

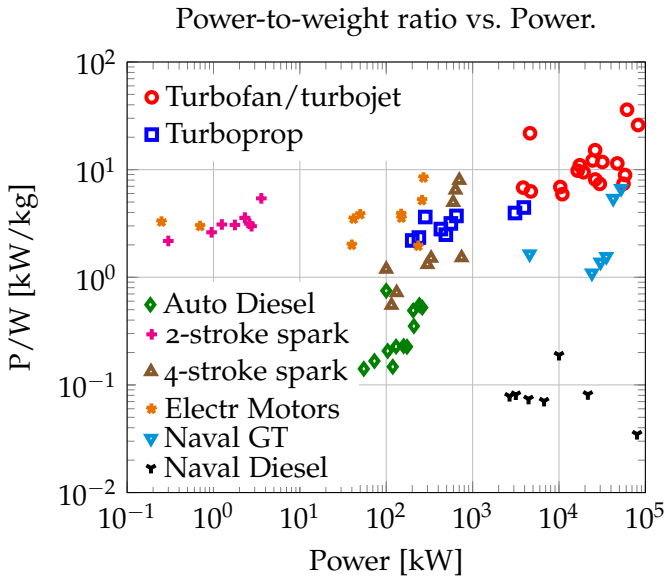

Figure 4: Comparison between power-to-weight ratios of the existing engines.

Figure 3 shows that the most compact and light application of turbine engines is involved in cruise missiles, military devices in which the frontal area must be kept as small as possible. Unfortunately, very little data about Thrust Specific Fuel Consumption $TSFC = \dot{m}_f/\mathcal{T}$ and inlet air mass flow rate $\dot{m}_{air}$ are available in open literature for these engines. For the analysis proposed in this chapter, a Williams F107 engine is considered. Its specifications are taken from [1] and are shown in Section 2.2.

Figure 4 shows the power-to-weight ratio vs. power for every engine investigated in this work. On a $\mathcal{P}/\mathcal{W}$ vs. $\mathcal{P}$ map, it is desirable to obtain an engine as close as possible to the top. For the purpose of this work we are also interested in the area near 10^2 kW. Here we find the electric motors, which have the highest power-to-weight ratio: since they do not need mechanical parts to work, for a given power they are the lightest. Compression ignition (CI) engines for commercial vehicles have the lowest ratio, being generally heavier than spark ignition (SI) engines. Gasoline engines and turboprops stay in the middle and could also be used for the purpose of this work.

2.1.1 Weight and Size

Data about the engine size have been collected as well and are shown in Fig. 5. The model adopted for computing the size is the so called *box size*, meaning the maximum volume occupied by the machine. or a turbine engine, is given by the fan (or first rotor) diameter times the length. Obviously, this basic model is very sensitive to the presence

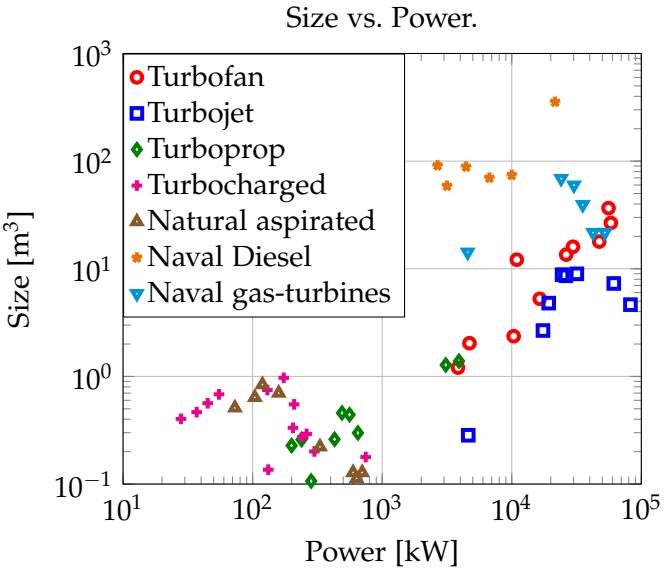

Figure 5: Size of the engines investigated for different power levels.

of large fans or long afterburners. More refined models should be adopted for a better size estimate.

Naval Diesel engines and naval gas turbines are notoriously massive and heavy; turbofan engines are generally bigger than turbojets, for the presence of the large front fan. Finally, reciprocating engines are the most compact and occupy the bottom-left part of the diagram.

2.2 AIRCRAFT CONFIGURATIONS

For a long range reconnaissance military UAV, the engine is expected to be efficient, light, compact, reliable and not very noisy. For the considerations made so far, the following technologies are discarded: turbofan, turbojet, naval large 2-stroke engines and naval gas turbines. All the others power sources will be tested to obtain a general idea of how suitable they are for our scope. The power target for this first analysis is 300 kW (later, higher powers will be studied). This can be obtained in several ways: by only one 300 kW engine, by two 150 kW engines in parallel, three of 100 kW, and so on. The choice of which one is the most convenient is one of the main topics of this thesis. Five different configurations are proposed:

CONF. A 3 turbocharged 4-stroke compression ignition (CI) engines [2], each one driving a propeller.

CONF. B 3 turbocharged 4-stroke spark ignition (SI) engines [3], each one driving a propeller.

CONF. C (HYBRID) 2 electric motors [4] plus one elecric generator [5] driven by a spark ignition engine [6] through a PTO connection.

Table 3: Specifications of the literature engines used in the preliminary analysis.

Config.	Engine name	Weight [kg]	Fuel cons. [kg/h]
A	Centurion/Thielert 135	134	21.43
B	ROTAX 915 IS/ISC	84	29.00
C	5.2 V10 FSI	220	58.97
D	EVD150/260+HVRcr	45.8	1379
E	Tomahawk F107	66	238.10

CONF. D 3 electric motors taking energy from a battery pack carried on-board [7].

CONF. E One single small gas turbine engine [1], driving a propeller by means of a gearbox.

Data concerning the literature engines involved in each configuration are reported in Table 3. In this analysis, a standard 76 kg propeller is considered [8] for each engine in configurations *A*-*D*. Moreover, a standard 15 kg two stage gearbox is added to the overall weight when needed. Electric motors in the range 100-200 hp (75-150 kW) generally have efficiencies between 0.94 and 0.97 [9]. Hence, in this analysis a 0.97 efficiency (defined as the ratio between output and input power) is assumed for each electric motor. For the engines installed in the configurations above, the data on fuel consumption (e.g. TSFC) are presented in Appendix A; they are taken from [1], [10], [11], [12] for the turbine engines, from [2] and [6] for reciprocating engines.

This preliminary analysis investigates the full aircraft weight for a mission. Given the same power level, the total weight of each configuration is given by the sum of the weights of the engines, the propellers, the gearboxes plus the fuel needed for each mission. Note that for configuration *D* the weight of the battery pack is considered instead of the fuel. A standard energy density of 0.645 MJ/kg is assumed, according to the current technology [7]. The results are shown in Fig. 6. The figure on the left is zoomed in the interval 0-6 hours to emphasize the short-flight zone.

While the dry weight is lower in the SI configuration, the CI engine benefits from a lower fuel consumption - the lines approach each other. *Hence, from* 20 *hours on, Diesel engines are the lightest devices for propelling a* 300 *kW aircraft*. This can be seen in Fig. 6, on the right. On the other hand, we see that configuration *D* is by far the heaviest, since the weight of the batteries available nowadays is still too high. An electric aircraft carrying batteries on board turns out to be con-

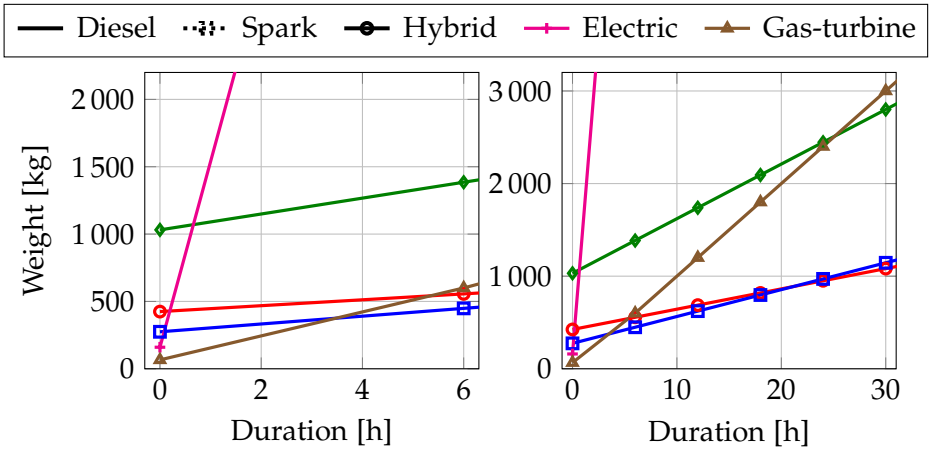

Figure 6: Total weight (dry engine plus fuel or battery) of the five configurations literature-engines-based. $\mathcal{P} \simeq 300$ kW.

venient only for very short missions, below 1 hour, and in extremely low power requirements, like aeromodeling or recreational drones.

The hybrid configuration C is somehow comparable with A and B, even though it is heavier in the whole range considered. This is mainly due to the offset of the generator's weight. The small turbine-based system is the lightest for short durations, then becomes heavier of the above mentioned configurations after few hours. This is due to the scale effects, which at small size dramatically reduce the efficiency, hence increasing the fuel consumption; moreover, military cruise missiles need powerful thrusts to obtain maneuverability and accelerations, then for them fuel consumption may be of secondary importance. It is well known that the advantage of using turbine engines increases with the power. Hence, a deeper analysis should be done for this technology.

Although more refined calculations are required, the simple analysis in this section clearly shows the potential of reciprocating engines for small aircrafts. Moreover, from this point on, the possibility of using an electric configuration is discarded, given the poor energy density of the batteries available nowadays. A deeper analysis will focus on IC engines and on gas turbine engines.

2.3 FINAL REMARKS

The previous discussion showed several engines' data that nowadays (or in the recent past) are produced and are mounted on aeronautical and automotive vehicles. A power-to-weight analysis has shown that electric motors, natural aspirated and turbocharged reciprocating engines are suitable to drive a lightweight aircraft with a power output around $300 - 500$ kW. In particular, electric motors are the lightest, *if only the engine weight is considered*. However, when taking into account

the weight of the batteries, the whole system is excessively heavy. This fact limits the use of large battery-pack for aeronautical purposes.

Layouts *A-B*, based on reciprocating engines, result in the lightest configurations, for their low specific fuel consumption as well as the lightweight of the engines itself. In particular (Fig. 6) Diesel engines appear to be the most convenient if the mission requires long time of flight in the same cruise condition. On the contrary, if short-flight missions are required, the turbine-based configuration *E* may be the lightest option, thanks to the engine lightweight.

The next chapter aims to confirm this behavior through a deep analysis of the thermodynamic cycles. In particular, 5 engines are selected from this section:

1. 4-stroke spark-ignition engine;
2. 4-stroke Diesel engine;
3. 2-stroke spark-ignition engine;
4. 2-stroke Diesel engine;
5. gas-turbine engine.

Every engine cycle is modeled and executed in MATLAB language.

REFERENCES

[1] EASA. *ICAO Aircraft Engine Emissions Databank*. Version 22nd. 2016. URL: https://www.easa.europa.eu/document-library/icao-aircraft-engine-emissions-databank.

[2] Continental motors. *Continental CD-135 data sheet*. Page retrieved on April 13, 2016. URL: http://continentaldiesel.com/typo3/index.php?id=59.

[3] Rotax Aircraft engines. *ROTAX 915 IS/ISC data sheet*. Page retrieved on April 19, 2016. URL: http://www.flyrotax.com/produkte/detail/rotax-915-is-isc.html.

[4] EVDrive electric motors. *VD Motor/Controller Packages*. Page retrieved on May 22, 2016. URL: http://www.evdrive.com/products/evd-motor-controller/.

[5] Winco Generators. *Model data sheet*. Page retrieved on April 13, 2016. URL: http://www.wincogen.com/W165FPTOT-18/.

[6] US Environmental Protection Agency EPA. *Engine Certification Data*. Page retrieved on April 13, 2016. URL: https://www3.epa.gov/otaq/certdata.htm.

[7] Green Car Congress. *Panasonic Develops New Higher-Capacity 18650 Li-Ion Cells*. December 25, 2009. URL: http://www.greencarcongress.com/2009/12/panasonic-20091225.html.

[8] G. Gardiner. *3-D preformed composites: The leap into LEAP*. Ed. by Composites World. March 4, 2014.

[9] U.S. Energy Information Administration. *Minimum efficiency standards for electric motors will soon increase*. September 26, 2016. Today in Energy. URL: https://www.eia.gov/todayinenergy/detail.php?id=18151.

[10] Stanford University. *Data on Large Turbofan Engines*. Page retrieved on May 22, 2016. URL: http://adg.stanford.edu/aa241/propulsion/largefan.html.

[11] Headquarters Air Force Directorate of Propulsion. "Data for some civil gas turbine engines." In: *The Engine Handbook*. Ohio: Wright-Patterson AFB, 1991. URL: http://www.aircraftenginedesign.com/TableB3.html.

[12] Jet Engine Specification Database. *Military Turbojet/Turbofan Specifications*. March 21, 2005. URL: http://www.jet-engine.net/miltfspec.html.

3 THERMODYNAMIC CYCLE ANALYSIS

In order to assess the performance of a certain engine, e.g. power, fuel consumption, efficiency, weight and geometry, two options are possible:

- look into the open literature and hope to find a (reliable) engine data-sheet;
- develop a numerical code able to compute the operative properties of an engine, given its geometry and some boundary conditions.

Although more complex, the second option allows greater flexibility, since any level of power can be theoretically assessed through the code; nevertheless, the real feasibility of the cycle computed is not guaranteed in reality, since mechanical limits may have not been considered or modeled properly. A deep research in the open literature was done and did not give good results, since industry is generally reluctant to let know the performance of the engine alone; the greater part of the data-sheet involve the use of the engine in the vehicle and their performance coupled.[1] These data are not useful for the present work.

For these reasons the numerical approach is the only way to estimate the engines capabilities at different operative conditions, such altitude, aircraft speed, rpm, equivalence ratio and others. From the previous section, five engines have been selected and a numerical MATLAB code has been developed for each one of them: 4-stroke spark ignition, 4-stroke compression ignition, 2-stroke spark ignition, 2-stroke compression ignition, gas turbine engine. The numerical codes are briefly discussed below.

3.1 4-STROKE SPARK IGNITION ENGINE

Is well known that a 4-stroke reciprocating engine's cycle is composed by five phases: compression, combustion and expansion, ex-

1 Data like the fuel consumption per kilometer are quite easy to find, but are very vehicle-dependent and ignore several other variables in that specific configuration, like rpm, velocity, turbocharging settings, altitude (if any) etcetera.

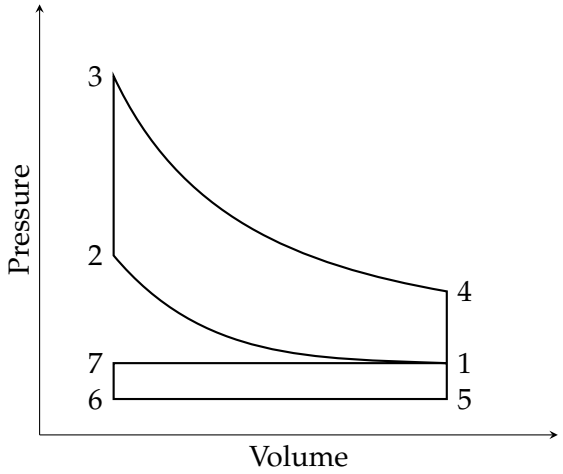

Figure 7: Volume-pressure diagram of an ideal 4-stroke turbocharged spark ignition engine.

haust, and intake. Distinguishing between each phase is not straightforward, since valve timing and spark timing make some of them partially overlapped. Among these phases, modeling the combustion process is by far the hardest challenge. Within few fractions of second physical, chemical and energetic transformations occur. Some simplifications are required to allow the code to be light and readable, without compromising the accuracy of the results. These assumptions will be explained when they are encountered.

The thermodynamic cycle of the engine is subdivided into 720°, i.e. two complete revolutions of the crank. The initial conditions at crank angle 1 are hard to be assessed, because they are the consequence of the previous cycle. Hence, the initial conditions of the cycle are taken from an ideal Otto cycle, performed in advance.

3.1.1 Ideal Cycle

The following theory is based on [1] and [2]. The ideal cycle of an ideal 4-stroke turbocharged reciprocating engine can be subdivided into five phases, evenly lasting 90° of crank angle: compression (1-2), combustion (2-3), expansion (3-4-5), exhaust (5-6-7) and intake (7-1) (see Fig. 7).

The two processes of compression and expansion are assumed to be adiabatic and reversible, hence isentropic. The specific heat ratio, γ, is constant and equal to 1.25. Hence,

$$p_1 V_1^{\gamma} = p_2 V_c^{\gamma} \tag{2}$$

and

$$p_4 V_1^{\gamma} = p_3 V_c^{\gamma} \tag{3}$$

and we get

$$\frac{p_2}{p_1} = \frac{p_3}{p_4} = \left(\frac{V_1}{V_c}\right)^{\gamma} = \varepsilon^{\gamma} = \left(\frac{T_2}{T_1}\right)^{\gamma/(\gamma-1)} = \left(\frac{T_3}{T_4}\right)^{\gamma/(\gamma-1)} \tag{4}$$

where ε is the compression ratio of the cylinder and V_c is the clearance volume. Thus,

$$\frac{T_2}{T_1} = \frac{T_3}{T_4} = \varepsilon^{(\gamma-1)} \tag{5}$$

and

$$\frac{p_3}{p_2} = \frac{p_4}{p_1} = \frac{T_3}{T_2} = \left(\frac{T_3}{T_1}\right)\left(\frac{T_1}{T_2}\right) = \frac{\Theta}{\varepsilon^{(\gamma-1)}} \tag{6}$$

naming Θ the temperature ratio of the cycle. Similarly,

$$\frac{T_4}{T_1} = \left(\frac{T_4}{T_3}\right)\left(\frac{T_3}{T_1}\right) = \frac{\Theta}{\varepsilon^{(\gamma-1)}}. \tag{7}$$

These relations allow to compute p, V, and T at points 1 to 4. In particular, the volumes are known since V_1 and V_2 are tied by ε, which is fixed, and $V_1 = V_4$ and $V_2 = V_3$. From ambient conditions, air is compressed by the turbocharger compressor. Being π_c the turbocharger compression ratio,

$$p_1 = \pi_c \cdot p_{amb} \tag{8}$$

$$T_1 = T_{amb} \cdot \pi_c^{\frac{\gamma-1}{\gamma}}. \tag{9}$$

p_2, p_3, p_4, T_2, T_3, T_4 come straightforward. The ambient conditions are known given the altitude of the aircraft.

In the ideal case, the combustion phase is instantaneous, and in this cycle is assumed to happen at constant volume. In addition, also the scavenging process, through which the exhaust gases are expelled from the cylinder, and the intake, in which fresh charge enters the cylinder, are instantaneous and happen at 4-5 and 6-7 respectively. Hence,

$$p_5 = p_6 = p_T \tag{10}$$

$$T_5 = T_6 = T_4 \tag{11}$$

and

$$p_7 = p_1 \tag{12}$$

$$T_7 = T_1 \tag{13}$$

where p_T denotes the pressure upstream to the turbocharger turbine.

3.1.2 Real Cycle

In the following real cycle modeling, the piston motion in the cylinder is discretized into 360° for the 2-stroke cycles and 720° for the

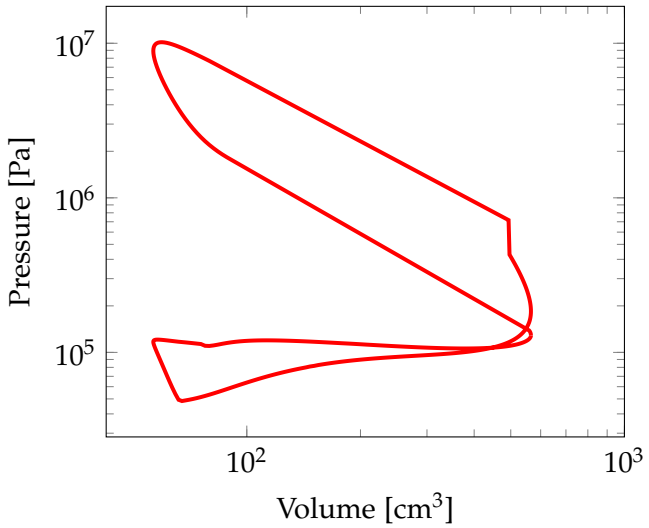

Figure 8: Example of a real spark-ignition cycle, obtained with the numerical code. Bore=8 cm, stroke=9 cm, 1800 rpm, $\varepsilon = 10$.

4-stroke cycles. The index i denotes the crank position, where $i = 1, 2, \ldots, 360$ $(or\ 720)$. The discretization is made as 1 crank degree = 1 step.

The real cycle starts with the piston at bottom dead center (BDC), ready for compression stroke. Both the valves are closed and pressure and temperature at the first crank angle ($i = 1$) are set equal to p_1 and T_1 respectively, found from the ideal case. These values will be refined later on. The compression stroke is characterized by

$$p_i = p_{i-1}\left(\frac{V_{i-1}}{V_i}\right)^{\gamma_c} \tag{14}$$

$$T_i = T_{i-1}\left(\frac{V_{i-1}}{V_i}\right)^{\gamma_c - 1} \tag{15}$$

where γ_c is the specific heat ratio of compression stroke, constant and equal to 1.4 for this phase only. A correspondent $\gamma_e = 1.3$ for expansion is considered. Note that, since $pV^\gamma = const$, in a $\log p - \log V$ diagram the compression and expansion phases are represented by straight lines of slope γ_c and γ_e respectively (Fig. 8). The compression phase continues until the spark ignites the charge. This happens at a certain crank angle (CA) before top dead center (TDC).

The fresh charge contained in the cylinder is constant throughout these phases, since air and fuel are mixed in the carburetor, prior to entering the cylinder. The overall mass is known by the perfect gas law applied at $i = 1$, while the amount of fuel is determined by the equivalence ratio:

$$m = \frac{p_1 V_1}{R T_1} \tag{16}$$

$$m_f = \frac{m}{1 + \alpha_{st}\Phi} \qquad \text{with } \alpha = \frac{m_{air}}{m_f} \tag{17}$$

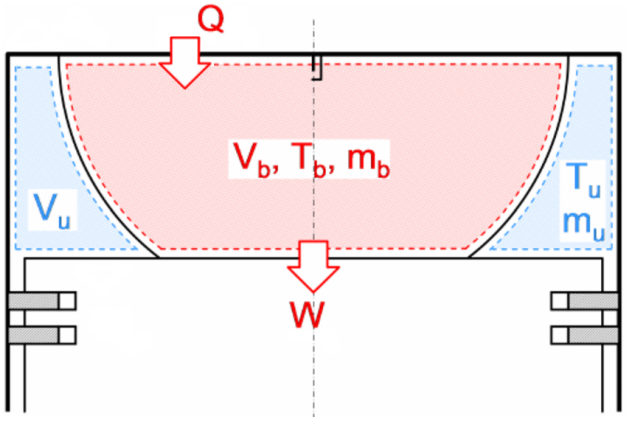

Figure 9: Two zone model, cylinder schematic.

At this point the combustion process starts and a specific function is called in the code. The volume available for combustion, $V(\theta)$, depends on crank angle and varies in time. The combustion model developed here is a two-zone model: the burning zone and the unburned zone (see Fig. 9). The former is the portion of the volume occupied by the burned gases, while the unburned zone contains the fresh charge. By hypothesis the two zones do not mix, remaining distinct throughout the process; however, their volumes V_b, V_u and temperatures T_b, T_u can change. Obviously, $V(\theta) = V_b(\theta) + V_u(\theta)$. Finally, the two zones are assumed to have the same pressure, which changes in time.

Chun and Heywood [3] outline pros and cons of assuming exact or approximated values of specific heat ratios during combustion. The paper demonstrates that the use of a single, average, constant value for the whole process and for both the zones do not compromise the accuracy of the computations. The value suggested by the authors is $\gamma_b = 1.25$.

3.1.2.1 *Combustion: Energy conservation*

In a closed control volume, the first law of thermodynamics states:

$$U = Q - W \tag{18}$$

where U is the internal energy of the cylinder contents, W is the work and Q is the heat. The heat is taken with positive sign when entering the control volume; the work is positive when it is done *by* the the gases *to* the surroundings, hence when it is leaving the volume (see again Fig. 9). The subscript b stands for *burned*, u stands for *unburned*. The derivative on time gives:

$$\dot{U} = \dot{Q} - \dot{W} \tag{19}$$

1. $U = m_u c_{vu} T_u + m_b c_{vb} T_b$

$$\dot{U} = \dot{m}_u c_{vu} T_u + m_u c_{vu} \dot{T}_u + \dot{m}_b c_{vb} T_b + m_b c_{vb} \dot{T}_b$$
$$\dot{U} = m\left[-\frac{dx_b}{d\theta}\omega c_{vu} T_u + (1-x_b) c_{vu}\dot{T}_u + \frac{dx_b}{d\theta}\omega c_{vb} T_b + x_b c_{vb}\dot{T}_b \right]$$

2. $\dot{Q} = \dot{Q}_{ch} - \dot{Q}_{ht}$
   1) $\dot{Q}_{ch} = \dot{m}_f LHV$
      $\dot{Q}_{ch} = m_f \frac{dx_b}{d\theta}\omega LHV$
   2) $\dot{Q}_{ht} = hA(T_b - T_w)$
3. $\dot{W} = p\frac{dV}{dt}$
   $\dot{W} = p\omega\frac{dV}{d\theta}$

where ω is the rotational speed, m_f is the fuel mass, x_b is the mass fraction burned, LHV is the fuel Low Heating Value, h is the heat transfer coefficient, T_w is the temperature of the cylinder walls, which is assumed constant for simplicity, and $\frac{dx_b}{d\theta}$ is the burning rate with respect to the crank angle.

The mass fraction burned is given by the Wiebe function:

$$x_b = 1 - exp\left[-c\left(\frac{\theta - \theta_0}{\Delta\theta}\right)^{r+1} \right] \tag{20}$$

where θ is the crank angle, θ_0 is the start of combustion, $\Delta\theta$ is the total combustion duration ($x_b = 0$ to $x_b = 1$), and c and r are adjustable parameters. The function is reported in Fig. 10, for variable values of c, and in Fig. 11 for variable values of r. Varying c and r changes the shape of the curve significantly. In particular, the change of c acts as a delay in the end of the combustion, while r acts like a trigger in the very beginning of the process. According to [1], actual mass fraction curves have been fitted with $c = 5$ and $r = 2$.
Substituting the equations above in Eq. 19 gives:

$$\begin{aligned} -m_f\frac{dx_b}{d\theta}\omega LHV + hA(T_b - T_w) + p\omega\frac{dV}{d\theta} + \\ + m\left[-\frac{dx_b}{d\theta}\omega c_{vu} T_u + (1-x_b)c_{vu}\dot{T}_u + \right. \\ \left. + \frac{dx_b}{d\theta}\omega c_{vb} T_b + x_b c_{vb}\dot{T}_b \right] = 0 \end{aligned} \tag{21}$$

i.e. a differential equation in T_b, T_u. To proceed further, models for the thermodynamic properties of the burned and unburned gases are required.

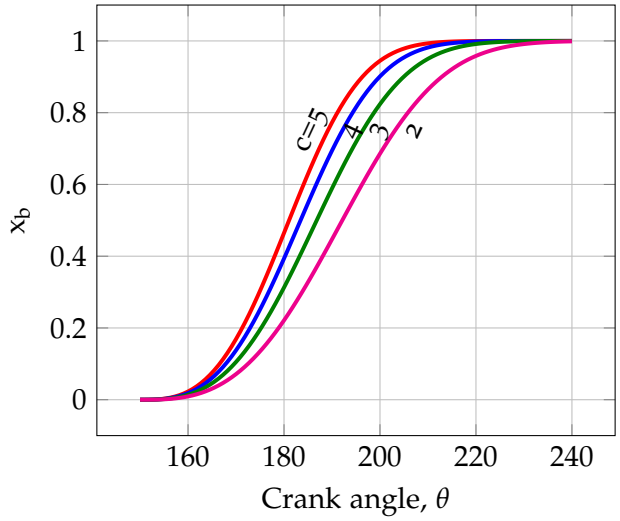

Figure 10: Wiebe function; $r = 2$, $\theta_0 = 150$, $\Delta\theta = 60$.

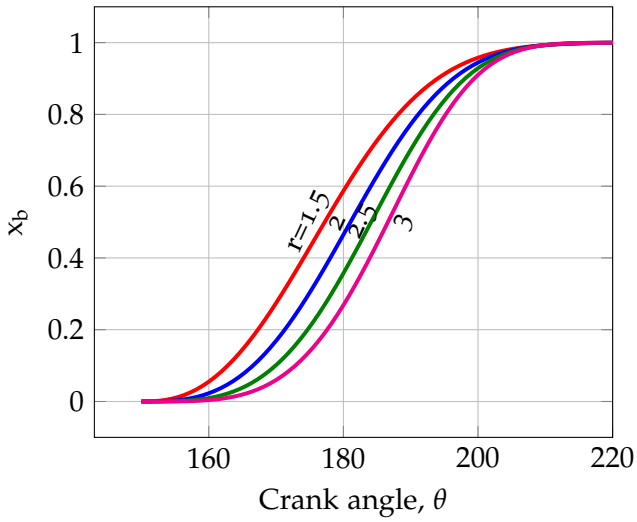

Figure 11: Wiebe function; $c = 5$, $\theta_0 = 150$, $\Delta\theta = 60$.

3.1.2.2 *Conservation of Mass*

$$\frac{V}{m} = \int_0^{x_b} v_b dx + \int_{x_b}^1 v_u dx \tag{22}$$

$$pv_b = R_b T_b \qquad pv_u = R_u T_u \tag{23}$$

Combining Eqs. 22 with 23 gives:

$$\frac{pV}{m} = x_b R_b \bar{T}_b + (1 - x_b) R_u \bar{T}_u \tag{24}$$

where

$$\bar{T}_b = \frac{1}{x_b} \int_0^{x_b} T_b dx \qquad \bar{T}_u = \frac{1}{1 - x_b} \int_{x_b}^1 T_u dx \tag{25}$$

An isentropic compression from an initial uniform state can be assumed for the unburned gas:

$$\frac{\bar{T}_u}{T_0} = \left(\frac{p}{p_0}\right)^{(\gamma-1)/\gamma} \tag{26}$$

We need to obtain two formulations in the form $T_u = f(t, p)$ and $T_b = f(t, p)$ in order to substitute them into the main Eq. 21. On so doing we will be able to close the problem and put it in the form $\dot{p} = f(t, p)$ (please, note that if T_u, T_b are known, also $\dot{T}_u = \frac{dT_u}{dt}$ and $\dot{T}_b = \frac{dT_b}{dt}$ are known as well).

By assuming a uniform temperature of the burned and unburned phases, it is possible to say $\bar{T}_b \simeq T_b$ and $\bar{T}_u \simeq T_u$. In that way it is possible to rearrange Eq. 26 as

$$T_u = T_0 \left(\frac{p}{p_0}\right)^{(\gamma-1)/\gamma} \tag{27}$$

Substituting into Eq. 24 we obtain

$$T_b = \frac{1}{m R_b x_b} \left[pV + (x_b - 1) m R_u T_u \right] \tag{28}$$

which can be finally used to proceed further. (27) and (28) and their derivatives (29) and (30) are all we need to close the problem.

$$\dot{T}_u = T_0 \left(\frac{\gamma - 1}{\gamma}\right) \left(\frac{p}{p_0}\right)^{(-1/\gamma)} \frac{\dot{p}}{p_0} \tag{29}$$

$$\begin{aligned} \dot{T}_b = {} & \frac{-\omega \frac{dx_b}{d\theta}}{m R_b x_b^2} \left[pV + (x_b - 1) m R_u T_u \right] + \\ & + \frac{1}{m R_b x_b} \left[V\dot{p} + \frac{dV}{d\theta} \omega p + \frac{dx_b}{d\theta} \omega m R_u T_u + (x_b - 1) m R_u \dot{T}_u \right] \end{aligned} \tag{30}$$

Substituting $\dot{T}_b$ (Eq. 30) and $\dot{T}_u$ (Eq. 29) in Eq. 21, a differential equation in p only is obtained. It comes in the form $\dot{p} = f(t, p)$.

For simplicity, let us define:

$$A_1 = -m_f \frac{dx_b}{d\theta} \omega LHV \tag{31}$$

$$A_2 = hA(T_b - T_w) \tag{32}$$

$$A_3 = p\omega \frac{dV}{d\theta} \tag{33}$$

$$A_4 = -m \frac{dx_b}{d\theta} \omega c_{vu} T_u \tag{34}$$

$$A_5 = m(1 - x_b) c_{vu} T_0 \left(\frac{\gamma - 1}{\gamma} \right) \left(\frac{p}{p_0} \right)^{-1/\gamma} \tag{35}$$

$$A_6 = \cancel{m} \frac{dx_b}{d\theta} \omega c_{vb} \frac{1}{\cancel{m} R_b x_b} \left[pV + (x_b - 1) m R_u T_u \right] \tag{36}$$

$$A_7 = \cancel{m} \cancel{x_b} c_{vb} \left\{ \frac{-\omega \frac{dx_b}{d\theta}}{\cancel{m} R_b \cancel{x_b^2}} \left[pV + (x_b - 1) m R_u T_u \right] \right\} \tag{37}$$

$$A_8 = \frac{\cancel{m} \cancel{x_b} c_{vb}}{\cancel{m} R_b \cancel{x_b}} \left(\frac{dV}{d\theta} \omega p + \frac{dx_b}{d\theta} \omega m R_u T_u \right) \tag{38}$$

Hence, we can write:

$$A_1 + A_2 + A_3 + A_4 + A_5 \frac{\dot{p}}{p_0} + A_6 + A_7 + A_8 + \\ + \frac{c_{v,b}}{R_b} \left[V\dot{p} + (x_b - 1) m R_u T_0 \left(\frac{\gamma - 1}{\gamma} \right) \left(\frac{p}{p_0} \right)^{-1/\gamma} \frac{\dot{p}}{p_0} \right] = 0 \tag{39}$$

Defining

$$A_9 = A_1 + A_2 + A_3 + A_4 + A_6 + A_7 + A_8 \tag{40}$$

$$A_{10} = \left[\frac{A_5}{p_0} + \frac{c_{vb}}{R_b} V + \frac{c_{vb}}{R_b} (x_b - 1) m R_u T_0 \left(\frac{\gamma - 1}{\gamma} \right) \left(\frac{p}{p_0} \right)^{-1/\gamma} \frac{1}{p_0} \right] \tag{41}$$

we finally obtain

$$\dot{p} = -\frac{A_9}{A_{10}} \tag{42}$$

which is a compact way to write the ode in the form $\dot{p} = f(t, p)$.
A correlation for the heat transfer h coefficient is required. In this analysis the Annand [4] correlation is used:

$$\left(\frac{hB}{k} \right) = a \left(\frac{\rho \bar{S}_p B}{\mu} \right)^b \tag{43}$$

The value of a varies with intensity of charge motion and engine design. Generally, $0.35 \leq a \leq 0.8$ with $b = 0.7$. Gas properties are evaluated at the cylinder-average charge temperature:

$$\bar{T}_g = \frac{pV\bar{M}}{m\tilde{R}} \tag{44}$$

$$\bar{M} = x_b M_b + (1 - x_b) M_u \tag{45}$$

$$\bar{S}_p = \frac{2LN}{60} \tag{46}$$

$$k = \frac{\mu c_{pb}}{Pr}; \tag{47}$$

where $\bar{M}$ is the average molecular mass of the gases contained in the cylinder, $\bar{S}_p$ is the mean piston speed, N is the engine rpm, L and B are the piston stroke and bore respectively, k is the wall thermal conductivity, $Pr = 0.7$ is the Prandtl number, μ is the viscosity of the cylinder contents, computed by Shuterland's correlation

$$\mu = \mu_{ref} \left(\frac{\bar{T}_g}{T_{suth}} \right)^{1.5} \left(\frac{T_{suth} + 110.4}{T_g + 110.4} \right) \tag{48}$$

where $\mu_{ref} = 1.716 \cdot 10^{-5} \ \frac{kg}{m \cdot s}$ and $T_{suth} = 291 \ K$. Cylinder gases then follow a polytropic expansion until exhaust valve is opened, some degree before bottom dead center. When exhaust valve opens, the cylinder pressure is above the exhaust manifold pressure and a *blowdown* process occurs. During this process, the gas which remains inside the cylinder expands polytropically.

A displacement of gas out of the cylinder follows the blowdown process as the piston moves from BDC to TDC. As long as a pressure difference between the cylinder and the manifold is present, the suction of the gases will be added to the scavenging process; during this phase the cylinder volume reduces, causing a rise in pressure.

3.1.2.3 *Flow Trough Valves*

When a pressure difference is present between two points of a duct, a mass flow rate from the high pressure zone towards the low pressure zone is established. The smallest cross area of the duct, if present, is called *throat*. In reciprocating engines this scenario is typical of the valves connecting the manifolds to the cylinders. The system is represented in Fig. 12.

For given values of p_0 and T_0 (the stagnation conditions), the maximum mass flow occurs when the velocity at the throat equals the speed of sound. This condition is called *choking* or *critical flow*. When the flow is choked the pressure at the throat, p_T, is related to the stagnation pressure p_0 as follows:

$$\frac{p_T}{p_0} = \left(\frac{2}{\gamma + 1} \right)^{\gamma/\gamma - 1} \tag{49}$$

This ratio is called *critical pressure ratio* and depends on γ only. For $\gamma = 1.4$ the critical pressure ratio is 0.528. For subcritical flow, the real mass flow rate established in the duct is

$$\dot{m} = \frac{C_D A_T p_0}{\sqrt{R T_0}} \left(\frac{p_T}{p_0} \right)^{1/\gamma} \left\{ \frac{2\gamma}{\gamma - 1} \left[1 - \left(\frac{p_T}{p_0} \right)^{(\gamma-1)/\gamma} \right] \right\}^{1/2}. \tag{50}$$

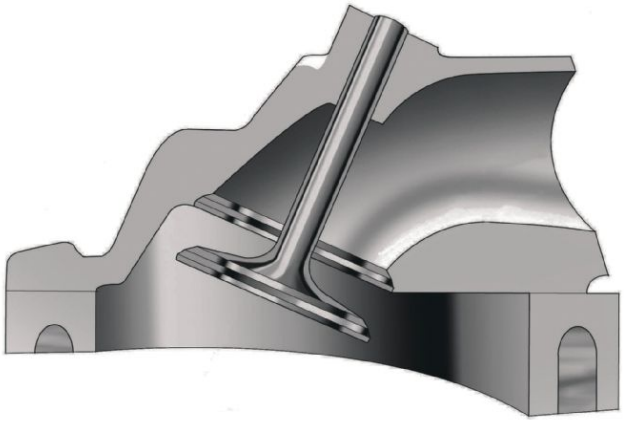

Figure 12: Representation of a cylinder valve.

while, for a choked flow,

$$\dot{m} = \frac{C_D A_T p_0}{\sqrt{RT_0}} \gamma^{1/2} \left(\frac{2}{\gamma + 1} \right)^{\gamma + 1/2(\gamma - 1)}. \tag{51}$$

If the flow is entering the cylinder, p_0 is the intake manifold pressure and p_T in the cylinder pressure. If the flow is exiting, p_0 is the cylinder pressure and p_T is the exhaust manifold pressure.

The value of C_D and the choice of valve reference area (which in this case represents the throat area) are linked together ([1], pag. 226). In this analysis the reference area adopted is the so-called valve *curtain area*:

$$A_T = A_C = \pi D_v L_v \tag{52}$$

where D_v and L_v are the valve diameter and lift respectively. Note that the passage area is not constant, since the valve lift L_v depends on θ.

The effective flow area is defined by

$$A_E = C_D A_C. \tag{53}$$

The discharge coefficient C_D strongly depends on L_v/D_v, and can be estimated through experiments (see Fig. 13). Since L_v/D_v changes in time, then C_D, A_C and $\dot{m}$ change in a complex way (see Eq. 51). However, by assuming a fixed L_v/D_v it is possible to know C_D and so the passage area. Typical maximum values of L_v/D_v are 0.25 [1].

The mass flow rate $\dot{m}(i)$ depends on cylinder pressure $p_0(i)$ (see Eq. 50-51). However, the cylinder pressure depends on the mass con-

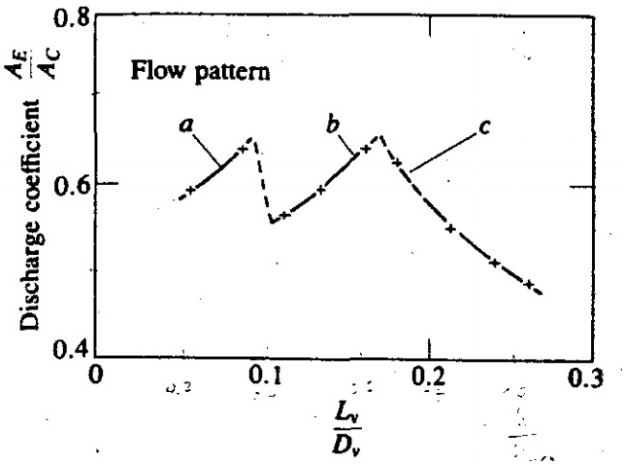

Figure 13: Discharge coefficient versus valve lift-over-diameter ratio. Image courtesy of Heywood [1].

tained in the volume (perfect gas law), which in turn depends on the mass flow entering and exiting the volume:

$$\begin{aligned} p_0(i) &= \rho(i) R \bar{T}(i) \\ &= \frac{m(i)}{V(i)} R \bar{T}(i) \\ &= \frac{m(i-1) + \left[\dot{m}_{in}(i) - \dot{m}_{out}(i)\right] \Delta t}{V(i)} R \bar{T}(i) \end{aligned} \tag{54}$$

where i indicates the crank angle, $\bar{T}$ is the average temperature between the cylinder and the manifold gases, and Δt is the time step of the computation. For this reason, an iterative process is needed: $p_0(i-1)$ is used to compute $\dot{m}(i)$ with Eq. 50 or 51, and this value is used in Eq. 54 to find a new value of pressure. The cycle is repeated until convergence. Attention should be paid during the overlap period, in which both the intake and exhaust valve are open: in this case, $\dot{m}_{in}$ and $\dot{m}_{out}$ are computed, and both are used in Eq. 54.[2]

The intake pressure depends on the compressor design. Assuming a single stage, centrifugal compressor for commercial purpose, the compression ratio depends on the Mach number at blade tip, the compressor efficiency and the blade shape. Experience shows that an optimized impeller works with a compression ratio around 3. Hence, given a cruise altitude, the intake pressure is fixed.

The intake process is basically equal to the blowdown and scavenging processes. The pressure in the intake manifold is higher than the one in the cylinder, and fresh charge is pumped in. The intake valve is kept open far after BDC, in order to enhance the loading of the cylinder; in fact, in turbocharged engines, during the beginning of

2 During the *pure* intake and exhaust phase, only one between $\dot{m}_{in}$ and $\dot{m}_{out}$ is different than zero.

compression the pressure in the cylinder is still lower than the manifold pressure. New charge enters the cylinder until the inlet valve closes; we are now into a new cycle, beyond 720°.

The intake process lasts until the intake valve closes, which generally happens several degrees after BC, exploiting the flow's inertia in order to fill the cylinder with fresh charge as much as possible. When the valve closes, the cylinder state is described by a pressure, temperature and mass content that very unlikely will be the same as those at the same crank angle computed before. In particular, performing the intake process until inlet valve closing corresponds to start from a different value of p_1, T_1, m. At this point, it is possible to perform a new cycle, with a compression stroke starting from the new values. New properties will be computed by the combustion process which will affect the following phases. The convergence is reached when the thermodynamic properties at the end of the intake process match the starting ones of the previous iteration under a certain tolerance. Convergence is generally obtained in 2-3 iterations.

Although this iterative procedure is required to "close" the loop in a p-V diagram, the real behavior of a reciprocating engine is fully unsteady and properties vary from one cycle to the other. Hence the perfect match of the properties is not strictly required.

3.1.2.4 *Work and Power*

Just as a remainder, the work W associated to a closed cycle is given by the integral

$$W = \oint p \, dV \tag{55}$$

that, discretized in the numerical code, is

$$W = \int_1^{720} p \, dV \simeq \sum_{i=1}^{720} p_i \, \Delta V_i = \sum_{i=1}^{720} p_i (V_i - V_{i-1}). \tag{56}$$

where $V_0 = V_{720}$.

In the four-stroke engine cycle, work is done on the piston during the intake and the exhaust processes. The work done by the cylinder gases on the piston during exhaust is

$$W_e = \int_{361}^{540} p \, dV \simeq \sum_{i=361}^{540} p_i \, \Delta V_i (< 0). \tag{57}$$

The work done by the cylinder gases on the piston during intake is

$$W_i = \int_{541}^{720} p \, dV \simeq \sum_{i=541}^{720} p_i \, \Delta V_i (> 0). \tag{58}$$

The net work to the piston over the exhaust and intake strokes, the *pumping* work, is

$$W_p = W_e + W_i. \tag{59}$$

The *compression* work made by the piston to the cylinder gases is given by

$$W_c = \int_1^{180} p\, dV \simeq \sum_{i=1}^{180} p_i\, \Delta V_i (< 0). \tag{60}$$

Finally, the *useful* work made during the expansion phase is

$$W_u = \int_{181}^{360} p\, dV \simeq \sum_{i=181}^{360} p_i\, \Delta V_i (> 0). \tag{61}$$

Engine's *thermal efficiency* is defined as

$$\eta_{th} = \frac{W}{m_f LHV} = \frac{\mathcal{P}}{\dot{m}_f LHV}. \tag{62}$$

The definition of W depends on authors. Some consider $W = W_u + W_c$, others take into account the pumping work too: $W = W_u + W_c + W_p$. In this analysis the second approach is adopted, as suggested by [1]. Power is defined as

$$\mathcal{P} = \frac{W\, rpm}{60\, n_r} \tag{63}$$

where n_r is the number of shaft revolutions per engine firing. A four-stroke engine fires once every two revolutions ($n_r = 2$), while a two-stroke engine fires every revolution ($n_r = 1$). This explains why, theoretically, a two-stroke engine delivers twice the power than a four-stroke, given the same rpm and engine geometry.

3.2 4-STROKE COMPRESSION IGNITION (DIESEL) ENGINE

The main difference between a spark ignition (SI) engine and a compression ignition (CI) engine is the combustion process. In the former the charge is composed by a premixed mixture of air and fuel, while in the latter only air is drawn into the cylinder and fuel is injected in another moment. Hence, the greater difference in the numerical code is the combustion function. Other smaller differences are also present and are here discussed.

3.2.1 Ideal Cycle

Ideal relations similar to those of Section 3.1.1 can be derived for the Diesel cycle, taking into account the different mechanism of ignition and combustion. The volume-pressure diagram of an ideal Diesel cycle is shown in Fig. 14. The *cutoff ratio* V_3/V_c is quite arbitrary, but it is not very important for the rest of the discussion.
The relation between temperatures is:

$$\frac{T_3}{T_2} = \frac{V_3}{V_c} = \left(\frac{T_3}{T_1}\right)\left(\frac{T_1}{T_2}\right) = \frac{\Theta}{\varepsilon^{(\gamma-1)}} \tag{64}$$

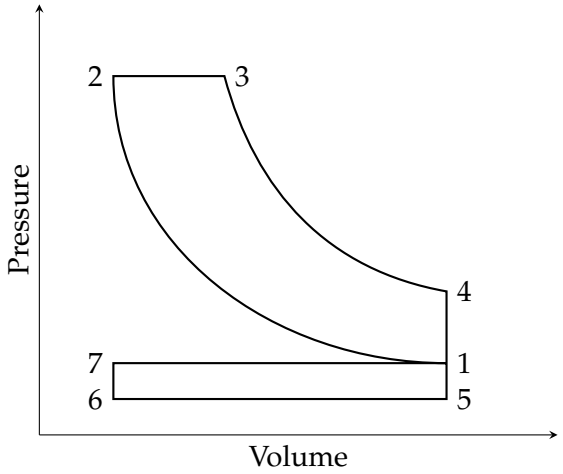

Figure 14: Volume-pressure diagram of an ideal 4-stroke turbocharged compression ignition engine.

Further, since $p_2 = p_3$ and $p_1 V_1^\gamma = p_2 V_c^\gamma$, we get

$$\frac{p_2}{p_1} = \frac{p_3}{p_1} = \varepsilon^\gamma \tag{65}$$

Moreover,

$$\frac{p_3}{p_4} = \left(\frac{V_1}{V_3}\right)^\gamma = \left[\left(\frac{V_1}{V_c}\right)\left(\frac{V_c}{V_3}\right)\right]^\gamma = \left(\frac{\varepsilon V_c}{V_3}\right)^\gamma \tag{66}$$

hence,

$$\frac{p_4}{p_1} = \frac{p_3}{p_1}\frac{p_4}{p_3} = \left(\frac{V_3}{V_c}\right)^\gamma \tag{67}$$

Further,

$$\frac{T_2}{T_1} = \left(\frac{p_2}{p_1}\right)^{\frac{\gamma}{\gamma-1}} \tag{68}$$

Finally,

$$\frac{T_4}{T_1} = \left(\frac{T_4}{T_3}\right)\left(\frac{T_3}{T_1}\right) = \left(\frac{T_3}{T_1}\right)\left(\frac{p_4}{p_3}\right)^{\frac{\gamma-1}{\gamma}} \tag{69}$$

3.2.2 Real Cycle

The following model is substantially very similar to the SI model described in Sec. 3.1.2. The main difference is the way the combustion process is modeled. The real mechanism of fuel injection is extremely complex and a strict reproduction of the phenomena involved would require the use of Computational Fluid Dynamics (CFD). Moreover, "combustion process" is a general term comprehending a series of distinct phenomena as vaporization, mixing, ignition and burning of the fuel-air mixture. All these processes are heterogeneous, unsteady, turbulent, multiphase.

A strict analysis of the combustion process is actually not required for the scope of this thesis. In fact, the study of the thermodynamic cycle requires information about:

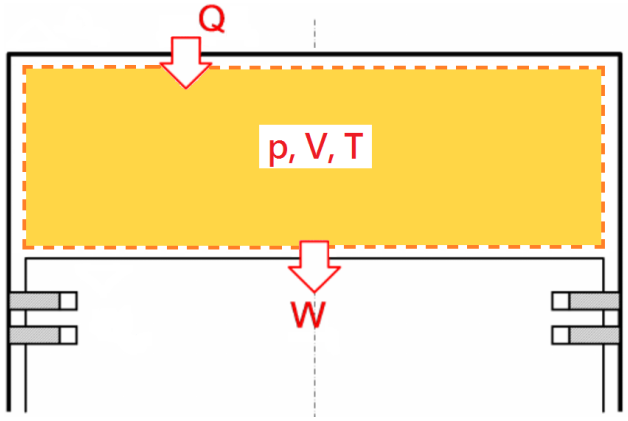

Figure 15: Single zone model, cylinder schematic.

- combustion start;
- combustion extinction;
- amount of heat released.

The grater complexity of studying the combustion kinetics would certainly add information of the first two types; however, experience outlines typical ignition delays and combustion durations in terms of crank angle degrees (see Sec. 3.2.2.3). Hence, these experimental data can be sufficient in this work.

Concerning the third bullet, chemical kinetics could theoretically predict the combustion efficiency and the presence of unburned fuel. Again, this value can be introduced in the code according to common values reported in literature, for any operative condition.

The combustion model considers a single zone contained in the cylinder, with uniform pressure and temperature (Fig. 15). This simplifying assumption allows to obtain acceptable accuracy within reasonable computational cost. The fuel injection is assumed to happen in the liquid phase. Although simplified, this model should be enough accurate for our scope.

3.2.2.1 *Combustion: Energy Conservation*

$$U = Q - W \tag{70}$$

where U is the internal energy of the cylinder contents, W is the work and Q is the heat. The heat is taken with positive sign when entering the control volume; the work is positive when it is done *by* the gases *to* the surroundings, hence when it is leaving the volume. The time derivative gives:

$$\dot{U} = \dot{Q} - \dot{W} \tag{71}$$

Each term must be modeled consequently:

1. $\dot{U} = \dot{m}c_v T + mc_v\dot{T} = \dfrac{R}{\gamma - 1}(\dot{m}T + m\dot{T})$
2. $\dot{Q} = \dot{Q}_{ch} - \dot{Q}_{ht} + \dot{Q}_{sens}$
   1) $\dot{Q}_{ch} = \dot{m}_{burn} LHV$
   2) $\dot{Q}_{ht} = hA(T - T_w)$
   3) $\dot{Q}_{sens} = \sum_i \dot{m}_i h_i - \sum_j \dot{m}_j h_j$
3. $\dot{W} = p\dfrac{dV}{dt} = p\dot{V}$

where Q_{ch} is the energy released by the combustion, Q_{ht} is the heat lost to the cylinder walls, which are at constant temperature T_w, Q_{sens} is the sensible energy of those masses entering and leaving the volume (only fuel injection is considered; crevice losses and leakages are neglected), m is the cylinder mass at each timestep $\big(m(t) = m_{air} + m_f(t)\big)$, LHV is the fuel Low Heating Value.

Assembling the terms we get the following equation:

$$\frac{R}{\gamma - 1}(\dot{m}T + m\dot{T}) = \dot{m}_{burn} LHV - hA(T - T_w) + \dot{m}_{inj} h_i - p\dot{V} \tag{72}$$

3.2.2.2 *Perfect Gas Law*

At the beginning of combustion, only air is contained in the volume. By deriving in time the perfect gas equation

$$pV = mRT \tag{73}$$

we obtain

$$\dot{p}V + p\dot{V} = \dot{m}RT + m\dot{R}T + mR\dot{T} \tag{74}$$

Rearranging,

$$\dot{T} = \frac{\dot{p}V + p\dot{V} - \dot{m}_{inj}RT - m\dot{R}T}{mR} \tag{75}$$

where the temperature T is simply given by the perfect gas law:

$$T = \frac{pV}{mR} \tag{76}$$

By substituting Eqs. 75 and 76 into Eq. 72 and rearranging:

$$\frac{R}{\gamma - 1}\Big[\cancel{\dot{m}_{inj}T} + \frac{1}{R}(\dot{p}V + p\dot{V} - \cancel{\dot{m}_{inj}RT} - m\dot{R}T)\Big] = \dot{m}_{burn} LHV - hA(T - T_w) + \dot{m}_{inj} h_i - p\dot{V} \tag{77}$$

$$\frac{1}{R}(\dot{p}V + p\dot{V} - m\dot{R}T) = \frac{\gamma - 1}{R}\big[\dot{m}_{burn} LHV - hA(T - T_w) + \dot{m}_{inj} c_p T_f - p\dot{V}\big] \tag{78}$$

$$\dot{p} = \frac{\gamma - 1}{V}\left[\dot{m}_{burn} LHV - hA\left(\frac{pV}{mR} - T_w\right) + \dot{m}_{inj} c_p T_f - p\dot{V}\right] - p\left(\frac{\dot{V}}{V} - \frac{\dot{R}}{R}\right) \quad (79)$$

Eq. 79 is a differential equation in the form $\dot{p} = f(t, p)$. V and $\dot{V}$ are known from the cylinder geometry and rpm. The term A in the above equation is the area subject to heat transfer. It is given by:

$$A(\theta) = A_{fix} + A_{var}(\theta) \begin{cases} A_{fix} = \dfrac{\pi B^2}{2} + \dfrac{4V_c}{B} \\ A_{var}(\theta) = \dfrac{4\left(V(\theta) - V_c\right)}{\pi B^2} \end{cases} \quad (80)$$

The fixed term is composed by the piston crown area plus the cylinder top wall plus the lateral cylinder walls of the clearance volume, which are always exposed to the gases. The variable term is the lateral surface of the cylinder that is gradually uncovered during piston motion.

The presence of the term $\dot{R}$ increases the overall complexity of the problem. A possible solution is the shifting of the value of R in time between two typical values: 289 [J/kgK] for the exhaust gases, and 273 [J/kgK] for the fresh charge. The rate of burning is modeled by the Wiebe function (Eq. 20) [1].

$$R = x_b R_1 + (1 - x_b) R_2 \quad (81)$$

$$\dot{R} = \frac{dR}{dx_b}\frac{dx_b}{d\theta}\frac{d\theta}{dt} \quad (82)$$

$$x_b(\theta) = 1 - exp\left[-c\left(\frac{\theta - \theta_0}{\Delta\theta}\right)^{r+1}\right] \quad (83)$$

$$\frac{dx_b}{d\theta} = \frac{c(r+1)}{\Delta\theta}\left(\frac{\theta - \theta_0}{\Delta\theta}\right)^{r} exp\left[-c\left(\frac{\theta - \theta_0}{\Delta\theta}\right)^{r+1}\right] \quad (84)$$

$$\dot{R} = (R_1 - R_2)\omega\frac{c(r+1)}{\Delta\theta}\left(\frac{\theta - \theta_0}{\Delta\theta}\right)^{r} exp\left[-c\left(\frac{\theta - \theta_0}{\Delta\theta}\right)^{r+1}\right] \quad (85)$$

In order to implement the combustion model on MATLAB `ode45` solver, a characteristic shape of fuel injection $\dot{m}_{inj}$ and the fuel burning rate $\dot{m}_{burn}$ should be defined. This is done in the following section.

3.2.2.3 *Fuel Injection*

The inlet fuel mass flow rate is given by the fuel flow through a nozzle:

$$\dot{m}_{inj} = C_D A_{inj}\sqrt{2\rho_f \Delta p} \quad (86)$$

$$m_{inj} = C_D A_{inj}\sqrt{2\rho_f \Delta p}\,\frac{\Delta\theta}{6\,rpm} \quad (87)$$

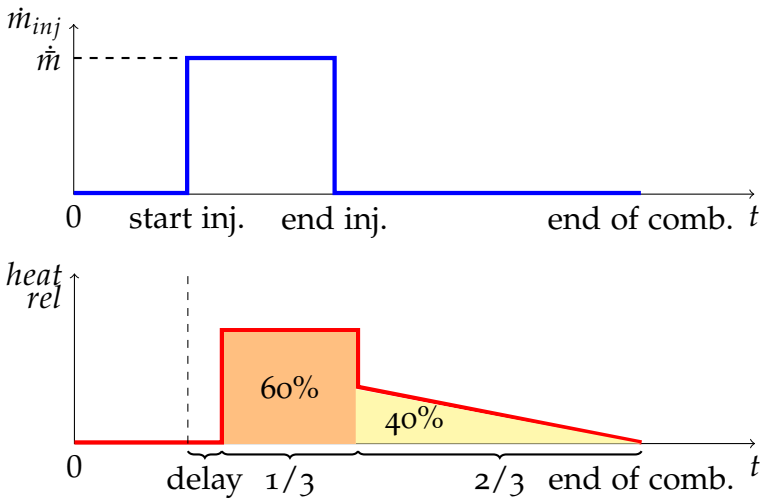

Figure 16: Fuel injection and heat release profile according to [1].

where A_{inj} is the nozzle area, ρ_f is the fuel density, Δp is the pressure drop across the injector, C_D is the discharge coefficient, and $\Delta\theta$ is the length of injection (in degrees). The C_D, A_{inj}, ρ_f and $\Delta\theta$ are fixed, while m_{inj} is an input parameter. It follows that Δp[3] can be obtained by the second equation and substituted into the first. The magnitude of fuel mass flow rate is then known. Standard Diesel injectors usually operate with fuel-injection pressures between 200 and 1700 atmospheres ([1], pag. 522).

It is well known that the fuel injection and the heat release do not take place simultaneously. The *ignition delay* in a Diesel engine is defined as the time (or crank angle) interval between the start of ignition and the establishment of the flame. Heywood ([1], pg. 503) indicates that typical ignition delays lie between 5° and 9°. The real injection profile is available only from experimental data; in this analysis a step function is assumed to approximate the injection rate; a heat release profile is also assumed, including an ignition delay and reproducing the heat release time distribution (Fig. 16).

The overall injection profile depends on many aspects and its shape may vary a bit; however, the length of injection is typically around 20 crank degrees. The heat release distribution, according to [1] pag. 513, says that about 60% of the fuel burns in the first one-third of the total combustion period. This is the main contribute to combustion and is modeled as a rectangle of unknown height; the remaining 40% is consumed linearly until there is fuel to sustain the combustion. Since the total heat released and the areas are known (60%-40%), with elementary algebra it is possible to fully characterize (length and height) these shapes.

The start of injection is at 15° before TDC, and is manually moved backwards up to 20° with increasing rpm. The most difficult data to

3 Δp varies on time. In fact, $\Delta p(t) = p_{inj} - p_{cyl}(t)$.

be decided is the duration of the flame. This length strictly depends on chemical kinetics, fluid dynamics and piston mechanics. For these reasons it was decided to assume that the combustion extinguishes after 100° from the start of injection. From that point on a simple isentropic expansion is considered. Another difference with the 4-stroke SI model is that the mass contained in the cylinder is not the same along compression and expansion strokes, because of the fuel injection. The equivalence ratio is computed as the ratio between the instantaneous air-to-fuel ratio α and the stoichiometric ratio. $\alpha_{st} \simeq 14.5$ in Diesel engines.

3.3 2-STROKE SPARK IGNITION ENGINE

The MATLAB code developed here is inspired to the work of Sookdeo [5], even if several major changes were done. The work of Sookdeo aims to model an extremely small and fast rotating CI engine, while we are interested in traditional dimensions and rpm; for this reason, the engine geometry was rearranged. Moreover, the combustion model present in Sookdeo's work is oversimplified and fitted to experimental data performed by himself; it was necessary to implement a new combustion model (substantially equal to those previously explained) which have a general validity. Finally, a new heat transfer model was included.

A 2-stroke engine is composed by a certain number of cylinders, in which the piston divides two very important environments. One is the volume contained between the piston crown and the cylinder walls; the other one is the so-called *crankcase* environment, composed by the portion between the piston and the crankcase surrounding the shaft, plus a short inlet manifold from which the air is drawn into the cycle. A scheme of a two-stroke cylinder is shown in Fig. 17.

The MATLAB code evaluates five thermodynamic properties for each environment: cylinder pressure, mass of gases in cylinder, enthalpy, temperature and entropy. For each one of these unknowns an equation is required:

$$\begin{cases} pV = mRT & \text{Eq. of state} \\ m = m_0 + m_{in} - m_{out} & \text{Mass conserv.} \\ Q = Q_0 + Q_{in} - Q_{out} & \text{Energy conserv.} \\ Q = mc_vT & \text{1st Law of Therm.} \\ Q = TdS & \text{2nd Law of Therm.} \end{cases} \tag{88}$$

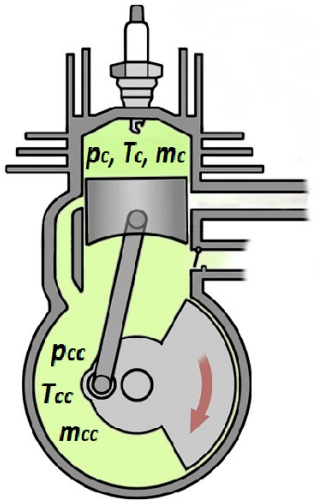

Figure 17: 2-stroke engine cylinder.

Deriving in θ, the system becomes:

$$\begin{cases} \dfrac{dp}{d\theta}V + p\dfrac{dV}{d\theta} = \dfrac{dm}{d\theta}RT + mR\dfrac{dT}{d\theta} & \text{Eq. of state} \\ \dfrac{dm}{d\theta} = \dfrac{dm_{in}}{d\theta} - \dfrac{dm_{out}}{d\theta} & \text{Mass conserv.} \\ \dfrac{dQ}{d\theta} = \dfrac{dQ_{in}}{d\theta} - \dfrac{dQ_{out}}{d\theta} & \text{Energy conserv.} \\ \dfrac{dQ}{d\theta} = \dfrac{dm}{d\theta}c_vT + mc_v\dfrac{dT}{d\theta} & \text{1st Law of Therm.} \\ \dfrac{dQ}{d\theta} = \dfrac{dT}{d\theta}S + T\dfrac{dS}{d\theta} & \text{2nd Law of Therm.} \end{cases} \tag{89}$$

Remember that, for the derivation chain rule,

$$\frac{d\cdot}{dt} = \frac{d\cdot}{d\theta}\frac{d\theta}{dt} \quad \Longrightarrow \quad \frac{d\cdot}{d\theta} = \frac{1}{\omega}\frac{d\cdot}{dt}$$

Equations 89 represent a system of five equations in five unknowns. Including the other set of five equations for the second environment, a 10×10 system is obtained. Every explicit linear system can be rearranged in matrix form: $\mathbf{Ax} = \mathbf{b}$. This problem comes in the form $\mathbf{M}(t, \mathbf{x})\dot{\mathbf{x}} = f(t, \mathbf{x})$. The MATLAB `ode45` solver is able to integrate the system of differential equations from t_0 to t_f given some initial conditions $\mathbf{x_0}$.

In this case, the problem is made by the following linear system:

$$\begin{bmatrix} V_c & -RT_c & 0 & -m_cR & 0 & & & & & \\ 0 & 1 & 0 & 0 & 0 & & & & & \\ 0 & 0 & 1 & 0 & 0 & & [\varnothing] & & & \\ 0 & -c_vT_c & 1 & -m_cc_v & 0 & & & & & \\ 0 & 0 & 1 & -S_c & -T_c & & & & & \\ & & & & & V_{cc} & -RT_{cc} & 0 & -m_{cc}R & 0 \\ & & & & & 0 & 1 & 0 & 0 & 0 \\ & & [\varnothing] & & & 0 & 0 & 1 & 0 & 0 \\ & & & & & 0 & -c_vT_{cc} & 1 & -m_{cc}c_v & 0 \\ & & & & & 0 & 0 & 1 & -S_{cc} & -T_{cc} \end{bmatrix} \frac{d}{d\theta} \begin{Bmatrix} p_c \\ m_c \\ Q_c \\ T_c \\ S_c \\ p_{cc} \\ m_{cc} \\ Q_{cc} \\ T_{cc} \\ S_{cc} \end{Bmatrix} = \frac{1}{\omega} \begin{Bmatrix} -\omega p_c \frac{dV}{d\theta} \\ \dot{m}_{cc} - \dot{m}_{out} \\ \dot{Q}_{in} - \dot{Q}_{out} \\ 0 \\ 0 \\ -\omega p_{cc} \frac{dV}{d\theta} \\ \dot{m}_{in} - \dot{m}_{cc} \\ \dot{Q}_{in} - \dot{Q}_{out} \\ 0 \\ 0 \end{Bmatrix}$$

with initial conditions

$$x_0 = \left\{ p_c^0 \quad m_c^0 \quad 0 \quad T_c^0 \quad 0 \quad p_{cc}^0 \quad m_{cc}^0 \quad 0 \quad T_{cc}^0 \quad 0 \right\}^T.$$

Initial pressure and temperature of the cylinder are assumed as $p_c^0 = 1.4\, p_{amb}$ and $T_c^0 = T_{amb} 1.4^{(\gamma-1)/\gamma}$. Further iterations will overwrite these values with the effective ones computed from the cycle. p_{cc}^0 and T_{cc}^0 are set equal to the conditions in the intake manifold: $p_{cc}^0 = \pi_c\, p_{amb}$ and $T_{cc}^0 = T_{amb} \pi_c^{(\gamma-1)/\gamma}$. Finally, initial masses m_c^0 and m_{cc}^0 are computed with the perfect gas law, given the temperature and the volume of each environment:

$$\begin{cases} m_c^0 &= m_{air} + m_f \\ &= (1+\alpha) m_{air} \\ &= (1 + \alpha_{st}\Phi) \dfrac{p_c^0 V_c^0}{R T_c^0} \\ m_{cc}^0 &= (1 + \alpha_{st}\Phi) \dfrac{p_{cc}^0 V_{cc}^0}{R T_{cc}^0} \end{cases} \tag{90}$$

Note that now α is defined as the fuel-to-air ratio. The system of differential equations is integrated along 360° with `ODE45` solver, obtaining the vector **x** at every crank angle. The MATLAB solver `ODE45` is based on an explicit second order accurate Runge-Kutta method. It is a single-step solver, meaning that in computing the solution at time *t*, it needs only the solution at the immediately preceding time point *t-1* [6]. The timestep used for the four reciprocating engine models was varied between one crank angle up to 1/16 of crank angle. Paying a moderate increase in computational time, no significant change in the results were noticed.

3.4 2-STROKE COMPRESSION IGNITION (DIESEL) ENGINE

The same considerations made for adapting the 4-stroke SI model to the 4-stroke CI model apply here. The code is substantially equal to the 2-stroke SI code, with the main exception of a different combustion model (see 3.2) and other minor changes concerning the air-fuel composition. Note that now the inzial conditions for the mass are:

$$\begin{cases} m_c^0 = m_{air} = \dfrac{p_c^0 V_c^0}{R T_c^0} \\ m_{cc}^0 = \dfrac{p_{cc}^0 V_{cc}^0}{R T_{cc}^0} \end{cases} \tag{91}$$

Table 4: Parameters chosen for the reciprocating engines models.

	4-stroke CI	4-stroke SI	2-stroke CI	2-stroke SI
ε	18	10	18	10
evc [deg]	20	20	-	-
evo [deg]	50	50	-	-
ivc [deg]	40	40	-	-
ivo [deg]	15	15	-	-
$\frac{\text{rod length}}{\text{crank length}}$	4	4	2	2
$c/r/\theta_0/\Delta\theta$	-	5/2/150/55	-	5/2/150/55
α_{st}	14.5	14.7	14.5	14.7

3.5 CONSIDERATIONS ON THE MODELS

The four reciprocating engine numerical models explained so far have been tested to assess their validity. This process is reported in Appendix C.

Table 4 reports the parameters which have been assumed in the MATLAB codes. Every value is taken according to [1], following typical values, rules of thumb and experience. ε is the compression ratio: typical values are above 15 for the CI engines and up to 12 for the SI engines; for this reason, 18 and 10 have been assumed respectively. Higher values imply higher pressures, hence ticker materials (extra weight) and risk of knocking for the SI engine. However, lower ε reduce the cycle efficiency.

The opening and closing of the intake and exhaust valves do not coincide with BDC and TDC in a real cycle; indeed, there exists a delay in both the valve closings, in order to maximize the exhaust gas scavenging and the cylinder filling with fresh charge. These two values are represented by exhaust valve closing delay (evc) and intake valve closing delay (ivc) respectively. For the same reasons, valves are opened far before the dead points: exhaust valve opening advance (evo) and intake valve opening advance (ivo) represent these values in terms of crank angle. These numbers can be moved around and, in some modern engines, are function of piston speed, i.e. engine rpm, allowing a fine regulation of the burning charge residence time and the maximization of the work. Obviously, no valves are involved in 2-stroke engines, since the cylinder filling and emptying processes are performed by the piston motion itself.

The ratio between the connecting rod length and the crank length depends on the engine application. Very small, fast-rotating engines as for radio-controlled aircraft and cars generally have a higher ratios in order to contain inertia forces. In fact, note that this ratio is propor-

tional to $1/stroke$. Large naval engines typically have small rotational speed and bore-to-stroke ratios, hence higher strokes.

The values of c, r, θ_0 and $\Delta\theta$ of the Wiebe function (Eq. **??**) represent the two constants of the equation, the fuel injection crank angle ($i = 180$ corresponds to TDC) and the burning duration in terms of crank angle. Note that injection is advanced with respect to TDC; this is generally named *spark advance* and in this analysis is set to 30°. The faster the rotational speed, the larger should be the spark advance allowing more time to the charge to ignite. CI engines do not work with this combustion model, hence these parameters do not apply.

Finally, the air-to-fuel stoichiometric ratio α_{st} is also reported in the table. For pure octane the stoichiometric mixture is approximately 14.7:1, while for Diesel fuel is around 14.5:1. Any mixture greater than α_{st} is considered a lean mixture; any less than α_{st} is a rich mixture.

3.5.1 Improvements of the models

The accuracy of the numerical codes can be improved in several ways:

- So far, the heat loss from the burning gases to the cylinder walls is modeled through the Annand's correlation [4]. Refined heat transfer models can be introduced in every combustion model, for example by accounting for a variable wall temperature, which depends on the gases temperature. Also, radiative heat transfer from the burning zone could be added to the convective one.

- Modeling the gradual opening and closing of the valves of the two 4-stroke engines, i.e. $L_v(\theta)$, should be done is more realistic results are expected; this implies that also the curtain area depends on θ. This dependence should be included in the computation of the instantaneous $\dot{m}$, Eq. 52. Further complexity is added if the valve lift is also a function of engine's rpm, i.e. $L_v(\theta, rpm)$.

- The 4-stroke Diesel model considers a single zone contained in the cylinder, with uniform pressure and temperature. Comparisons between this model and more accurate numerical models, CFD and/or experimental results should be performed; if needed, multiphase injection and evaporation might be considered.

- Improvements of the 4-stroke Diesel combustion model are possible in many directions: more complex heat release curve shape (possibly obtained by measurement); automatic regulation of injection timing with rpm; accounting for vaporization of droplets

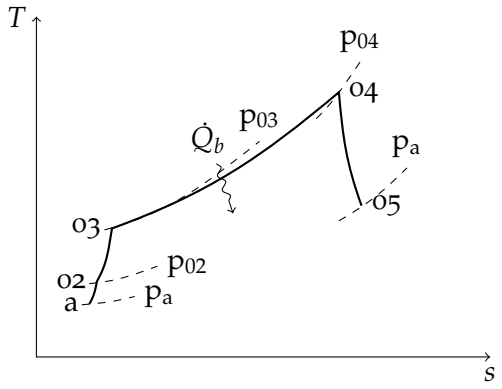

Figure 18: Temperature - specific entropy real Brayton cycle.

Table 5: Input parameters of the gas turbine numerical code.

Altitude [ft]	z	10000
Flight Mach Number	M_0	0.4
Diffuser PR	π_d	0.98
Comb. chamber PR	π_b	0.98
Combustion eff.	η_b	0.99
Mechanical eff.	η_m	0.98
Turbine inlet temp. [K]	T_{04}	1670

and computation of the delay; implementation of a multi-zone combustion model, able to model the effective combustion duration.

3.6 GAS TURBINE ENGINE

In this section, a cycle analysis of the gas turbine engine is performed to assess its efficiency for certain design choices, such as the overall compressor pressure ratio (OPR). The real thermodynamic cycle for the gas-turbine engine is the real Brayton cycle (Fig. 18). In this study, the compressor OPR $\pi_c = p_{03}/p_{02}$ and the turbine inlet total temperature T_{04} are design choices. The OPR is evenly distributed throughout the compressor stages. The following parameters are also introduced as input in the code: flow coefficient $\phi = V_x/U$, stage loading coefficient $\Psi = \Delta h_t/U^2$, degree of reaction $\mathcal{R} = \Delta h_r/\Delta h_{stage}$ and solidity $\sigma = c/s$. Other parameters are chosen as shown in Table 5.

Let the freestream be designated as station a at ambient pressure p_a and Mach number M; the inlet/diffuser reduces the flow to a low-speed flow before the compressor inlet; at station 02, $p_{02} = p_{01}/\pi_d$. The flow is further compressed to reach a total pressure $p_{03} = \pi_c\, p_{02}$ before it goes into the combustor; here, heat $\dot{Q}_b$ is added to increase

the flow temperature up to T_{04}. A small loss in total pressure along combustion is accounted, as $p_{04} = \pi_b p_{03}$. The high temperature and pressure gas finally expands through the turbine to ambient pressure $p_{05} = p_a$.

The value of OPR is of extreme importance, since it influences the thermal efficiency of the cycle. Apart from Rolls Royce, most of the aerospace companies are able to produce only two-spool engines, with OPR upper limited to 40, as the new CFM International LEAP (Leading Edge Aviation Propulsion) [7]. For this reason $\pi_c = 40$ is taken as a reference value for current technology and this value is used throughout the results. As a comparison, the results obtained by using $\pi_c = 60$ will be also plotted for showing the consequences of investing into this technology. At the present date, the only engine capable of such performance is the new *General Electric GE9X*. The following assumptions have been made:

1. no air bleeding from the compressor;
2. complete expansion ($p_5 = p_a$);
3. calorically perfect gas;
4. part of the turbine power is used to drive the compressor, part to drive the propeller.

Typically a compressor and turbine have many stages with approximately equal pressure ratios for each stage. However, a work by A. M. Frisch [8] showed that as the size of the compressor is reduced, the compression efficiency through each stage decreases due to increased losses. There are four major loss mechanisms for compressors: blade surface boundary layer dissipation, wake mixing dissipation, endwall boundary layer dissipation, and tip clearance flow dissipation. The efficiency loss related to these mechanisms is described in [9],[10],[11],[12]. As the size of a compressor decreases, the boundary layer and mixing losses increase due to decreased Reynolds number. The relative tip clearance increases significantly as the compressor blade is shortened, because the absolute tip gap cannot decrease proportionally due to manufacturing limitations, leading to substantially increased tip clearance loss. These losses strongly penalize the use of gas-turbine engines at very low power levels.

Accounting for all these forms of losses, it is possible to compute the adiabatic efficiency for the compressor. The adiabatic efficiency for the compressor and turbine are defined as:

$$\eta_c = \frac{\pi_c^{\left(\frac{\gamma-1}{\gamma}\right)} - 1}{\tau_c - 1} \tag{92}$$

$$\eta_t = \frac{\tau_t - 1}{\pi_t^{\left(\frac{\gamma-1}{\gamma}\right)} - 1} \tag{93}$$

where $\tau_c = T_{03}/T_{02}$, $\tau_t = T_{04}/T_{05}$, and $\pi_t = p_{04}/p_{05}$. The following steps are used in the cycle calculations.

1. INLET AND DIFFUSER SECTION: A-02

$$T_{02} = T_a\left(1 + \frac{\gamma - 1}{2}M^2\right) \tag{94}$$

$$p_{02} = \pi_d\, p_a\left[1 + \eta_d\left(\frac{T_{02}}{T_a} - 1\right)\right]^{\frac{\gamma}{\gamma-1}} \tag{95}$$

where γ is the air specific heat ratio, M is the flight Mach number, and η_d is the adiabatic efficiency of the inlet and diffuser.

2. COMPRESSOR: 02-03 The stagnation temperature ratio can then be calculated starting from the OPR $\pi_c = p_{03}/p_{02}$:

$$\tau_c = \frac{T_{03}}{T_{02}} = 1 + \frac{1}{\eta_c}\left(\pi_c^{(\frac{\gamma-1}{\gamma})e_c} - 1\right) \tag{96}$$

where η_c is the adiabatic efficiency of the compressor. The power needed to drive the compressor is then

$$\mathcal{P}_c = \eta_c \dot{m}_a c_p T_{02}(\tau_c - 1) \tag{97}$$

where η_c is the compressor isentropic efficiency, and $\dot{m}_a$ is the air inlet mass flow rate.

3. MAIN BURNER: 03-04 The air-to-fuel ratio $\alpha = \dfrac{m_a}{m_f}$ can be calculated by an energy balance at the combustor:

$$\eta_b Q_b \dot{m}_f T_m + \dot{m}_a c_p T_{03} = (\dot{m}_a + \dot{m}_f) c_p T_{04} \tag{98}$$

$$\alpha = \frac{\eta_b Q_b T_m - c_p T_{04}}{c_p(T_{04} - T_{03})} \tag{99}$$

where Q_b is the fuel low heating value, η_b is the combustion efficiency, and T_m is the average temperature between T_{03} and T_{04}. p_{04} can be determined as $p_{04} = \pi_b p_{03}$.

4. TOTAL TURBINE POWER: 04-A Finally, the hot gases are expanded through the turbine to produce enough power to drive the compressor and other utilities.

$$\mathcal{P}_t = \eta_t(\dot{m}_a + \dot{m}_f) c_p T_{04}\left[1 - \left(\frac{p_a}{p_{04}}\right)^{\frac{\gamma-1}{\gamma}}\right] \tag{100}$$

where η_t is the turbine isentropic efficiency. The net shaft power output of the turbine is $\mathcal{P}_s = \mathcal{P}_t - \mathcal{P}_c$. The overall thermal efficiency of the engine is then $\eta_{th} = \dfrac{\mathcal{P}_s}{\dot{m}_f Q_b}$.

Previous works by the same authors of this work showed the benefits of burning extra fuel in the first stages of the turbine [13],[14],[15]. The so-called *turbine-burner* technology allows significant increases in specific thrust (ST) with only small increases in thrust specific fuel consumption (TSFC). Future studies might consider use of the turbine burner for the production of auxiliary power.
The fuel to air ratio is computed from an energy balance at the combustor; inlet air lass flow air is fixed once flight Mach number and external conditions are known.

REFERENCES

[1] J. B. Heywood. *Internal Combustion Engine Fundamentals*. 1st ed. II. McGraw-Hill Science/Engineering/Math, 1988. Chap. 5.

[2] T. Bose. *Airbreathing Propulsion: An Introduction*. Ed. by Springer-Verlag. 1st ed. Springer Aerospace Technology. New York, 2012.

[3] K. M. Chun and J. B. Heywood. "Estimating Heat-Release and Mass-of-Mixture Burned from Spark-Ignition Engine Pressure Data." In: *Combustion Science and Technology* 54 (1987), pp. 133–143.

[4] W. J. D. Annand. "Heat Transfer in the Cylinders of Reciprocating Internal Combustion Engines." In: *Proceedings of the Institution of Mechanical Engineers* 177.36 (1963), pp. 973–996.

[5] T. Sookdeo. "Performance Measurement, Simulation, and Analysis of the Cox Tee Dee 0.010, the World's Smallest Production IC Engine." Master of Science Thesis. University of Maryland, College Park, 2006.

[6] J. R. Dormand and P. J. Prince. "A Family of Embedded Runge-Kutta Formulae." In: *Journal of Computational and Applied Mathematics* 6 (1980), pp. 19–26.

[7] CFM International. *The Leap Engine. Performance. Execution. Technology.* Retrieved October 12, 2016. 2016. URL: https://www.cfmaeroengines.com/engines/leap/.

[8] A. M. Frisch. "Scaling Effects on the Performance and Efficiency of Gas Turbine Engines." Master of Science Project. University of California, Irvine, 2014.

[9] F. M. White. *Viscous Fluid Flow*. New York: The McGraw-Hill Companies, Inc., 2006.

[10] D. K Hall. *Performance Limits of Axial Turbomachine Stages*. Technical Manual. Department of Aeronautics and Astronautics, MIT. Boston, 2011.

[11] O. Sharma and T. Butler. "Predictions of Endwall Losses and Secondary Flows in Axial Flow Turbine Cascades." In: *Journal of Turbomachinery* 109.2 (1987), pp. 229–236.

[12] J. Denton. "The 1993 IGTI Scholar Lecture: Loss Mechanisms in Turbomachines." In: *Journal of Turbomachinery* 115.4 (1993), pp. 621–656.

[13] W. A. Sirignano and F. Liu. "Performance Increases for Gas-Turbine Engines Through Combustion Inside the Turbine." In: *Journal of Propulsion and Power* 15.1 (1999), pp. 111–118.

[14] F. Liu and W. A. Sirignano. "Turbojet and Turbofan Engine Performance Increases Through Turbine Burners." In: *Journal of Propulsion and Power* 17.3 (2001), pp. 695–705.

[15] W. A. Sirignano, D. Dunn-Rankin, F. Liu, B. Colcord, and S. Puranam. "Turbine Burners: Performance Improvement and Challenge of Flameholding." In: *AIAA Journal* 50.8 (2012), pp. 1645–1669.

Part II

RESULTS

4 ENGINES COMPARISON

The following sections will show several aircraft configurations, with engines and propellers arranged in different ways. The basic hypothesis behind this discussion is that the propeller efficiency is unitary. In other words, it is assumed that the propeller acts as a screw in the air *without slipping*, i.e. by transforming the whole input power into useful thrust.

4.1 APPLICATION OF THE MODELS

The five numerical codes are used to compute several properties of the engines, including thermal efficiency. As explained in the introduction chapter 1, the power range around 100 kW is the one affected by low turbine efficiency. This is the result that must be reached by each numerical model. More precisely, it was decided to investigate the following scenarios:

- Power equal to 75, 100, 125 and 150 kW;
- Altitude equal to 10 000, 15 000 and 20 000 feet.

By considering every combination of the five engines selected with the parameters above, 60 simulations have been performed in total (Fig. 20-22). In order to obtain an engine with the desired power, minimum weight and maximum efficiency, an optimization process is needed. This process is explained here.

4.1.1 Optimization Process

The whole engine design allows the following parameters to be modified in the numerical code:

- equivalence ratio;
- engine rpm;
- engine size (bore, stroke and n° of cylinders).

all the other variables being constant. A restriction to the efficiency-maximization process is that the equivalence ratio and the engine rpm must remain within reasonable limits for these applications, i.e.

$\Phi = 0.8 - 1.5$ and $rpm = 1200 - 5000$. The optimization scheme is reported in Fig. 19.
Here is an example of the optimization process. Let us consider the 4-stroke spark ignition engine; assume a flight altitude (z=10 000). Cruise flight Mach is 0.4. For the IC engines in Fig. 20 and 21, the cylinder geometry (bore=8 cm, stroke=9 cm) is kept constant with altitude and power. For a certain rpm and equivalence ratio, a power is obtained from the code: this is the power obtained from one cylinder. This power must be multiplied for an hypothetical number of cylinders, in order to obtain the target power of the whole engine, say 125 kW. Actually, few attempts are needed to obtain exactly 125 kW. Some finer adjustments of rpm and equivalence ratio can be done here, as well as changing the number of cylinders. The number of cylinders increases from 4 to 6 for powers higher than 100 kW to obtain better efficiencies.

Once the power target is matched (within fractions of kW), the thermal efficiency of the engine can be computed by

$$\eta_{th} = \frac{\mathcal{P}}{\dot{m}_f LHV} \tag{101}$$

where P is the total power delivered from the engine (125 kW) and $\dot{m}_f$ is the sum of the fuel consumption of every cylinder. The weight of this configuration is evaluated by means of the correlation in Sec. 2, optimized with the coefficients of Table 2.1.

At this point, bore, stroke, and flight altitude are maintained constant, while rpm and equivalence ratio are modified. With these variations, a (slightly) different efficiency is obtained, although the power is still matching the target. The turbocharging option for altitude compensation allows to limit the efficiency depletion.

4.1.2 Numerical Simulations Results

Fig. 20-22 show the result of this optimization process, presenting the engines with the highest efficiency only. The results show that Diesel engines are more efficient than their gasoline counterpart, and the 4-stroke technology is more efficient than the 2-stroke; the gas turbine is the direct competitor of the 4-stroke Diesel engine from thermal efficiency viewpoint (Fig. 20).

For this reason the further discussion will be based on these two options only, the others being discarded (Fig. 21-22).

Two important questions are aimed to be answered in this study.

1. Which one between Diesel engine and gas turbine is the best choice to accomplish a long mission?

2. Which engine-propeller layout (number, connections, size) gives the best performance?

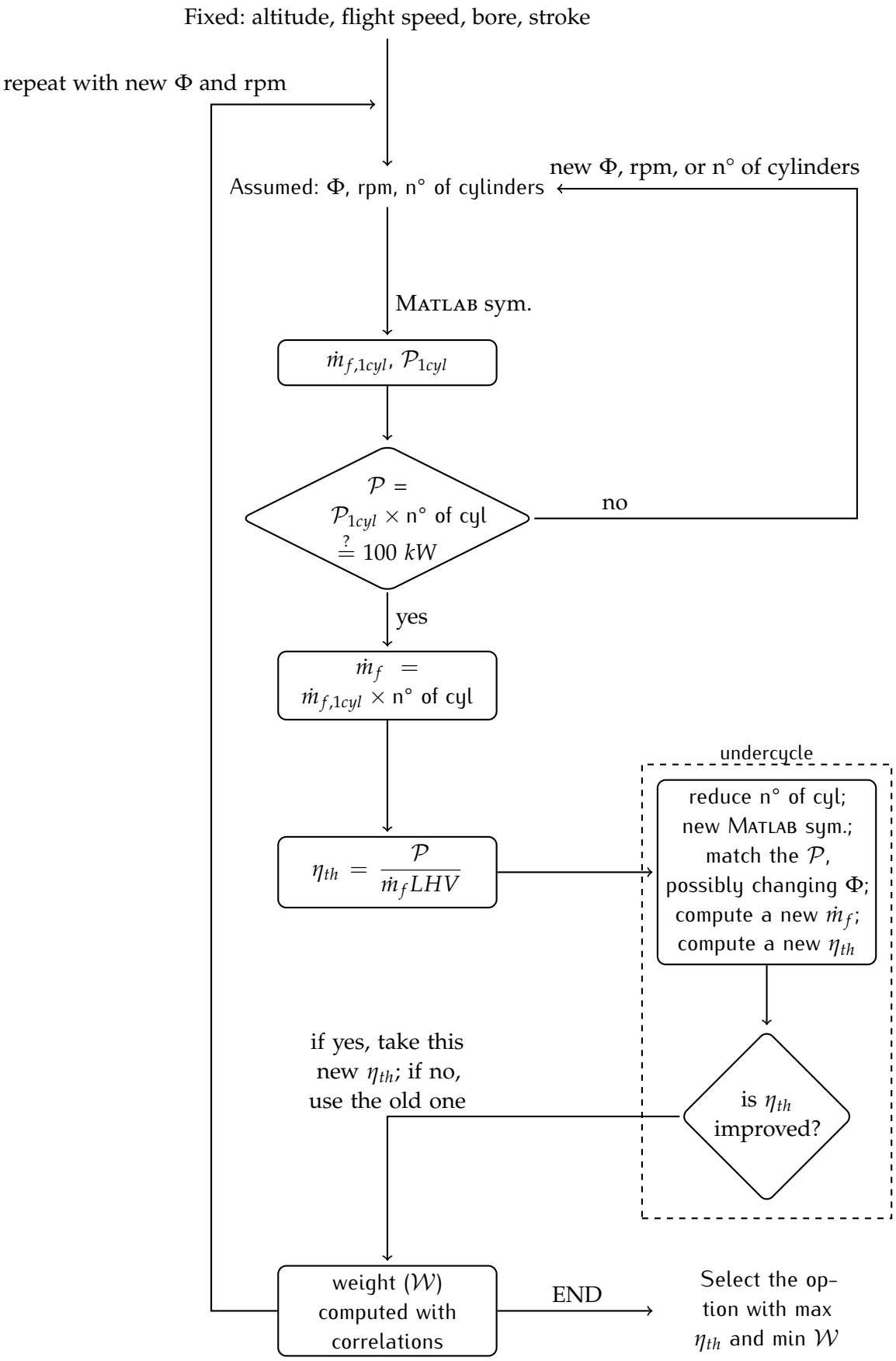

Figure 19: Optimization process.

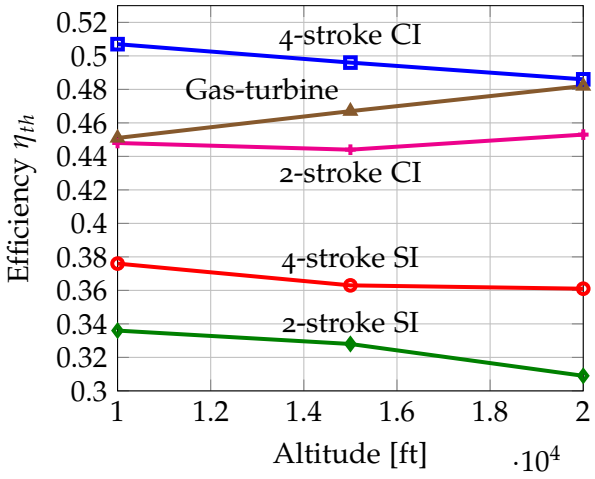

Figure 20: Thermal efficiency of the five engines modeled by the MATLAB codes; power: 150 kW.

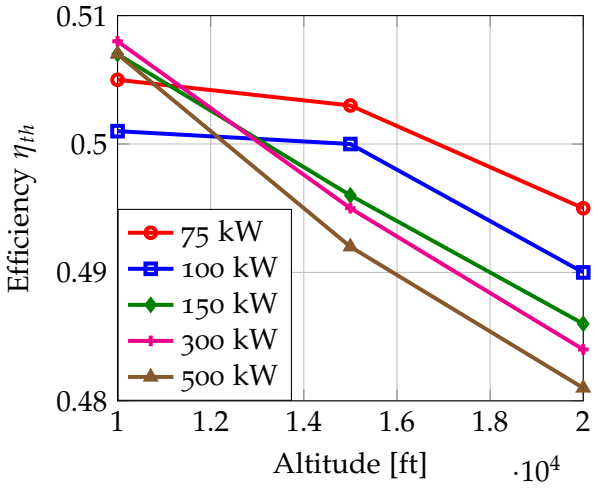

Figure 21: Four-stroke Diesel engine efficiency as function of flight altitude.

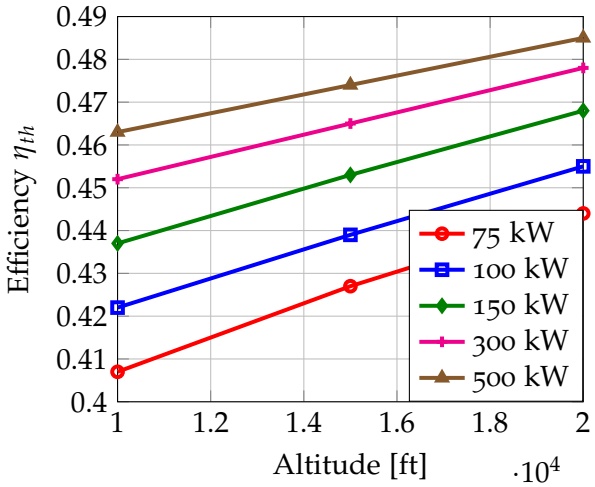

Figure 22: Gas-turbine engine efficiency as function of flight altitude; OPR=40.

The second question requires consideration of two different overlapping effects: the weight and efficiency gain obtained by the choice of an engine-propeller layout instead of another, and the thrust benefit coming from a better choice of propeller size and number. For this reason, these two effects are studied separately. In this chapter the engines only are compared, regardless of propellers size and efficiency; in Chapter 5 the propeller theory defines the gain in thrust obtained by a certain propeller design; finally, Chapter 6 briefly describes the criteria to put together the two effects.

4.2 LAYOUT SELECTION

Engines can be arranged on the aircraft in many ways, to obtain the same power. Simplified sketches are shown in Fig. 23.

A. single engine - single propeller;

B. single engine - belt transmission - three propellers;

C. three engines - three propellers;

D. single engine - electric generator - two electric motors - three propellers.

The following hypothesis are also assumed:

- the turbine engine requires a gearbox to reduce the rpm from $\simeq 10^4$ to $\simeq 2000 - 3000$, the typical range in which propellers operate efficiently;
- the mechanical connection between the IC engine or electric motor, and the propeller, is 100% efficient and does not require a gearbox;
- the aircraft power is distributed evenly between the engines.

Data about the devices involved are reported in Table 6. The weight of each component depends on its size and configuration, hence on the power it works with. The alternator and the electric motor hare chosen because they are designed to deliver a power of 100 kW. The gearbox is of the kind generally used in aeronautical applications, i.e. a planetary gearbox. Finally, the belt transmission chosen is a general device for mid-low rotational speed applications.

In order to obtain a certain power output, and accounting for the efficiencies listed in the table, the engines will have to deliver a power a bit higher. To obtain that power, a certain engine geometry and size is needed, like bore, stroke, number of cylinders, turbocharger size, etc. This translates in an estimate of the engine weight, which is known by means of correlations in Sec. 2.1.

Table 6: Weight and efficiency of the mechanical devices involved in the configurations.

Component	Weight [kg]	Symbols		Efficiency %
Alternator Converter	10	Alt	η_{conv}	80 [1]
Belt Transmission	20	$=$	η_{mech}	95 [2]
Electric Motor	45	EM	η_{el}	97 [3]
Gearbox	15	GB	η_{gear}	90 [4]

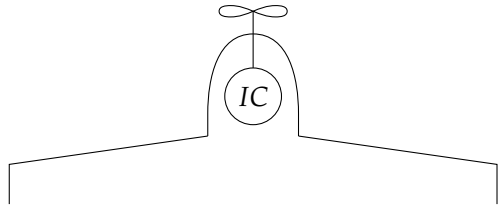

(a) *Configuration A, IC-based.*

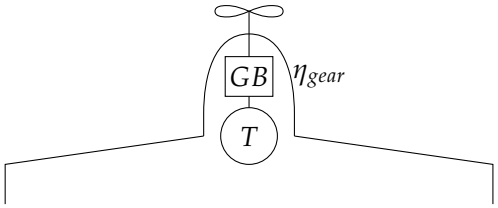

(b) *Configuration A, turbine-based.*

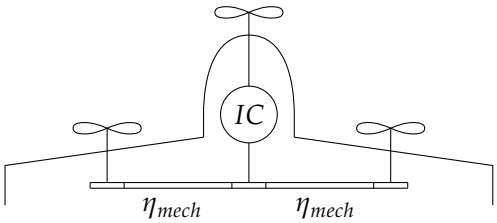

(c) *Configuration B, IC-based.*

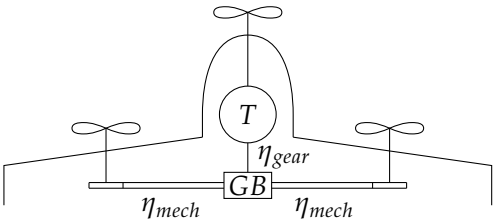

(d) *Configuration B, turbine-based.*

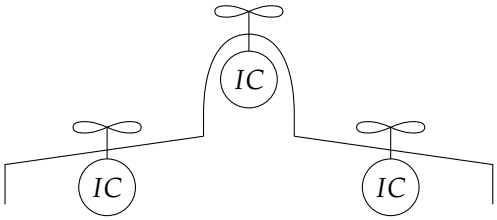

(e) *Configuration C, IC-based.*

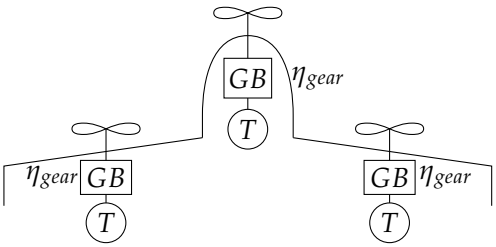

(f) *Configuration C, turbine-based.*

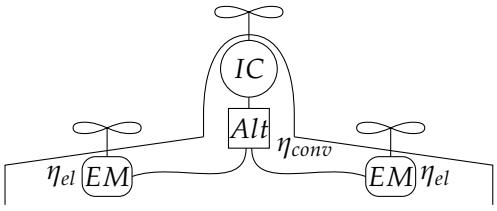

(g) *Configuration D, IC-based.*

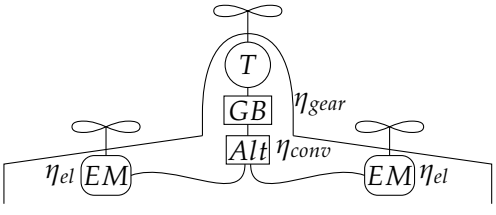

(h) *Configuration D, turbine-based.*

Figure 23: Configurations considered for the analysis.

Concerning the Diesel-based configurations, the lightest is always the one with one single large engine driving its own propeller (configuration A). This arrangement is the lightest because it does not require any additional weight from belt transmissions or alternators, as in the other configurations. Moreover, the number of components constituting the *working chain* is minimum, so the product of inefficiencies is not deteriorated as it would be with a large number of elements.[1] On so doing, the engine must deliver less power to obtain the desired power output, implying less fuel consumption.

Compared to A:

- configuration B requires the use of the transmission, which adds weight and inefficiency to the whole system. Hence, there is the need of a slightly more powerful engine and additional weight;
- since the weight of an IC engine do not scale linearly with power, the use of 3 smaller engines in configurations C results heavier and less efficient;
- the transformation from mechanical energy to electrical energy is the main source of inefficiency, which translates in a larger engine needed to provide the same output power. Hybrid configuration D is the heaviest among the four, mainly because of the higher fuel consumption and also, of lesser importance, because of the higher weight of the components.

The same considerations apply for the turbine-based configurations. In other words, the lightest configuration is still the one with one single large turbine driving a propeller; however, the large difference in the rotational speed of the two shafts requires the use of a geared connection between the two parts. The lightness of the turbine is then compensated by the additional weight of the gearbox. The fuel consumption of the three-turbines, three-propellers configuration C is higher than the one with one engine only, due to the scale effects. The smaller is the turbine, the less efficient it is. Moreover, the sum of three small turbines exceeds the weight of a single bigger turbine, for two reasons: the presence of three gearboxes instead of one, and the non-linear relation between power and weight.

4.2.1 Altitude Compensation and Flammability Limits

If the flight altitude changes, the environmental conditions change as well. The main consequence on the engine is the so called *density effect*: as the altitude increases, the air density decreases, and the intake

1 In a mechanical system, the efficiency of the whole system depends on the efficiency of the single element constituting the chain and on the way they are assembled. If the elements are arranged in series, the overall efficiency of the system is given by the product of each single element efficiency: $\eta = \eta_1 \cdot \eta_2 \cdots \eta_n$.

manifold, for a fixed cross section area and airspeed velocity, ingests less air. As a result, the machine operates with lower working charge, either it is a internal combustion engine or a turbine engine. On the other hand, the combustion process requires the equivalence ratio Φ to be within the *flammability limits*, in order to obtain a proper combustion. Hence, for a fixed Φ the fuel amount that is possible to inject is lower than it would be at lower altitude. Since $\mathcal{P} \propto \dot{m}_f W$, lower power is obtained.

The ignition range of a mixture depends on pressure, chamber architecture and the couple oxidizer-fuel adopted. As a general trend, by decreasing the pressure, the range becomes narrower and the mixing requirement more stringent. Spark-ignition (SI) engines usually operate stoichiometric or slightly rich, while compression-ignition (CI) engines operate slightly or very lean. In SI engines the fresh charge is composed by a premixed mixture of air and fuel. The spark ignites the charge when proper conditions of pressure, temperature, mixing and Φ are present in the combustion chamber. The upper limit for the pressure is the one dictated by the engine *knocking*. Knock occurs when combustion of the air/fuel mixture in the cylinder does not start off correctly in response to ignition by the spark plug, but one or more pockets of air/fuel mixture explode outside the envelope of the normal combustion front. CI engines, instead, are not tied to knocking, since the charge is composed by air only and can not ignite unless fuel in injected. Moreover, every hydrocarbon fuel has its own Carbon and Hydrogen content, which corresponds to a different amount of Oxygen required for burning. If an amount of air is stoichiometric for a certain fuel, it may be lean or rich for a different fuel. Finally, the value of Φ with which the engine operates is also dictated by environmental regulations in order to control the exhaust pollutants.

Since Φ is bounded by the reasons mentioned above, often the turbocharging option is adopted. By the introduction of an higher amount of air with respect to the one *naturally aspirated* by the engine, it is possible to inject more fuel still maintaining the correct equivalence ratio. By acting on the turbocharger's rpm, it is then possible to tune the engine power to the desired value.

This is the reason why the engines' size and geometry[2] are kept constant with altitude, and so are their powers, by means of acting on the turbocharger and the engine rpm. As a drawback, the engine's fuel consumption and thermal efficiency change with altitude. These values as a function of flight altitude are shown in Table 7.

2 Hence, the weight.

Table 7: Thermal efficiency and fuel consumption of each engine involved in the analysis for different altitudes.

	10000 ft		15000 ft		20000 ft	
	η_{th}	[lt/h]	η_{th}	[lt/h]	η_{th}	[lt/h]
A-IC	49.38	71.25	49.05	71.44	48.97	71.57
A-Turbo	46.06	84.51	47.36	82.21	48.55	80.12
B-IC	49.23	73.59	48.95	73.97	48.80	73.47
B-Turbo	46.06	84.51	47.36	82.21	48.55	80.12
C-IC	50.10	69.31	50.10	70.00	49.00	71.51
C-Turbo	42.49	91.59	44.23	88.07	45.83	84.94
D-IC	48.80	85.70	49.43	84.63	47.92	87.32
D-Turbo	46.38	97.41	47.65	94.76	48.82	92.41

4.3 CONSTANT THRUST PROFILE

Figure 24 shows the total fuel weight that must be carried onboard to accomplish a *constant-cruise mission* (constant flight speed) *up to* 50 *hours* at different altitudes; the flight speed is *highly subsonic.* The four configurations of Sec. 4.2 are compared. The engine fuel consumption is represented by the slope of the lines.

Not surprisingly, the reciprocating engine suffers the higher weight of the components, and for short missions this is the major source of weight. In this scenario, the turbine configuration is preferred. However, there is a crossing point in which the reciprocating engine's higher efficiency takes over the turbine. From that point on, the turbine configuration requires more fuel to be carried onboard, and the internal combustion engine becomes the lightest option.

4.4 VARIABLE THRUST PROFILE

In the reality, a constant cruise mission (i.e., constant thrust, speed and altitude) is far from being existent. Instead, there are always variations of these parameters as a consequence of throttling up or down the engine, taking-off or landing. During the rolling and climbing phases the aircraft accelerates, so the velocity increases continuously; in addition, the takeoff speed is based on the weight of the airplane, which is still unknown (actually, it is the goal of this analysis). Since the engine's thermodynamic cycle depends on the aircraft velocity, the problem highly increases its complexity.

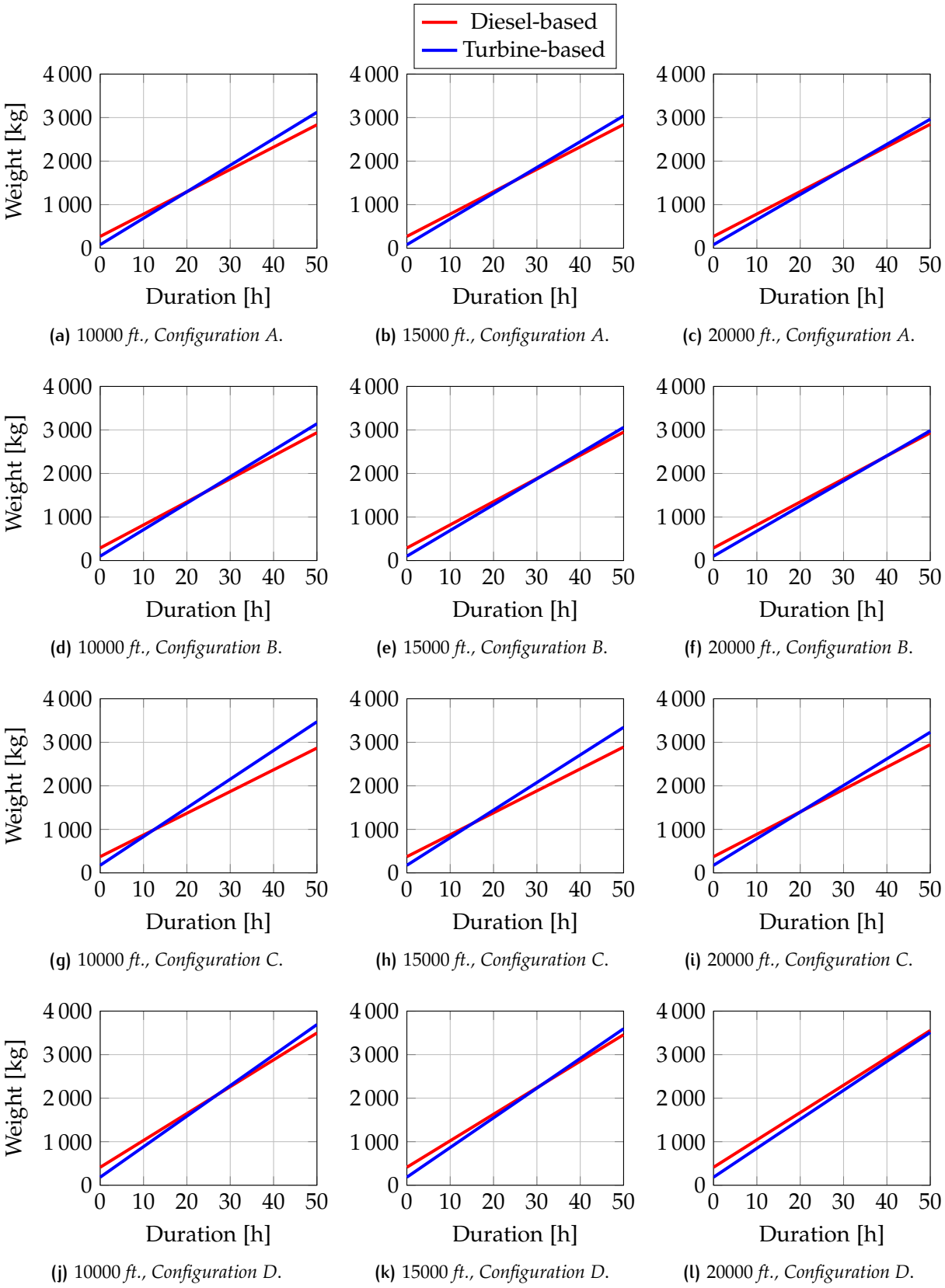

(a) 10000 *ft.*, *Configuration A.* **(b)** 15000 *ft.*, *Configuration A.* **(c)** 20000 *ft.*, *Configuration A.*

(d) 10000 *ft.*, *Configuration B.* **(e)** 15000 *ft.*, *Configuration B.* **(f)** 20000 *ft.*, *Configuration B.*

(g) 10000 *ft.*, *Configuration C.* **(h)** 15000 *ft.*, *Configuration C.* **(i)** 20000 *ft.*, *Configuration C.*

(j) 10000 *ft.*, *Configuration D.* **(k)** 15000 *ft.*, *Configuration D.* **(l)** 20000 *ft.*, *Configuration D.*

Figure 24: Comparison between each configuration for different missions and altitudes.

Changes in aircraft velocity and/or thrust can be assessed together by looking at the engine's power. If variations of power are introduced in the mission, for whichever reason, two levels of simplification are possible:

1. the more rigorous way to proceed would be to iterate on the fuel weight, assuming a guess value m_0 (for instance the weight given by a chosen constant-thrust mission from Section 4.3). Along the mission, the weight reduces continuously by the burning of the fuel: the weight at a generic moment $\bar{t}$ is:

$$m(\bar{t}) = m_0 - \int_0^{\bar{t}} \dot{m}_f(t)dt \tag{102}$$

where $\dot{m}_f(t)$ is the instantaneous fuel consumption, unknown.[3] Moreover, during the climbing phase the altitude changes continuously, hence the engine keeps working with changing inlet conditions. Hence it is

$$\dot{m}_f = \dot{m}_f(z, m(\bar{t}), \mathcal{P}) \tag{103}$$

which makes the problem strongly coupled. Eq. 102 and 103, together with models for the aircraft trajectory, definitions of thrust, drag and lift, plus appropriate boundary conditions, constitute a differential problem that can be solved by means of numerical methods, such as finite differences.

The iteration takes place if the mass of the fuel reaches zero before the end of the mission, whose length has been fixed when m_0 was chosen; in this case, a different value of m_0 is needed to restart the computations.

2. a much simpler approach is to neglect the dependence of the fuel consumption by the altitude and the instantaneous weight of the aircraft, i.e.

$$\dot{m}_f = \dot{m}_f(\mathcal{P}). \tag{104}$$

Although very strong, this hypothesis suggests that the fuel consumption depends on the engine throttling only. In other words, this simplification consists in the study of a flying aircraft whose engine keeps working on the ground, with constant inlet conditions. This approach clearly overestimates the fuel consumption: in fact, the thermodynamic cycle becomes more efficient as the external temperature decreases, hence when flying at higher altitudes. The results of this analysis are influenced by this hypothesis, but, although overestimated, they still provide a sufficient accuracy.

The value $\dot{m}_f$ can be obtained by the MATLAB numerical code developed for this study and described in Chap. 3, once the

3 Note that $m_0 = m_{struct} + m_{payload} + m_{engine} + m_{fuel}$.

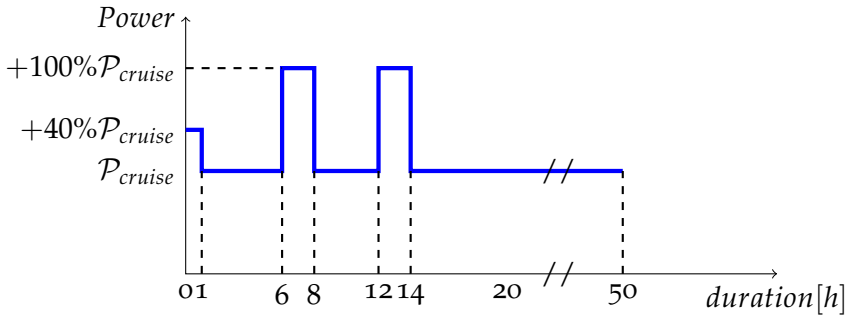

Figure 25: Power demand profile during a 50 hours mission.

altitude is fixed. This simplified approach is adopted in this study.

The results of Section 4.3 are different if variable thrust is required in the mission. This variation is simulated by means of 3 short phases of high power demand (Figure 25). The first one relates to take-off, while the other two simulate a scenario in which extra thrust and/or extra auxiliary power is required. The interested reader can find the reason for this profile in App. B.

Only the 10000 ft. cruise altitude is chosen for this comparison, since similar considerations are valid for the other altitudes.

4.5 COMPARISON OF PROPOSED MISSION PROFILES

Figure 26 shows the comparison between the constant-cruise and the varying-power mission. By the request of different amounts of power, the crossing point changes position for every arrangement. Compared to the constant-cruise profile, the crossing point shifts backwards in configurations A, B and C, while in the hybrid configuration D it shifts afterwards. Both the advance and the delay, however, are between 0.5 and 2.5 hours.

The reason for this behavior is here explained. The slope of the lines represents the fuel consumption of each engine or each system of engines. It is known from previous discussions and from Section 4.3 that the 4-stroke Diesel engine requires less fuel per unit time than the turbine engine, for the same power; in other words, the former is more fuel-efficient. This behavior is maintained as long as the power is kept around 300-350 kW. However, the extra power required by the mission force the engines to work up to +100% the normal functioning, hence up to 700 kW. It is then necessary to mount a bigger turbine which can withstand this power requirement. In this range, the turbine engine is large enough to limit the typical scaling effects due to the small scales. Phenomena like profile losses, endwall losses and tip clearance losses become less severe and the turbine engine is more efficient compared to the small scales.

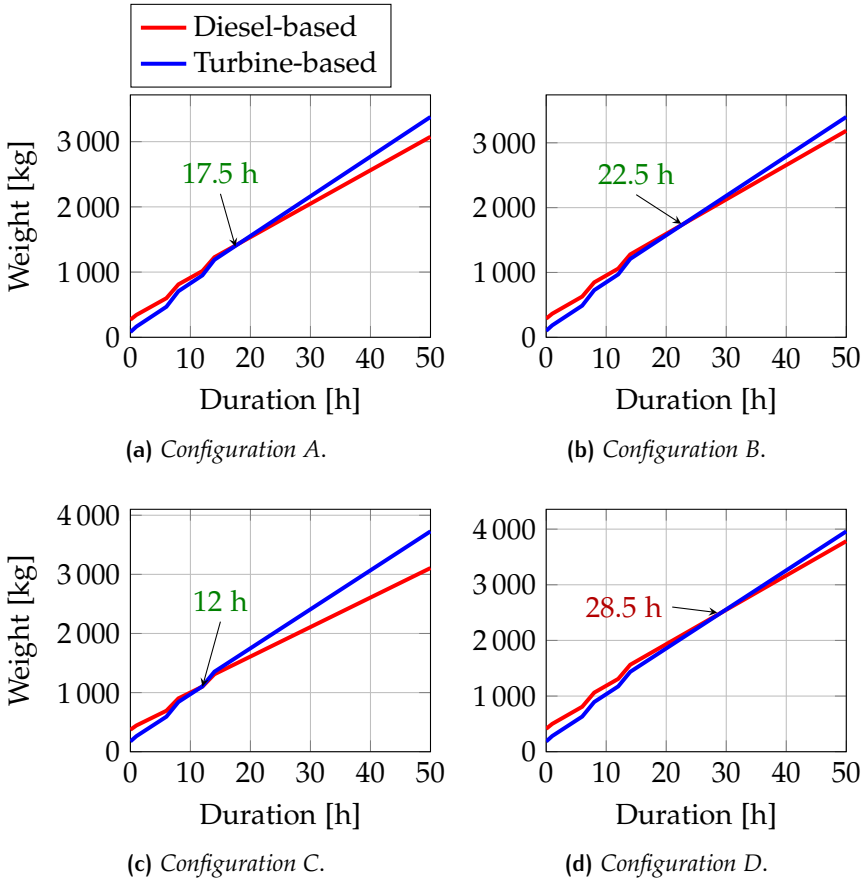

(a) *Configuration A.* **(b)** *Configuration B.*

(c) *Configuration C.* **(d)** *Configuration D.*

Figure 26: Comparison between Diesel-based and turbine-based configurations. Altitude=10000 ft.

This behavior underlines the importance of choosing carefully which power source has to be adopted in this range of applications. If the mission duration is shorter than the crossing point, the turbine engine is more convenient thanks to its compactness and lightness. If the mission is longer, the use of a Diesel engine is preferable thanks to its higher efficiency.

From the previous analysis it is clear that the most appealing layout is configuration A, with a single engine driving a large propeller, either by means of a gearbox or by a direct mechanical connection. The wise reader should have already noted that a gearbox and a propeller variable-pitch system are always needed, to obtain good propeller efficiency in a wide range of rpm. However, so far the study focused on the engine efficiency only and aimed to point out the relations between engine's power, weight and the way the various arrangements influence the overall weight. The following chapter will focus on the propeller analysis, and will help to understand which configuration is more likely to be used if the propeller efficiency is taken into account.

REFERENCES

[1] R. Bosch GmbH. *Automotive Handbook*. 8th ed. pag. 993. printed in Germany: Horst Bauer, 2011.

[2] Inc. Carlisle Power Transmission Products. *Energy Loss and Efficiency of Power Transmission Belts*. Ed. by Belt Technical Center. Springfield, Missouri, 2009.

[3] EVDrive motors. *High Performance EVD Motor/Controller IP67 Drive Sub-Systems*. Ed. by EVDrive Research. Portland, Oregon, 2016.

[4] B. R. Höhn, K. Stahl, and P. Gwinner. "Light-Weight Design for Planetary Gear Transmissions." In: *Geartechnology* (2013). Ed. by Randall Publications LLC.

5 PROPELLER ANALYSIS

5.1 MOMENTUM THEORY

The efficiency of a piston engine-propeller combination depends on a proper match of the propeller to the engine as well as a match of the two to the airframe; aerodynamically, one strives to select a propeller that provides a high efficiency for cruise and a high static thrust for take-off. These two requirements are easier to satisfy with a variable pitch propeller. A fixed pitch propeller is usually a compromise between these two operating regimes. The terms constant pitch, fixed pitch and variable pitch are somewhat confusing. A constant pitch propeller is one whose pitch does not vary with radius. "Fixed" or "variable" pitch refers to whether or not the whole blade can rotate about an axis along the blade in order to vary the pitch angles of the blade sections all along the blade (this is called *feathering*). Some propellers are equipped with governors to maintain a constant rpm as the engine throttle is varied. This is done by increasing the blade pitch angles as the propeller rpm tends to increase due to increased power or, vice versa, by decreasing the pitch for reduced power. Such propeller is called a "constant speed" propeller [1].

According to the early literature a propeller can be seen as an "airscrew" which screws itself through the surrounding air. By applying the classical momentum theory to a control volume including the actuating disc and its surroundings, an important result is obtained:

$$\mathcal{P} = \mathcal{T}(\mathcal{V} + w) \tag{105}$$

where $\mathcal{T}$ is the thrust, $\mathcal{P}$ is the power, $\mathcal{V}$ is the true airspeed and w is the induced velocity. This important result states that the power required by the propeller equals the product of its thrust and the velocity *through* the propeller. This can be divided into two parts. The first part is defined as the useful power:

$$\mathcal{P}_u = \mathcal{T}\mathcal{V}. \tag{106}$$

The second part is known as the induced power:

$$\mathcal{P}_i = \mathcal{T}w. \tag{107}$$

The induced velocity is given by the relation ([1], chap. 6):

$$w = \frac{1}{2}\left[-\mathcal{V} + \sqrt{\mathcal{V}^2 + \left(\frac{2\mathcal{T}}{\rho\mathcal{A}}\right)} \right] \tag{108}$$

where ρ is the air density at the local altitude and $\mathcal{A}$ is the disc area. In forward flight, an ideal efficiency can be defined as the ratio of the useful power to the total power:

$$\eta_{id} = \frac{\mathcal{T}\mathcal{V}}{\mathcal{T}(\mathcal{V} + w)} = \frac{1}{1 + (w/\mathcal{V})}. \tag{109}$$

It is interesting to note that, as V increases, the ideal efficiency is seen to approach unity. By applying typical numbers to Eq. 109 it is easy to obtain efficiencies around 95%. However, η_{id} given by the momentum theory is optimistic and represents an upper limit that is really not attainable: with the same numbers, the actual propeller efficiency is closer to 85%.

At low speeds (e.g., during the take-off roll), the efficiency is difficult to estimate. At zero forward speed, the efficiency of a propeller is zero by definition, even though its thrust is not zero. In fact, for the same shaft power, a variable pitch propeller will produce the most thrust at zero advance velocity (i.e., its static thrust is greater than the thrust produced in forward flight).

5.2 MOMENTUM – BLADE ELEMENT APPROXIMATED THEORY

More reliable evaluations of propeller efficiency are attainable if the blade theory is considered, which is described in detail in [1] and is briefly outlined here.

The thrust and the power of a propeller are normally expressed in coefficient form. These non-dimensional coefficients are defined in various ways, depending on what particular reference areas and velocities are used. Test results on propellers almost always define the thrust coefficient, C_T, and power coefficient, C_P, as follows:

$$C_T = \frac{\mathcal{T}}{\rho n^2 D^4} \tag{110a}$$

$$C_P = \frac{\mathcal{P}}{\rho n^3 D^5} \tag{110b}$$

where n is the rotational speed in revolutions per second and D is the propeller diameter. All the others quantities must be expressed in consistent units. One of the most famous coefficient used in propeller analysis is the advance ratio J, defined by

$$J = \frac{V}{nD}. \tag{111}$$

Thus, C_T and C_P are functions of J. The classical definition of propeller efficiency (analogous to Eq. 109)

$$\eta_{prop} = \frac{\mathcal{T}\mathcal{V}}{\mathcal{P}} \tag{112}$$

can be also expressed in terms of C_T, C_P and J, becoming

$$\eta_{prop} = \frac{C_T J}{C_P}. \tag{113}$$

Equations 110 are very convenient to have a quick description of a propeller behavior. However, they don't take into account the real aerodynamics of the blades. The value of thrust, for example, depends on the distribution of the aerodynamic forces of the blade and on the blade pitch, angle of attack, rpm, geometry and length. Thrust is strictly connected to the lift formation; however, since the pressure difference across the blades must vanish at the tips, lift vanishes at the tips too, which generally means that the local angle of attack at the tip must be zero. A trailing vortex system, helical in shape, is generated by the propeller in a manner similar to a finite wing. Considerations on the induced velocity and on the wake created by the fluid-structure interaction also apply. In fact, the propeller does not behave as a perfect "airscrew", but slips partially when screwing into the air stream; tangential components induced on the downstream air translate in the formation of a wake. Turbulent structures and vorticity in the wake imply additional drag, hence more thrust is needed to compensate it.

Equations 110 can be applied to a blade element and integrated along the radius accounting for the blade geometry and the local air stream properties. This process may require a few iterations and the aid of a numerical solver. Some useful relationships are reported here by applying some fairly accurate approximation. C_T and C_P become

$$C_T = \frac{\pi^3 \sigma}{24} \bar{C}_L f(\lambda) \tag{114a}$$

$$C_P = J C_T + \frac{\pi^4 \sigma}{8} \bar{C}_D g(\lambda). \tag{114b}$$

where

$$\sigma = \frac{\mathcal{B} c}{\pi \mathcal{L}} \qquad \lambda = \frac{\mathcal{V}}{\omega \mathcal{L}} \tag{115}$$

$$f(\lambda) = \left(1 + \lambda^2\right)^{\frac{3}{2}} - \lambda^3 \tag{116}$$

$$g(\lambda) = \frac{1}{2}\left[\left(1+\lambda^2\right)^2\left(2+\lambda^2\right) - \lambda^4 \log \frac{1+\sqrt{1+\lambda^2}}{\lambda}\right]. \tag{117}$$

$\bar{C}_L$ and $\bar{C}_D$ indicate average values of lift and drag coefficient respectively, $\mathcal{B}$ is the number of blades, c is a reference chord length, $\mathcal{L}$ is

n° of blades	$\mathcal{B}$	3
lift coefficient	C_L	1
lift over drag ratio	L/D	10
chord length	c	$0.075 \cdot D$

Table 8: Blade geometry assumptions.

the blade length (measured from the tip to the rotational axis, neglecting the hub distance), and ω is the rotational speed in radiants per second.

The term JC_T in the expression for C_P represents the useful power. The remaining term in C_P is the profile power, that is the power required to overcome the profile drag of the blades. The induced power is missing; experience shows that the induced power can be approximated by

$$C_{Pi} \simeq 1.12 \frac{C_T}{2} \left[-J + \left(J^2 + \frac{8C_T}{\pi} \right)^{1/2} \right]. \tag{118}$$

C_P then becomes

$$C_P = JC_T + \frac{\pi^4 \sigma}{8} \bar{C}_D g(\lambda) + C_{Pi}. \tag{119}$$

Given the geometry, forward speed and rotational speed of the propeller, C_T, C_P and J can be computed and finally the propeller efficiency can be obtained by applying the definition in Eq. 113.

5.3 PROPELLER EFFICIENCY EVALUATION

The aim of the present section is to map the propeller efficiency as function of propeller size and flight speed. The previous equations were implemented into a numerical MATLAB code. To do so, some values have been assumed and are reported in Table 8.

The blade theory shows that propeller efficiency increases when diameter and rpm are reduced (Fig. 27). Theoretically, the highest efficiency is obtained by the use of a single-blade propeller; however, single bladed propellers are not used because of dynamic imbalance. More blades are preferred, generally in the number between 3 and 6, and a decrease in the efficiency is obtained. Moreover, the maximum diameter of the propeller is tied by the tip speed, centrifugal forces, aeroelastic problems, ground clearance, vibrations and noise level. Generally, all the above mentioned problems can be mitigated by choosing shorter blades and by studying the dynamic interaction between the propeller, the engine and the structure. Finally, the rotating speed influence the aerodynamics of the blades and must lie in a certain range. A high rotational speed will induce off-design angles

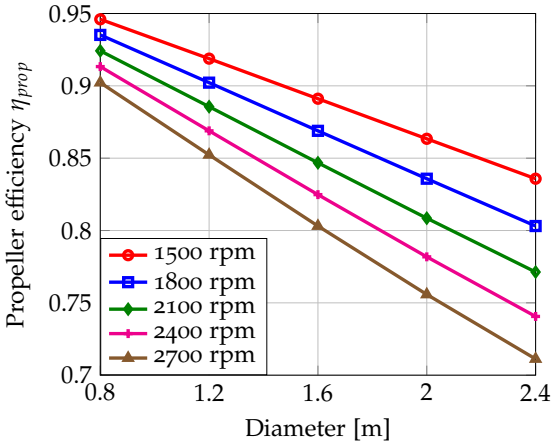

Figure 27: Propeller efficiency for different blade length and rpm. Mach: 0.3.

of attack on the blade, which is more prone to stall. Moreover, the tip speed should remain in subsonic (or at most transonic) range, to avoid or limit the formation of shock waves at the blade tips, generating a drop in the efficiency and noise. The lower limit for the rotational speed is given by the insufficient thrust production.

Propellers are known to work efficiently enough as long as the cruise Mach number is low, say below 0.5. As the flight speed increases, the efficiency decreases. From this value on, tip losses are the main source of inefficiency, which can be mitigated by shrouding the propeller into a ducted fan; hence, a basic fan engine is obtained.

Actually, the Mach number, the diameter and the rpm are not independent, but are linked by the tip speed limit. Anytime the aircraft is in motion the path of the blade tip through the air is a helix, and therefore, its velocity is the vector sum of the rotational velocity plus the translational velocity, also named *helical tip velocity*. Maximum helical tip velocity is an important parameter for propeller selection. In the absence of specific data from the manufacturer, it is safe to assume that the propeller efficiency begins to decrease dramatically when the helical tip Mach exceeds 0.85. That occurs because the local air velocity over the surface of the blade (near the point of maximum airfoil thickness) will reach Mach 1, and create a shock wave, separating the flow and dissipating energy.

The thrust produced by each engine can be obtained by solving Eq. 112 for $\mathcal{T}$:

$$\mathcal{T} = \frac{\mathcal{P}}{\mathcal{V}}\eta = \frac{\mathcal{P}}{\mathcal{V}}\frac{C_T}{C_P}J = \frac{\mathcal{P}}{\cancel{\mathcal{V}}}\frac{C_T}{C_P}\frac{\cancel{\mathcal{V}}}{nD} \implies \mathcal{T} = \frac{\mathcal{P}}{nD}\frac{C_T}{C_P}. \tag{120}$$

A clear interpretation of the above equation is that thrust is proportional to the input shaft power. For example, let assume that power is supplied by a single 300 kW engine to a large 2.4 m diameter propeller, rotating at 2077 rpm and M=0.3. It follows that $\mathcal{T} = 2356$ N.

But if we imagine to subdivide that power into three smaller engines of 100 kW each, driving three propellers large one-third and rotating at three times the previous example (0.8 m, 6232 rpm), with the same and $M_{TIP} = 0.85$, we obtain the exact same thrust. The reason is that, by linking the two propellers to have the same tip speed, they end up having the same efficiency.

However, it is obvious that propellers can not rotate as fast as that; very rarely rotational speeds exceed 3000 rpm, more likely lying in between 1500 and 2400 rpm. Reciprocating engines run between 1500 and 3500 rpm during cruise flight, with peaks up to 5000 rpm during take-off and climbing. The gearbox installed between the propeller and the engine shafts allows a gearing ratio generally between 1.5:1 and 2.5:1. Higher gearing ratios would require more (and larger) elements, causing additional weight, less reliability and cooling problems.[1]

The correct way to compare propellers of different size is then accounting for the rotational speed at which they are commonly operated. In the previous example, with a lower rotational speed, three smaller propellers large one-third (0.8 m) will produce 920 N thrust each, more than one-third of the big propeller. An important result comes from this analysis: propeller efficiency increases if the propeller is scaled down. Typical values of propeller efficiency are 85-89%, which are very close to those computed by CFD or with complex theories [2].

This section outlined the basic theory to access propellers performance under different operating conditions. It was showed that rpm, diameter and flight speed are connected each other and the reasons why some typical numbers are preferred. It is shown, from an analytical viewpoint, that higher efficiencies are attainable if smaller propellers are considered. For fixed shaft power, higher thrust is attainable if three smaller propellers are considered instead of a single larger one. Or, vice versa, the same total thrust can be obtained by the use of smaller propellers, hence limiting ground clearance and noise.[2]

5.3.1 Propeller Selection

The previous theoretical analysis is a good starting point for the estimate of the propeller efficiency. However, as always in engineering problems, one needs to rely on existing devices and on performance maps given by the manufacturers. This section will focus on the choice of real propellers. Roskam [3] contains 43 pages of propeller charts, taken from [4]. In particular, those diagrams in the form

1 The planetary gearbox is the most common solution for its compactness.
2 The noise produced by a rotating fan is proportional to the blade tip Mach number, which is generally lower in smaller propellers.

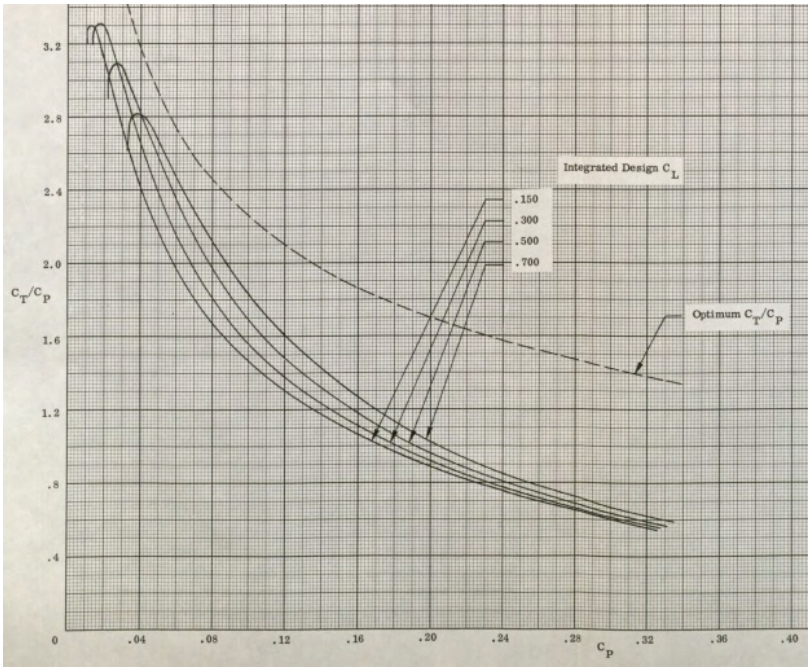

Figure 28: C_T as a function of $\bar{C}_L$ and C_P.

Advance ratio vs. Power coefficient are considered. To enter these diagrams, however, some design parameters must be fixed (Table 9).

The *activity factor* is just another way to define blade solidity; for example (see [1], pag. 365):

$$AF = \frac{100000}{16} \int_0^1 \left(\frac{c}{D}\right) x^3 dx \tag{121}$$

where $x = (r/R)$ and the integral may start either from 0 or from r_h, the radial coordinate of the blade hub.

The diagrams reported in Fig. 28-29 are taken from [4] and have been used to estimate the efficiency of the propellers in this analysis.

Table 9: Real propeller geometry assumptions.

n° of blades	$\mathcal{B}$	3
integrated lift coefficient	$\bar{C}_L$	0.7
Activity Factor	AF	100

5.4 PRELIMINARY DESIGN OF THE AIRCRAFT

The only thing left is to determine the amount of thrust needed to move the whole aircraft at take-off, which is the moment of maximum weight. In the previous sections, several scenarios have been presented. To proceed further, the following parameters need to be fixed:

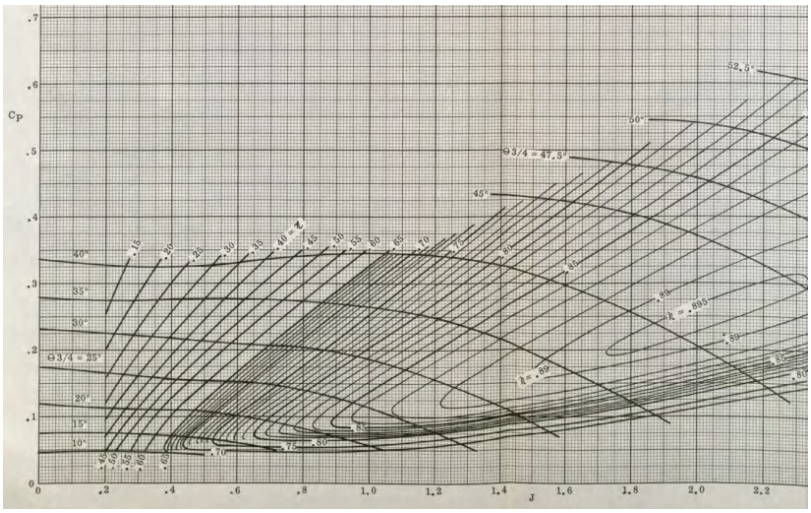

Figure 29: Propeller efficiency as a function of J and C_P.

- engine(s) power profile for the whole mission;
- mission duration;
- engine technology (Diesel or gas-turbine) and n°.

On so doing, the weight of the fuel W_{fuel} needed to accomplish the mission should be known. Moreover, the weight of the engines W_{engine} can be computed by means of correlations. The overall weight of the aircraft at take-off includes also the weight of the structure and the payload, which need to be modeled.

In his work, Raymer [5] suggests a procedure to estimate the "Design take-off gross weight", which is defined as the total weight of the aircraft as it begins the mission for which it was designed[3]. Design take-off gross weight can be divided into crew weight, payload (or passenger) weight, fuel weight, and empty weight. The empty weight includes the structure, engines, landing gear, fixed equipment, avionics and anything else not considered a part of crew, payload or fuel. Eq. 122 summarizes the take-off weight buildup:

$$\mathcal{W}_0 = \mathcal{W}_{crew} + \mathcal{W}_{payload} + \mathcal{W}_{fuel} + \mathcal{W}_e. \tag{122}$$

Being a UAV the target of this analysis, no crew is involved in the mission. The payload, not well defined yet, might be composed by electronic devices like cameras, avionics systems or weapons. Depending on the mission, it can be considered as an external input. Hence,

$$\mathcal{W}_0 = \mathcal{W}_{payload} + \mathcal{W}_{fuel} + \mathcal{W}_e \tag{123}$$

3 This is not necessarily the same as the "maximum take-off weight". In fact, many military aircraft can be overloaded beyond design weight, yet suffering from a reduced maneuverability.

The only unknown is the empty weight, which is a function of the total aircraft weight itself W_0. To simplify calculations, the empty weight can be expressed as a fraction of the total takeoff weight, i.e.

$$\mathcal{W}_0 = \mathcal{W}_{payload} + \mathcal{W}_{fuel} + \left(\frac{\mathcal{W}_e}{\mathcal{W}_0}\right)\mathcal{W}_0. \tag{124}$$

The empty-weight fraction W_e/W_0 can be estimated statistically from historical trends; data are shown in [5] and are fitted so that correlations are obtained. These fractions vary from about 0.3 and 0.7, and diminish with increasing total aircraft weight. Flying boats have the highest empty-weight fraction, long-range military aircraft have the lowest. This dependence can be expressed by the exponential equation (weights are expressed in pounds):

$$\frac{\mathcal{W}_e}{\mathcal{W}_0} = a\,\mathcal{W}_0^b \tag{125}$$

where a and b are coefficients depending on aircraft mission and size. Note that the empty-weight fraction depends on $\mathcal{W}_0$. The exponent b is a small negative number, which indicate that the empty weight fraction decreases with increasing take-off weight. For military long range aircraft, $a = 0.93$, $b = -0.07$. Equations 124 and 125 constitute a non-linear system of two equations in the two unknowns $\mathcal{W}_0$ and $\mathcal{W}_e$, which can be solved numerically.

Once the take-off gross weight is known, it is easy to compute the lift at take-off, which can be approximated equal to the aircraft full weight: $L = \mathcal{W}_0$. The remaining unknown in the estimate of the thrust is the L/D, or lift-to-drag ratio. L/D is highly dependent upon the wing span, shape and the design airfoil distribution. In this preliminary design, these data are still unknown to the designer; existing literature data is one means around this difficulty. If we assume the reconnaissance drone target of this thesis to be similar in shape (but bigger is size) to the General Atomics MQ-1 Predator, the same aspect ratio can be assumed: AR=19 [6]. The aspect ratio of the wing has historically been used as the primary indicator of wing efficiency. AR is defined as the square of the wing span divided by the wing reference area. Raymer suggests to correct the aspect ratio with the total aircraft wetted area, forming a new parameter, the "Wetted Aspect Ratio" WAR ([5], pag. 20):

$$AR = \frac{b^2}{A_{ref}} \tag{126a}$$

$$WAR = \frac{b^2}{A_{wet}} = \frac{AR}{A_{wet}/A_{ref}}. \tag{126b}$$

where A_{wet}/A_{ref} is the wetted-area ratio.

According to Raymer's work, we can assume for the present study that $A_{wet}/A_{ref} = 7$. Hence, $WAR = 2.7$. A scatter plot reporting L/D as function of WAR for many aircraft families is available. Being the MQ-1 Predator a fixed landing gear prop aircraft, a WAR of 2.7 corresponds to a $L/D = 15$. Finally, since L is known, the drag and the corresponding thrust can be computed.

Once the thrust is known, we can proceed further with the propeller selection. If three propellers are needed, for example, each one has to deliver one third the total thrust. Then, it is possible to choose a propeller from the diagrams in Fig. 28-29, by computing C_P, C_T, J, D, rpm and η_{prop} with the methodology showed in Sec. 5.2.

This design process is an iterative cycle in which convergence is not guaranteed. In other words, not necessarily there exists a solution (propellers geometry and number) for certain mission requirement. For example, given the engine power and an excessive long flight duration, the fuel weight might be too high to allow the aircraft to take-off, hence no propellers can give enough thrust, even with $\eta = 1$. Further iterations are needed, e.g. by adjusting the propellers number and geometry, the engines number and power, and in general by changing the whole aircraft assembly. This procedure will be discussed in the next chapter.

REFERENCES

[1] B. W. McCormick. *Aerodynamics, Aeronautics, and Flight Mechanics*. 2nd ed. Wiley, 1994. ISBN: 0471575062,9780471575061.

[2] L. Piancastelli, L. Frizziero, S. Pica, and G. Donnici. "High Altitude Operations with Piston Engines Power Plant Design Optimization, Part I: Introduction." In: *ARPN Journal of Engineering and Apllied Sciences* 11.5 (2006).

[3] C. T. Lan J. Roskam. *Airplane Aerodynamics and Performance*. Revised. Darcorporation, 2000. ISBN: 9781884885440,1884885446.

[4] Hamilton Standard. "Generalized Method of Propeller Performance Estimation." In: *United Aircraft Corp.* PDB (1963).

[5] D. Raymer. *Aircraft Design. A Conceptual Approach*. 2nd ed. 1992.

[6] U.S Air Force. *USAF MQ-1B fact sheet*. URL: http://www.af.mil/AboutUs/FactSheets/Display/tabid/224/Article/104469/mq-1b-predator.aspx.

6 REAL ENGINE-PROPELLER ASSEMBLY

6.1 NEW ENGINE–PROPELLER CONFIGURATIONS

The previous chapter has shown that propeller efficiency increases when diameter and rpm are reduced (Fig. 27). In terms of propeller efficiency, the use of multiple smaller propellers is favorable. This fact collides with the conclusions of Chap. 4, which suggested the use of a single, large propeller driven by a single engine. Choosing between these two opposite trends is not straightforward. A key point is understanding that the larger is the gas-turbine, the higher its efficiency, since the scale effects are reduced.

Instead, it is common experience in automotive industry that for a given shaft power, a smaller highly-loaded Diesel engine is more efficient than a larger one operated at lower rpm. In other words, when the engine is throttled down, less rpm are obtained and less fuel is burned per unit time, producing less power, but in a more efficient way. The higher efficiency of the thermodynamic cycle of this scenario can be due to different reasons. At lower rpm the time available for combustion is higher; if in spark-ignition engines the spark timing can be regulated as a function of rpm, this is not possible in compression-ignition engines. At high piston speeds the air-fuel mixing and the time for flame propagation are poor, producing a combustion inefficiency. Moreover, higher thermal losses through the walls are experienced at higher rpm. Finally, the amount of fuel injected is controlled by means of a pressure drop through a nozzle; this process is much harder to be linked to the engine rpm, with respect to the spark advance fine regulation. The mismatch between fuel and air mass flow rates usually brings a shift from the usual equivalence ratios, generating poor combustion efficiency.

Another issue is that propeller efficiency varies by just few percentage when varying the diameter (typical numbers are 85%-88%, obtained via experimental test and proved by CFD [1]), while scaling up or down the engine is much more significant in terms of percentage.

Configurations B and D (Fig. 23) could become competitive only if the thrust gain given by the use of multiple propellers overcomes the weight- and efficiency-penalization due to: electrical conversion

of the generator, mechanical friction of belt transmission, and the additional weight of multiple propellers instead of one. Unfortunately, all these negative effects outweigh the thrust gain from multiple propellers, and for this reason the electric propulsion and the mechanical transmission are definitively discarded.

It is conceivable to exploit the previous considerations by imaging two new configurations:

A. single turbine - single (larger) propeller;

B. multiple Diesel engines - multiple (smaller) propellers.

On so doing, the turbine becomes as efficient as possible, with the larger propeller being lighter than many smaller propellers and not constituting a big disadvantage in terms of efficiency. The multiple reciprocating engines experience a higher efficiency and also benefit from the (little) propeller thrust gain, paying the price of a higher dry weight of the entire assembly. The number of Diesel engines is decided after computations.

6.2 REFINING THE COMPUTATIONS

6.2.1 Constant Cruise Mission

The algorithm describing the procedure to fully characterize the aircraft performing a constant cruise mission is reported in Fig. 30. The iterations stop when convergence is reached, i.e. when the engine power is enough to take-off the full aircraft weight and the propellers manage to deliver enough thrust.

The algorithm requires the choice of:

- altitude and flight Mach number;
- mission duration;
- engines' number and power;
- propellers number and preliminary geometry;
- $\mathcal{W}_{payload}$.

Since the main power source can be distributed among a certain number of engines, the same subdivision can be considered for the thrust among many propellers. The right side of the algorithm then involves the choice of the propeller, which has been described in Sec. 5.2.

Fuel consumption can be computed with the MATLAB codes developed, while engines' weight can be estimated with correlations. The rest of the left side of the figure is the procedure outlined in Sec. 5.4. If $\mathcal{T}$ is not the desired one, two choices are possible: for small adjustments it is sufficient to modify the propeller geometry; otherwise it is necessary to vary the number and power of engines and propellers.

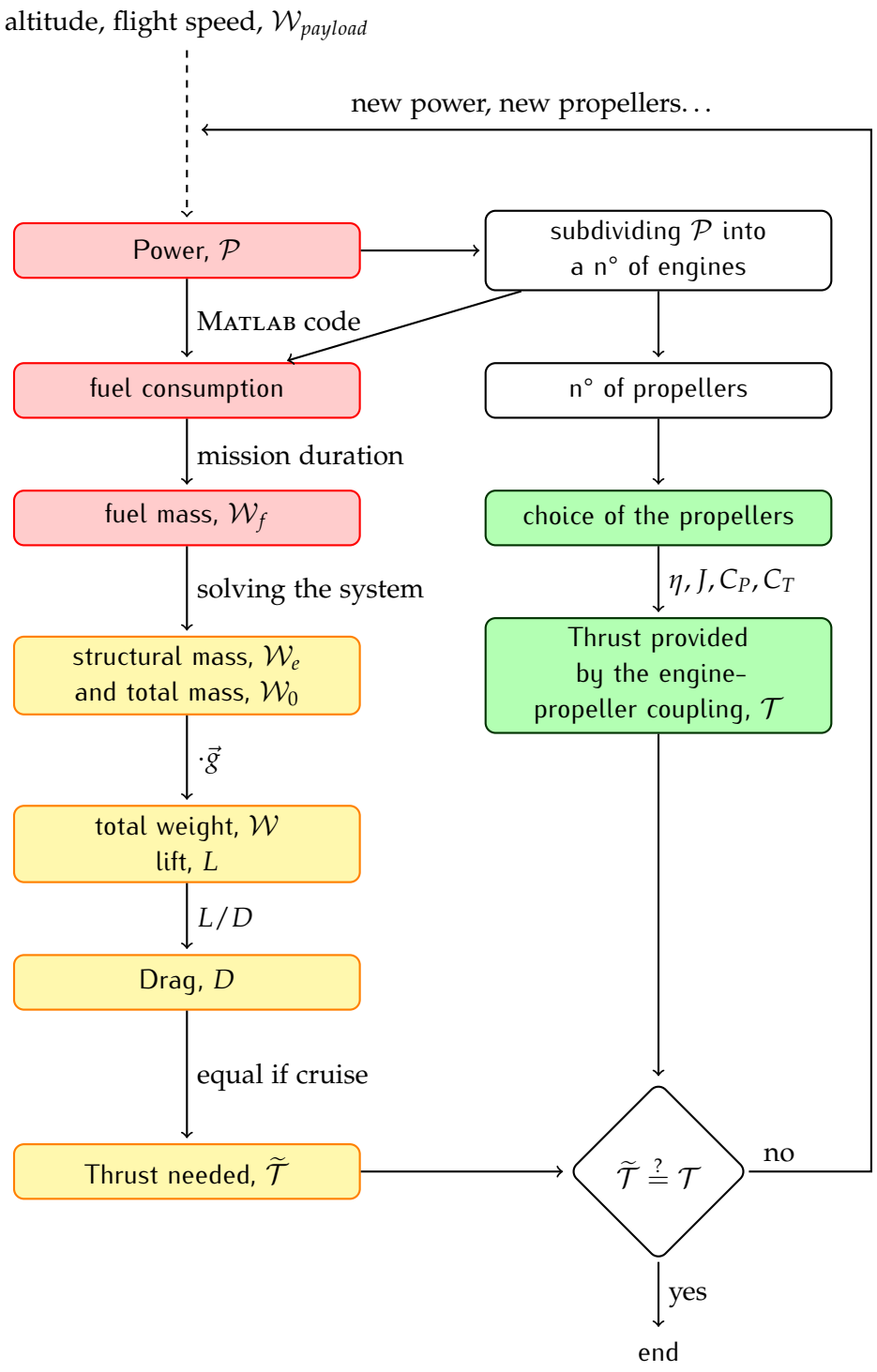

Figure 30: Iterative process required to find the engine power.

6.2.2 Variable Power Mission

It is clear that a scenario in which the power requirement varies during the mission is much more complex. In fact, starting from the top of the diagram, there might be the case in which the flight speed is not constant, because of a variable thrust profile (i.e., accelerations). Hence, we would have *flight speed (t)*. The power delivered by the engine varies during the mission for the same reasons: $\mathcal{P}(t)$. It is easy to see that all the other parameters in the scheme become time-dependent, including the propeller performance, $\eta(t)$. As a result:

- if extra power is used for auxiliary power onboard and not for accelerating, (i.e., *flight speed = const.*), the thrust needed to move the aircraft must *always* match the thrust available by the propellers. In short, $\widetilde{\mathcal{T}}(t) = \mathcal{T}(t) \; \forall \; t$;
- if the power variation is made to obtain an acceleration, in those moments it is allowed to have $\widetilde{\mathcal{T}}(t) \neq \mathcal{T}(t)$, while *flight speed* $\neq$ *const.*
- a combination of the two above, in which part of the power is used onboard for utilities ($\mathcal{P}_u$) and part is converted in thrust.

These considerations are summarized in the algorithm in Fig. 31. The exact solution of this problem is beyond the scope of this thesis. The procedure would require the implementation of the algorithm proposed, where the thermodynamic MATLAB code simulating the engine operation (red), the aircraft weight estimation (yellow), and the computation of the propellers performance (green) are joined together in a single numerical program.

Improvement

Do it.

To be even more strict, a varying altitude along the mission (simulating the climbing and the approaching phases) should be involved in the iterative process too.

In this work some hypothesis are made:

- $\mathcal{V} = const$ with the exception of the take-off, when an acceleration is needed. The mission profile is assumed to not require any acceleration during flight, but only auxiliary power onboard;
- variable pitch propellers are assumed. On so doing the engine's rpm can be decoupled from the propeller rotational speed, which remains constant. On so doing, the input torque to the propeller varies with the input power, but the work made by the blade to the surrounding air is damped with the variable pitch. This allows to have constant η, J, C_P, C_T;

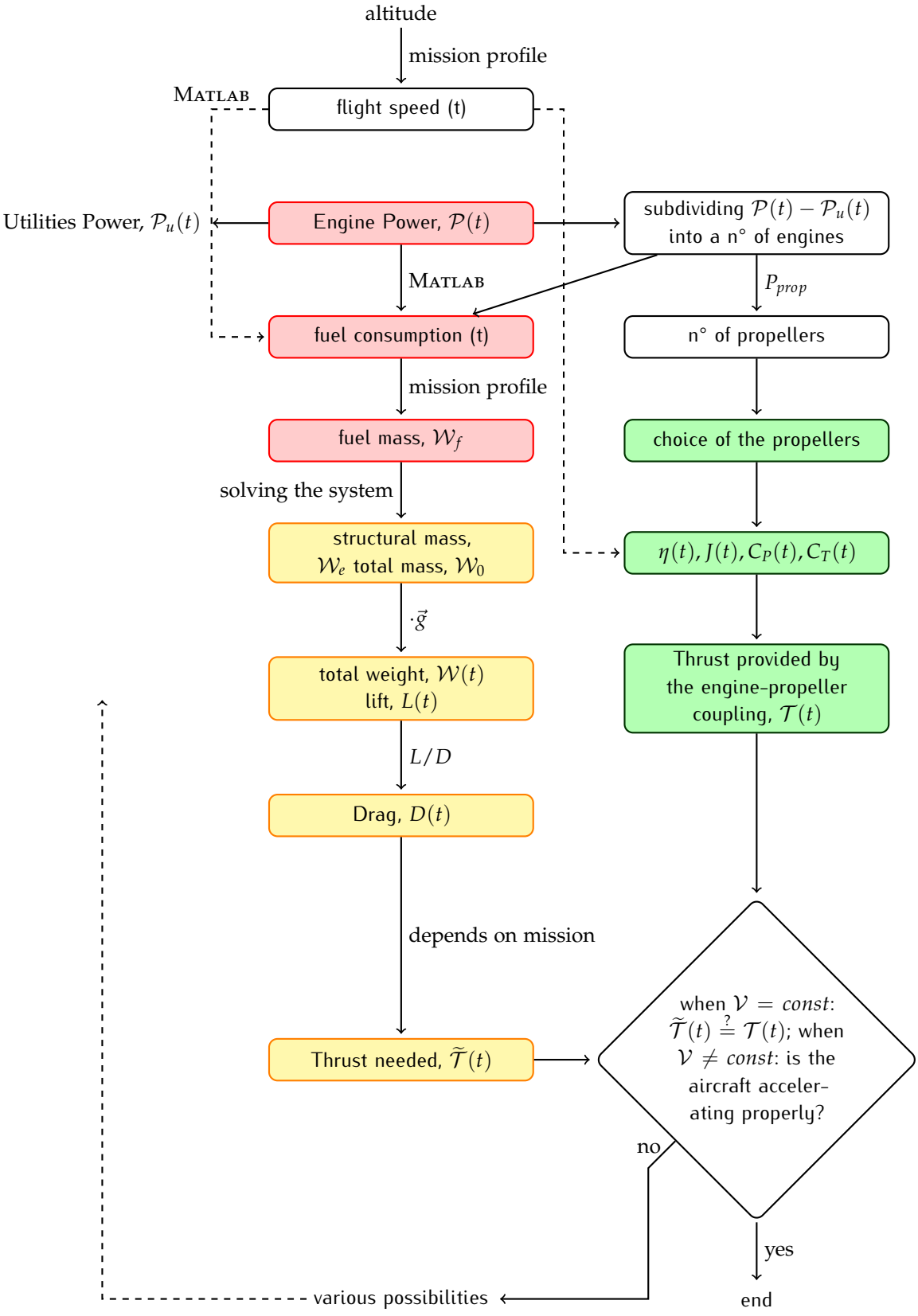

Figure 31: Iterative process required to find the engine power.

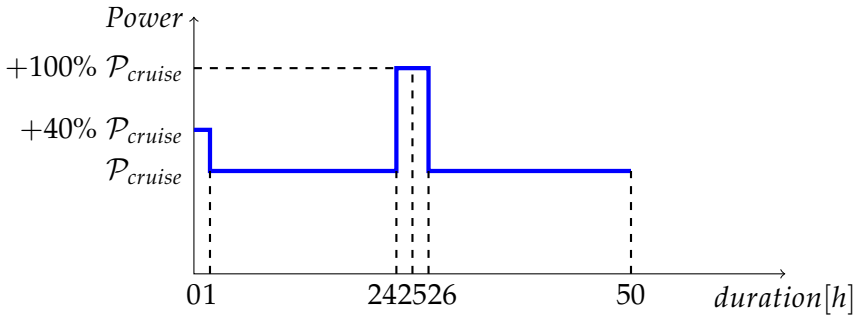

Figure 32: Power requirement profile for 50 hours mission.

- with respect to Section 4.4 and to the power profile in Fig. 25, a more realistic power profile is now considered (Fig. 32). There is one power peak at half mission, lasting two hours and representing the duty to be accomplished at the furthest point from the base, and one smaller power request at take-off, one hour long.

When the decision block is reached, the thrust at take-off should be checked, i.e. the thrust developed by the propellers must grant the acceleration needed to reach the take-of speed. Here is the procedure: the difference between the thrust and the drag is the net force, $T - D = F$. The net uniform acceleration is given by $a = F/\mathcal{W}_0$. Hence, since the take-off velocity is fixed (see Sec. B.1), that velocity will be reached after $s = \mathcal{V}_{TO}/a$ seconds.

If this duration is within a certain range, e.g. between 10 and 20 seconds, then the acceleration is considered acceptable, else a different thrust must be provided.

6.3 RESULTS

When convergence is reached, the aircraft engines and propellers are fully sized. The configurations obtained are tested over missions up to 50 hours. While the turbine configuration is tied to be single engine-single propeller, the Diesel configuration can be designed to be made by two-two, three-three, and four-four of these elements. The results of the iterations are shown in Tab. 10. Concerning the turbine technology, a compression ratio $\pi = 40$ represents the current state of the art [2],[3]. A comparison with an advanced $\pi = 60$ is presented, showing the potential of investing in this technology; however, increasing π certainly involves an increase in dimension and weight.

The propellers selected from the last iteration are reported in Table 11. The weight of each propeller is based on data sheets available in literature [4]; those selected are aluminum made.

The results for the constant-cruise mission are shown in Fig. 33. For short durations the gas-turbine is lighter than the Diesel compounds,

Table 10: Performance data of the updated configurations.

name of config.	D4	D3	D2	T1, $\pi = 40$	T1, $\pi = 60$
n° of propellers	4	3	2	1	1
Engines	4 Diesel	3 Diesel	2 Diesel	1 Turbine	1 Turbine
Power [kW]	125 each	169 ea	260 ea	594	594
Dry weight [kg]	154 ea	196 ea	257 ea	70	around 80
Fuel cons. [lt/h]	24.02 ea	33.29 ea	52.92 ea	134.16	123.33

Table 11: Performance data of the propellers selected.

n° of propellers	4	3	2	1
Diameter [m]	1.5	1.7	2.1	2.3
rpm	2500	2300	2000	1900
η_{prop}%	89.5	89.0	88.5	88.0
J	2.10	2.02	1.88	1.81
C_P	0.252	0.234	0.190	0.289
C_T	0.201	0.201	0.200	0.198
n° blades	3	3	3	3
Weight [kg]	28	33	37	39
Input power [kW]	125	169	260	535
Thrust [N]	859	1146	1721	3587
Tot Power needed [kW]	500	507	520	535
Tot Thrust [N]	3436	3438	3442	3587

with the four-engines four-propellers being the heaviest. Around twenty-three hours flight the Diesel configurations take over the turbine, thanks to their higher efficiency. For longer missions, the four-engines four-propellers is the best configuration because of the lowest fuel consumption of the smaller engines; however, adding more elements to a system generally decreases its reliability. A cutting-edge turbine with $\pi = 60$ would shift the crossing point up to thirty-one hours, thanks to the higher efficiency. Its dry weight is estimated to be approx. 10 kilograms larger than the $\pi = 40$ turbine.

Fig. 34 takes into account also the additional thrust for take-off and the auxiliary power phase, simulating a specific requirement to be accomplished at half mission. It is showed that the crossing point shifts a little bit towards longer durations: the Diesel configurations take over the $\pi = 40$ gas-turbine around twenty-five hours flight. With an

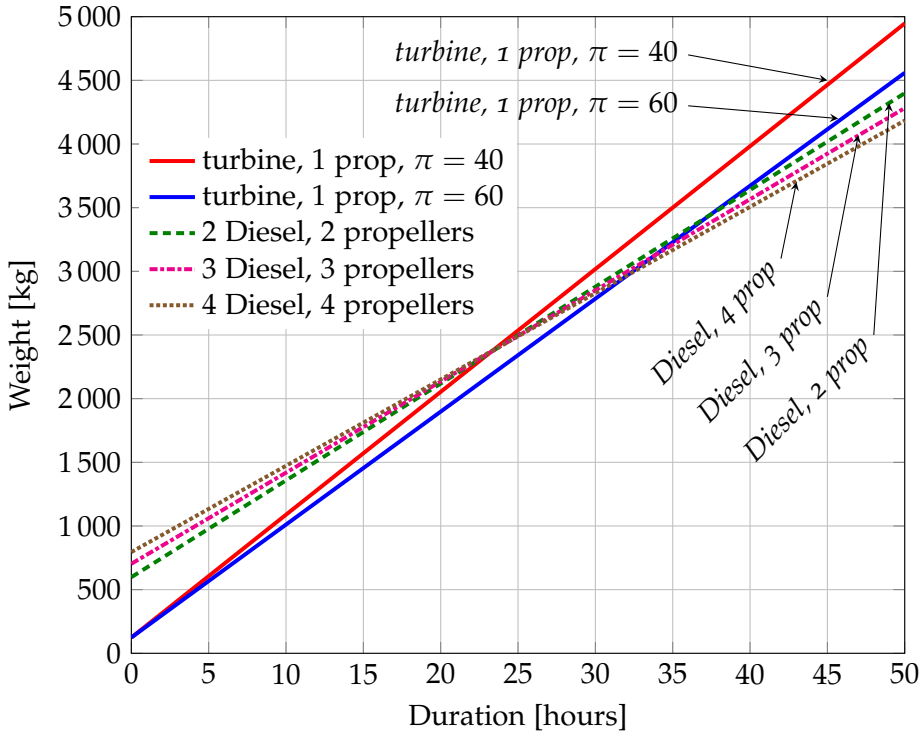

Figure 33: Comparison between different configurations; constant cruise mission. Altitude=10000 ft, flight Mach=0.4.

increased compression ratio of 60, the turbine engine could extend its convenient range up to thirty-four hours in the near future. This right-shift of the crossing point (compared to the constant-cruise mission) is due to a different increase of fuel consumption between the configurations. The Diesel engines, in particular, undergo a remarkable decrease in efficiency past the design point, when very high rpm are imposed. The gas-turbine too shows a decrease in efficiency when shifting from its design point, but less abrupt than in the IC engines. Hence, the increase in the curve slope is less severe, and the crossing point shifts towards longer durations.

6.4 COST CONSIDERATIONS

By looking at Fig. 33-34, the difference in terms of fuel weight for a 50 hours mission is between 300 and 500 kg, depending on which configurations are compared.[1] Let us compare the $\pi = 40$ and $\pi = 60$ turbine-based configurations and the four turbocharged Diesel engine-based configuration. The scope of this section is to estimate the savings resulting from the choice of the latter option.

First, the difference in fuel must be computed (Table 12).

1 A minor difference is also given by the engine dry weight; however, compared to the fuel weight, this is an order of magnitude lower.

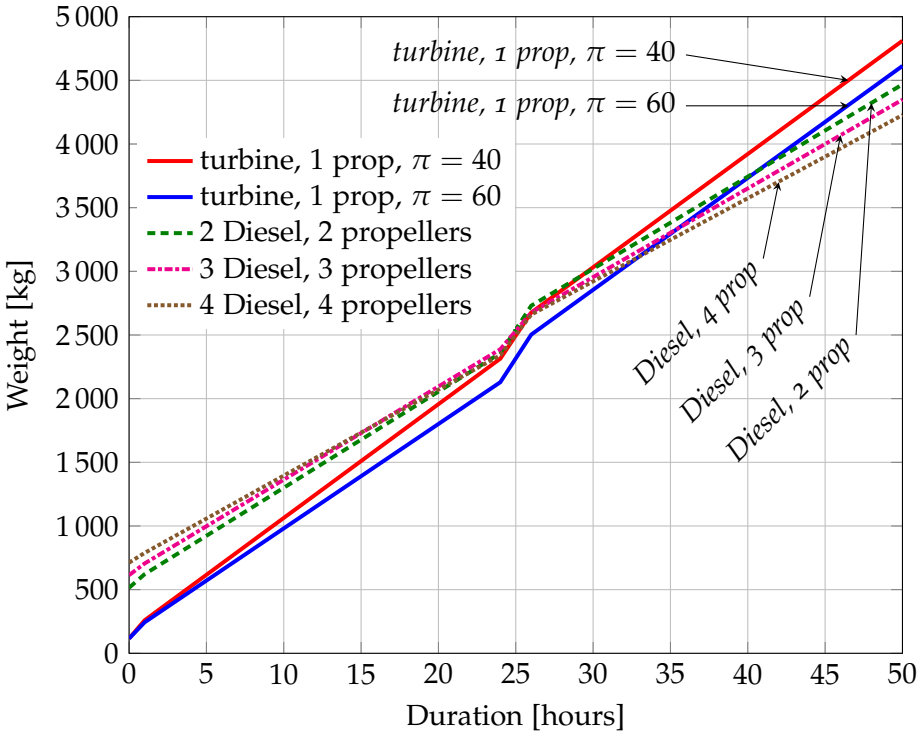

Figure 34: Comparison between different configurations; variable power mission. Altitude=10000 ft, flight Mach=0.4.

The price of the fuel fluctuates daily; at 30 September 2016, the average US cost of standard aviation fuel kerosene (Jet Fuel, Jet-A) is 1.42 $ per gallon [5]. This means that every tank refill translates into the cost reported in Table 13:

On top of this, two more elements have still to be taken into account: the cost of the engine itself and the cost of the propellers. The Cessna 172 Skyhawk is one of the most famous aircraft ever built and mounts a 160 hp (120 kW) Diesel engine, approximately the power of the Diesel engine in our analysis. The Continental Diesel 155 has a cost estimated around 65 000 $, including the gearbox and the propeller [6]. On the other hand, a Pratt-Whitney PT6A-60A is a turbine

Table 12: Difference in weight between the four-Diesel four-propellers configuration and the turbine configurations.

	D4	T1 ($\pi = 40$)	T1 ($\pi = 60$)
W_{TOT} [kg]	4320	4800	4580
- W_{engine} [kg]	4×154	70	80
- $W_{propellers}$ [kg]	4×28	39	39
= W_{fuel} [kg]	3592	4691	4461

Table 13: Price of a full load of fuel for a 50 hours mission.

	D4	T1 ($\pi = 40$)	T1 ($\pi = 60$)
Cost of fuel	1871 $	2444 $	2326 $

Table 14: Price of the propellers involved in the configurations.

	D4	T1 ($\pi = 40$)	T1 ($\pi = 60$)
*FC*7391 series	$4 \times 25\,000$ $		
*B*3*N*10 series		45 000 $	45000 $

engine in the range 800-1000 hp (600-755 kW); this engine might be suitable for this study, and has a unit price of 955 000 $ (in 2015) [7]. This price includes the cost of gearbox.

The cost of the propeller is very model- and make-dependent. In the iterative process made so far, the *Hartzell Propellers Inc.* was chosen as a reference. To be consistent with that choice, two aluminum propellers are selected from this manufacturer [8]; their price are reported in Table 14.[2]

Summing up:

	D4	T1 ($\pi = 40$)	T1 ($\pi = 60$)
Cost of fuel [$]	1871	2444	2326
Cost of propellers [$]	$4 \times 25\,000$	45 000	45 000
Cost of engine [$]	$4 \times 65\,000$	955 000	ND
Total [$]	361 871	1 002 444	ND

Quite obviously, it is shown that the cost of the fuel is marginal compared to the rest of the assembly. Hence, excluding this voice, the price of the once-for-all purchase is obtained. The cost of the Diesel-based configuration is about one-third the cost of the gas-turbine.

Concerning the third column, the cost of a new gas-turbine engine is the sum of several unknown parameters. It is not only the cost of the engine itself, but also the cost of the research behind it. The exact estimate of a new technology would require a specific research that is not the scope of this work. In any advance, the higher pressure ratio would imply strong financial and time efforts. The final retail price, however, could be in the same order of magnitude of the previous engine, which in turn will become out-dated, and cheaper.

Other issues that have not been taken into account in this cost analysis are:

2 The prices are averaged among the huge quantity of versions available in the data sheet.

- maintenance costs: overhaul, replacing of parts, inspections;
- cost of certifications and approvals;
- installation and delivery costs.

The choice of four Diesel engines implies four times the cost of one inspection (and repairing); also, the probability of a failure is four times increased. Many problems still plague these engines and especially the problem with reliability, low Time Between Overhaul (TBO) or Time Between Replacement (TBR), maintenance availability and cost [9]. The choice of the turbine instead of the Diesel engine, indeed, is based on reliability issues too, since the turbine technology has a lower shutdown rate per hour of flight. Finally, other aspects to take into account are: noise, vibrations, compactness, emission of pollutants, need of extremely variable power (as in aerobatic vehicles).

This section aimed to give a very general guideline about the costs of the configurations proposed, and do not expect to be exact nor complete. Nevertheless, it points out the two main aspects concerning the cost of each configuration: first, the 4-stroke Diesel assembly involves less expensive engines, and second, every long flight is cheaper because of the lower fuel consumption. The lower amount of fuel required for a long mission implies savings for every flight made, which may justify the higher rate of maintenance. Moreover, a smaller and lighter tank is required, with the benefit of lower structural weight and size.

REFERENCES

[1] L. Piancastelli, L. Frizziero, S. Pica, and G. Donnici. "High Altitude Operations with Piston Engines Power Plant Design Optimization, Part I: Introduction." In: *ARPN Journal of Engineering and Apllied Sciences* 11.5 (2006).

[2] CFM International. *The Leap Engine. Performance. Execution. Technology.* Retrieved October 12, 2016. 2016. URL: https://www.cfmaeroengines.com/engines/leap/.

[3] L. Piancastelli, L. Frizziero, and I. Rocchi. "Feasible Optimum Design of a Turbocompound Diesel Brayton Cycle for Diesel-Turbo-Fan Aircraft Propulsion." In: *International Journal of Heat and Technology* 30.2 (2012), pp. 121–126.

[4] Hartzell Propeller Inc. *Propeller Owner's Manual and Logbook*. Version 14. Piqua, OH 45356-2634 U.S.A.

[5] International Air Transport Association (IATA). *Fuel Price Analysis*. URL: http://www.iata.org/publications/economics/fuel-monitor/Pages/price-analysis.aspx.

[6] Aircraft Owners and Pilots Association (AOPA). *Little Diesel, Big Fuel Savings*. URL: https://www.aopa.org/news-and-media/all-news/2015/february/pilot/f_diesel.

[7] J. Kasper O. Balle (Forecast International). *About the Pratt & Whitney PT6A*. URL: http://www.fi-powerweb.com/Engine/PW-CANADA-PT6A.html.

[8] Hartzell Propeller Inc. *2016 Price List*. Piqua, OH 45356-2634 U.S.A.

[9] N. E. Daidzic, L. Piancastelli, and A. Cattini. "Diesel engines for light-to-medium helicopters and airplanes (Editorial)." In: *International Journal of Aviation, Aeronautics, and Aerospace* 1.3 (2014). URL: http://commons.erau.edu/ijaaa/vol1/iss3/2.

7 CONCLUSIONS AND FUTURE WORK

7.1 CONSLUSIONS

In this work a method for choosing the best engine and layout to drive a lightweight long-range UAV was proposed. Particular attention was given to the engine technology used, as well as the arrangement of the engines onboard and to the connections with the propellers. A lack in literature studying the scenario between 200 and 500 kW and missions beyond 20 hours was present.

Many power sources have been selected for this study. Several existing engines were classified basing on their power, weight, size and fuel consumption. Comparisons among them outlined the reciprocating engines and the turbine technology as the most promising. Electric propulsion was discarded because of the exceeding weight of the batteries; turbocharging was preferred to the natural aspirated counterpart for internal combustion engines.

Five engines were selected: 2 and 4 stroke, spark- and compression-ignition turbocharged engines, and the gas-turbine engine. A Matlab code was written for each, simulating their thermodynamic cycle. Output properties as power, efficiency and fuel consumption were obtained, for different levels of power and altitude. A best-fit correlation was developed to estimate the engines weight. Different arrangements of engine-propellers were proposed.

An analysis of the propeller efficiency was also made, by means of theoretical concepts and experimental diagrams. It was outlined that smaller slow-rotating propellers give a better propeller efficiency. A preliminary sizing of the aircraft was performed as well. Finally, the overall system composed by structure, payload, engines and propellers was optimized for a 50 hours mission, in order to obtain the highest thermal efficiency and the lowest weight.

The thermal analysis has shown the advantages of replacing a small gas-turbine with one or more turbocharged 4-stroke Diesel engines. Increases in efficiency and decreases in fuel consumption can result. These advantages can translate to increases in range and/or flight duration, plus a reduction in fuel tank volume and weight.

The use of multiple Diesel engines, coupled with the same number of propellers, results in lower fuel weight for missions beyond the 23-25 hours flight; if a high-performance turbine is used, the range is extended to 31-34 hours in the next future. The presence of the turbocharger for altitude compensation allows to keep the IC engine at its best performance over a larger flight envelope.

Replacing a gas-turbine with multiple Diesel engines presents problems concerning the reliability of the system, as well as noise, vibrations and size, which are very important requirements in a long-duration UAV. However, the use of reciprocating engines allows savings for purchase, maintenance and refueling. Considerations on efficiency and weight have shown the non-feasibility of using mechanical connections between one engine and multiple propellers, nor the use of electric generators to drive electric motors. The availability of more efficient electric generators and batteries could cause reconsideration of the hybrid and pure-electric options in the future.

7.2 SUGGESTIONS FOR FUTURE WORK

The accuracy of the numerical codes has already been discussed in Sec. 3.5.1. More realistic heat transfer models can be implemented, accounting for radiative and convective heat transfer through a temperature-variating wall. Gradual opening and closing of intake and exhaust valves should be included, also, timing should be function of rpm, e.g. delaying the inlet valve closing for enhancing the cylinder scavenging at high rpm. More refined combustion models could be included in the cycle; experiments should be performed to simulate the real heat release curve for the Diesel combustion model. Modeling the turbocharger operation by translating maps into functions could be considered, synchronizing its capabilities within the rest of the code. Finally, the accuracy of the numerical codes should be compared with real engines and/or CFD simulations in a more strict fashion.

Concerning the flight simulations, more realistic missions could be considered, e.g. accounting for altitude variation during the mission. Moreover, the power of the engine should consider the decrease of the aircraft weight during the mission due to the fuel consumption. It should be given a try to include these variations into an algorithm able to compute the aircraft weight at every instant.

A more detailed cost analysis should be performed if needed, including an estimate of maintenance costs and mean time to failure; include issues that possibly drive the choice of a certain technology, as size, vibrations and noise. Further improvements in IC engines efficiency and weight include different arrangements of the turbochargers: it is conceivable to save weight and volume if a single turbocharger could supply air to multiple engines simultaneously.

Part III

APPENDIX

A ENGINES REVIEW

In this chapter a collection of engines in presented. This is the product of a deep research through several data sheets. All the engines presented are or have been on the market, i.e. no prototypes have been considered.

The engines are classified according to their power, fuel consumption and size. Unfortunately, turbojet and turbofan engines are commonly rated with their thrust, instead of power. In order to make comparisons, the power of each engine must be computed. The following procedure is applied, according to [1]. By assuming the aircraft as a black box, with $\dot{m}_{air}$ and $\dot{m}_f$ entering and $(\dot{m}_{air} + \dot{m}_f)$ exiting the boundaries, with a perfectly adapted nozzle, the following relations are derived:

$$\begin{cases} \mathcal{T} = (\dot{m}_{air} + \dot{m}_f)\mathcal{V}_{jet} - \dot{m}_{air} V \\ \Delta KE = \dfrac{1}{2}\left[(\dot{m}_{air} + \dot{m}_f)\mathcal{V}_{jet}^2 - \dot{m}_{air}\mathcal{V}^2\right] \\ \mathcal{P} = \mathcal{V}\mathcal{T} = \mathcal{V}\left[(\dot{m}_{air} + \dot{m}_f)\mathcal{V}_{jet} - \dot{m}_{air}\mathcal{V}\right] \\ TSFC = \dfrac{\dot{m}_f}{\mathcal{T}} \end{cases} \tag{127}$$

where T is the net thrust, ΔKE is the rate of change of kinetic energy, P is the power associated with propelling the aircraft, and $TSFC$ is the thrust specific fuel consumption.

The above 4 equations contain 5 unknowns: $\dot{m}_f, \mathcal{V}, \mathcal{V}_{jet}, \Delta KE, \mathcal{P}$. The other terms as $T, \dot{m}_{air}, TSFC$ should be given from data sheets.

If $\mathcal{T}$ is the static thrust at sea level, $\mathcal{V} = 0$ in this condition and the third equation drops. Hence, the remaining system of 3 equations in 3 unknowns $(\dot{m}_f, \mathcal{V}_{jet}, \Delta KE)$ can be solved.

$$\begin{cases} \mathcal{T} = (\dot{m}_{air} + \dot{m}_f)\mathcal{V}_{jet} \\ \Delta KE = \dfrac{1}{2}\left[(\dot{m}_{air} + \dot{m}_f)\mathcal{V}_{jet}^2\right] \\ TSFC = \dfrac{\dot{m}_f}{\mathcal{T}} \end{cases} \tag{128}$$

Else, if one of the information is missing (because confidential), or if the thrust is not the static one, the previous simplification can not be done; another information should be given, e.g. $\mathcal{V}$. or $\dot{m}_f$. Turbofan

and turbojet engines specifications are shown in Table 15. Information about fuel consumption was not collected, both because generally these data are confidential and very hard to find on official sources, and also because these engines exceed the power required for this analysis. In can be seen that the power-to-weight ratio spans over a wide range: it goes from 6 to 11 for turbofan, and from 9 to 36 for turbojet: a variation between two and four times. Let us analyze this parameter.

The main drivers of the power-to-weight ratio are the power, the dry weight, the fuel consumption and the mission length. The influence of the power on $\mathcal{P}/\mathcal{W}$ is quite obvious. However, the fuel weight is given by the mission length times the fuel consumption, which in turn depends on the power. At lower power both Diesel and turbine engines require a lower fuel mass flow rate, but how much lower? For the turbine engines, for instance, fuel consumption depends both on size (scale effects deteriorate the efficiency) and on inlet air mass flow rate (to match the correct air to fuel ratio), which again depends on the inlet air velocity, i.e. on the power of the engine ($\mathcal{P} \simeq \mathcal{TV}$). In addition, all this is very technology dependent: significant deviations from a somehow "standard" trend are possible, depending on the modernity of the engine (cutting edge materials, new technologies, etc.) and on the engine architecture (the amount of by-pass and the presence of the afterburner influence the fuel mass flow rate). And this, very often, translates in a lack of data in open literature.

It is worthwhile to remind that, in the end, this work aims to evaluate the fuel consumption of each technology, in order to assess its efficiency. However, a comparison on the specific fuel consumption between IC engines and gas turbines is somehow meaningless, since the former is thrust-specific, the latter is power-specific. To compute the power of the turbine engines (for comparing them in a "power-specific way") again the fuel mass flow rate and the inlet mass flow rate are needed. Same problems as above: 1) lack of data, 2) fuel mass flow rate depends on the power, which is unknown.

Specifications of cruise missiles are shown in Table 16. A comparison between these engines and internal combustion engines is made harder in the power range between 100 and 1000 kW, since most of the specifications of cruise missiles are confidential. For this reason cruise missiles are ranked only with their thrust, since it was impossible to obtain data about $\dot{m}_{air}$ and $TSFC$, needed to compute their power.

An electric motor is an electrical machine that converts electrical energy into mechanical energy. In this work these devices are generally intended as composed by a rotor, a stator and windings (wires that are laid in coils, usually wrapped around an iron magnetic core). No major distinction is made between the various technologies. Concerning the electric motors in Table 18, note that the power-to-weight

Table 15: Turbofan and Turbojet specifications.

	Model	Weight [kg]	Size $[m^3]$	Power [kW]	$\frac{\mathcal{P}}{\mathcal{W}}\left[\frac{kW}{kg}\right]$
Turbofan	$ALF502H$	565	1.21	3846	6.81
	$AE-3007$	752	2.04	4717	6.27
	$TAY620$	1500	2.36	10347	6.90
	$BR710-A1$	1851	12.14	10938	5.91
	$CF34-10E$	1682	5.26	16452	9.78
	$PW2037$	3247	13.53	26303	8.10
	$JT-9D-7R4$	4029	16.01	29698	7.37
	$CF6-80C2$	4144	17.88	47339	11.42
	$GE90$	7550	36.62	55854	7.40
	$Trent800$	6531	26.64	58188	8.91
Turbojet	$JT12A-8$	212	0.28	4617	21.78
	$JT8D-219$	2041	4.80	19286	9.45
	$JT3C-7$	1585	2.67	17413	10.99
	$AL-7F$	2010	8.82	24462	12.17
	$YJ93$	1728	8.61	26192	15.16
	$J58$	2700	8.98	31787	11.77
	$F135-PW100$	1701	7.30	61285	36.03
	$Olympus593$	3175	4.64	82430	25.96

Table 16: Cruise missiles specifications.

	Model	Weight [kg]	Size $[m^3]$	Thrust [N	$\frac{\mathcal{T}}{\mathcal{W}}\left[\frac{N}{kg}\right]$
Cruise missiles	$Kh-55$	95	0.07	4448	46.82
	$AGM-86ALCM$	66.2	0.10	2700	40.79
	$AGM-129ACM$	73	0.05	4450	60.96
	$Tomahawk$	66	0.07	3114	47.18

ratio differs of at least one order of magnitude between the engine alone and when it is coupled with batteries.

In Tables 19 and 20 each reciprocating engine is classified along with the number of strokes (two or four) and the ignition technique (spark or compression). Pay attention to the fact that the last six elements of Table 20 are actually Formula 1 engines. This is the reason for their remarkable high Power-to-Weight ratio.

Finally, some specifications involving the electric generators investigated are shown in Table 22. These devices are commonly produced in two types: one is a massive machine including a reciprocating engine. The crankshaft is mechanically linked with the generator itself; often the rpm matching is obtained trough the use of a gearbox. These devices are very large and heavy, definitely not suitable for aeronautic purposes, but quite common as assistance power source in industrial applications. The other type does not include the engine, and are commonly called *alternators*. Hence these machines are smaller and portable. In fact, the power is taken from a power source, such as an IC engine, by the use of a *PTO*, or *Power Take Off*. It is a system comprising a splined output shaft on a tractor or truck, which can be easily connected and disconnected to the generator side.

REFERENCES

[1] N. Cumpsty. *Jet Propulsion: A Simple Guide to the Aerodynamic and Thermodynamic Design and Performance of Jet Engines*. Cambridge University Press, 1997.

Table 17: Turboprop engines specifications.

	Model	Weight [kg]	Size [m^3]	Power [kW]	$\frac{\mathcal{P}}{\mathcal{W}}\left[\frac{kW}{kg}\right]$
Turboprop	$RR500$	102	0.26	238.6	2.34
	$M250$	78	0.11	283	3.63
	$AE-2100$	783	1.28	3096	3.95
	$PT6B-37A$	175	0.30	650	3.71
	$M601D-1$	197	0.46	490	2.49
	$TPE331-43A$	153	0.26	429	2.80
	$AllisonT56$	880	1.39	3915	4.45
	$GEH75$	177	0.44	560	3.16
	$RR300$	91	0.23	200	2.20

Table 18: Electric motors specifications. Y = batteries included, N = batteries not included.

	Model	Weight [kg]	Power [kW]	$\frac{\mathcal{P}}{\mathcal{W}}\left[\frac{kW}{kg}\right]$	Batteries
Electric	$OSMG9505$	0.076	0.25	3.29	N
Motors	$OSMG9538$	0.234	0.5	2.14	N
	$Siemens$	50	260	5.20	N
	$Hi-PaDrive$	120	235	1.96	N
	$Yuneec$	20	40	2.00	N
	″	115	40	0.35	Y
	$TeslamodelS$	32	270	8.44	N
	″	622	270	0.43	Y
	$SolarImpulseII$	158	13.5	0.09	Y
	$EVD150/260$	45.8	80	1.75	N

Table 19: Turbocharged engines specifications.

	Model	Weight [kg]	Size [m3]	Power [kW]	$\mathcal{P}/\mathcal{W}$ [kW/kg]	n° of strokes	Technology
Turbocharged	$PF4-53T$	572	0.748	130	0.23	2	*Diesel*
	$PF6V53T$	769	0.97	174	0.23	2	*Diesel*
	$MDITCGDBS-II$	270		46.3	0.17	4	*Diesel*
	$NEF2.6BS-II$	320		77	0.24	4	*Diesel*
	$NEF2.6BS-III$	320		81	0.25	4	*Diesel*
	$YC4108ZD$	370	0.466	37	0.10	4	*Diesel*
	$FordV8 6.0L$	438	0.273	242	0.55	4	*Diesel*
	$LD4B3.9-60G$	340	0.563	45	0.13	4	*Diesel*
	$4JB1T-1$	241	0.403	28	0.12	4	*Diesel*
	$YC4108ZC$	390	0.682	55	0.14	4	*Diesel*
	$FordV8 6.4L$	499	0.292	261	0.52	4	*Diesel*
	$FordV8 7.3L$	417	0.333	205	0.49	4	*Diesel*
	$MBE900$	594	0.55	209	0.35	4	*Diesel*
	$1.820vT$	183	0.136	132	0.72	4	*Spark*
	$2.0TFSI$	140		142	1.01	4	*Spark*
	$8.0W1664V$	490	0.178	746	1.52	4	*Spark*
	$BMWN63$	228	0.201	300	1.32	4	*Spark*

Table 20: Naturally aspirated engines specifications.

	Model	Weight [kg]	Size [m3]	Power [kW]	$\mathcal{P}/\mathcal{W}$ [kW/kg]	n° of strokes	Technology
Naturally Aspirated	$PF4-53N$	503	0.639	104	0.21	2	*Diesel*
	$PF3-53N$	438	0.511	73	0.17	2	*Diesel*
	$PF3-71N$	692	0.701	159	0.23	2	*Diesel*
	$PF4-71N$	807	0.839	119	0.15	2	*Diesel*
	$1VR-DF$	0.662		3.58	5.41	2	*Spark*
	$120AX$	0.65		2.31	3.55	2	*Spark*
	$104RX$	0.83		2.61	3.14	2	*Spark*
	$160RX$	0.925		2.76	2.98	2	*Spark*
	$15LA$	0.138		0.3	2.17	2	*Spark*
	$35AX$	0.363		0.95	2.62	2	*Spark*
	$55AXABL$	0.404		1.25	3.09	2	*Spark*
	$75AXABL$	0.578		1.77	3.06	2	*Spark*
	$120AX$	0.647		2.31	3.57	2	*Spark*
	$60EPIMercury$	98		45	0.46	4	*Spark*
	$5.2V10FSI$	220	0.222	331	1.50	4	*Spark*
	$P86$	95		537	5.65	4	*Spark*
	$E41-4$	120	0.128	596	4.97	4	*Spark*
	$P80$	98	0.113	634	6.47	4	*Spark*
	$P84$	89		671	7.54	4	*Spark*
	$P84/5$	92		690	7.50	4	*Spark*
	$P83$	88	0.128	701	7.97	4	*Spark*

Table 21: Gas turbines engines specifications.

	Model	Weight [kg]	Size [m^3]	Power [kW]	$\frac{\mathcal{P}}{\mathcal{W}}\left[\frac{kW}{kg}\right]$
Gas turbines	*LM*2500	22000	68.8	24050	1.09
(naval appl.)	*LM*2500	22707	39.4	35320	1.56
	*LM*6000	7863	21.73	52404	6.66
	*LM*500	2779	14.24	4570	1.64
	42*MW*	7863	21.7	42428	5.40
	30*MW*	21859	59.8	30200	1.38

Table 22: Electric generators specifications.

	Model	Weight [kg]	Size [m^3]	Output [kW]
Electric gen.	*QT*15068*KVAC*	1130	3.87	150
(engine incl.)	*RC*185*D.JD*3*FXSM*	2672	2.12	146
	300*REOZJ*	2449	6.81	300
	*CatC*9*GeneratorSet*	3402	21	300
	*KohlerDetroit*60	4536	11.2	300
	*SG*300	3180	11.87	300
	*QT*10068*GVAC*	1148	3.88	100
Alternators	*PTO*110.3	422	0.367	100
	*W*165*FPTOT*.18	682	0.623	165

B VARIABLE POWER PROFILE

Section 4.4 introduced the concept of variable power requirement. The profile of Fig. 25 and the correspondent power increments are justified by the following analysis.

B.1 TAKE-OFF PHASE

The analysis of this section is focusing on relating the engine's power with the useful thrust and the aircraft speed. Both these parameters are important in defining the take-off phase. In fact, we need to know whether a certain power increment (say, +40%) is able to guarantee enough thrust and velocity for taking off.

In aeronautics, $\mathcal{P}$, $\mathcal{T}$, and $\mathcal{V}$ are linked by the so called *propeller efficiency* ([1], pag. 351):

$$\eta_{prop} = \frac{\mathcal{T}\mathcal{V}}{\mathcal{P}}. \tag{129}$$

A propeller efficiency equal to 1 is now assumed for simplicity, but the real value can be computed in advanced phases of the design, as explained in Sec. 5. At cruise conditions:

- $\mathcal{P} = 300$ kW
- $M = 0.4 \implies \mathcal{V} = M \cdot c(z) \simeq 125$ m/s

Hence, $\mathcal{T}_{cruise} \simeq 2400$ N. In order to know the power at the take-off, both $\mathcal{T}_{TO}$ and $\mathcal{V}_{TO}$ must be estimated.

$\mathcal{T}_{TO}$ A reasonable approximation suggested by [2] is that the cruise thrust (in lbf) as a function of take-off thrust is given by

$$\mathcal{T}_{cruise} = 14300 \sin\left(\frac{\pi\,\mathcal{T}_{TO}}{200000}\right) \tag{130}$$

which can be solved for $\mathcal{T}_{TO}$. This correlation relates the performance of 26 large turbofan engines as reported in Svoboda [3]. Being the aircraft in this analysis orders of magnitude smaller than the ones studied by Svoboda, Eq. 130 tends to overestimate the value of $\mathcal{T}_{TO}$. Alternatively, a simpler correlation developed by Svoboda himself suggests that

$$\mathcal{T}_{cruise} = 200 + 0.2 \cdot \mathcal{T}_{TO} \tag{131}$$

where again the thrust are expressed in lbf. Although the Sforza's correlation is the best data fitting, Svoboda's correlation fits better the small engines below 10000 lbf (44482 N). For this reason, Svoboda's Eq. 131 is preferred. As a result, $\mathcal{T}_{TO} = 7562$ N.

$\mathcal{V}_{TO}$ Concerning the velocity at take-off, an approximation should be done here. Typical takeoff air speeds for jetliners are in the 240–285 km/h range. Light aircraft, such as a Cessna 150, take off at around 100 km/h [4]. Given the size of the drone investigated and the large amount of fuel onboard, a takeoff speed of 200 km/h is assumed. Hence, $\mathcal{V}_{TO} = 55.\bar{5}$ m/s.

From the above mentioned assumptions, the power during the takeoff is computed:

$$\mathcal{P}_{TO} = 7562 \times 55.\bar{5} \simeq 420 \text{ kW} \tag{132}$$

i.e. $+40\%$ compared to the power required during cruise.

B.2 AUXILIARY POWER PHASE

During the mission, it is conceivable that the power supplied by the engines is not constant. It may be due to a sudden extra thrust request (e.g. if targeted) or to a lower thrust demand as in the landing phase. Moreover, some auxiliary power might be needed onboard. Power peaks up to +100% may be needed for a short duration. In this scenario, the engine is highly loaded over its design point.

Such high power demands can be obtained by throttling up the engine, by injecting more fuel in the cylinders and consequently by increasing its rpm. On so doing, a higher air mass flow rate is needed due to the increased number of firings per minute. If the rpm increment is moderate, the engine itself can provide it by its *natural aspirated* operation; otherwise, the turbocharger setting is changed, essentially rotating faster. Despite the initial inertia, the pressure ratio increases with rpm, hence delivering more mass per unit time. However, by shifting from its design point, the turbocharger works less efficiently, and is more prone to stall. If a *wastegate*[1] turbine is present, its bypass ratio should be electronically controlled in order to provide the right amount of power to drive the compressor.

In any case, such demanding high-power profile can be actuated by the engine only for very short periods, to prevent overheating, fatigue, centrifugal forces and other phenomena which can bring the engine to failure. The double 2-hours peaks in this analysis of Fig. 25 is an enhanced scenario adopted here to obtain more visible results.

1 A wastegate is a valve that diverts exhaust gases away from the turbine wheel. Diversion of exhaust gases regulates the turbine rotational speed, which in turn regulates the rotating speed of the compressor. The primary function of the wastegate is to regulate the maximum boost pressure after the compressor, to protect the engine and the turbocharger.

REFERENCES

[1] B. W. McCormick. *Aerodynamics, Aeronautics, and Flight Mechanics*. 2nd ed. Wiley, 1994. ISBN: 0471575062,9780471575061.

[2] Sforza P. M. *Theory of Aerospace Propulsion*. 2nd ed. pag. 397. Butterworth-Heinemann, 2016.

[3] Svoboda C. "Turbofan Engine Database as a Preliminary Design Tool." In: *Aircraft Design* 3 (2000), pp. 17–31.

[4] Scott J. *Airliner Takeoff Speeds*. URL: http://www.aerospaceweb.org/question/performance/q0088.shtml.

C VALIDATION OF THE MATLAB MODELS

C.1 4-STROKE TURBOCHARGED DIESEL ENGINE

Fig. 35 and 36 show a comparison between the 4-stroke Compression-Ignition model performed on MATLAB and the existing Centurion 2.0 produced by Thielert AG. It is a 155 hp, 4 in-line cylinders, liquid-cooled turbocharged Diesel engine. Some of its specifications are reported in Table 23. The simulation is carried out at 15000 ft. (4600 m).

The fuel consumption and efficiency curves are not available for this engine. However, the performance curves shown in Fig. 36 reproduce accurately the relative standings of other engines of the same type. Fig. 36 also shows that the maximum efficiency is obtained at 2030 rpm, well below the peak power; the correspondent power supplied is $\simeq$ 75 kW. If the same analysis is carried at an altitude below 2000 m. amsl, the power supplied at maximum efficiency is very close to 97 kW, the one stated in the datasheet.

C.2 4-STROKE TURBOCHARGED SPARK-IGNITION ENGINE

The thermodynamic cycle of a 4-stroke spark-ignition engine has been investigated. The code has been compared with an existing engine, in

Table 23: Thielert AG Centurion 2.0 specifications.

Cylinder diameter	83 mm (3.26 in)
Piston stroke	92 mm (3.62 in)
Compression	18:1
Weight (empty)	134 kg (295.4 lbs)
Maximum output up to 2000 amsl	114 kW (155 hp)
Economical rating up to 2000 amsl	97 kW (132 hp)
Fuel consumption at cruise speed	18-22 l/h (4,7-5.8 gal/hr)

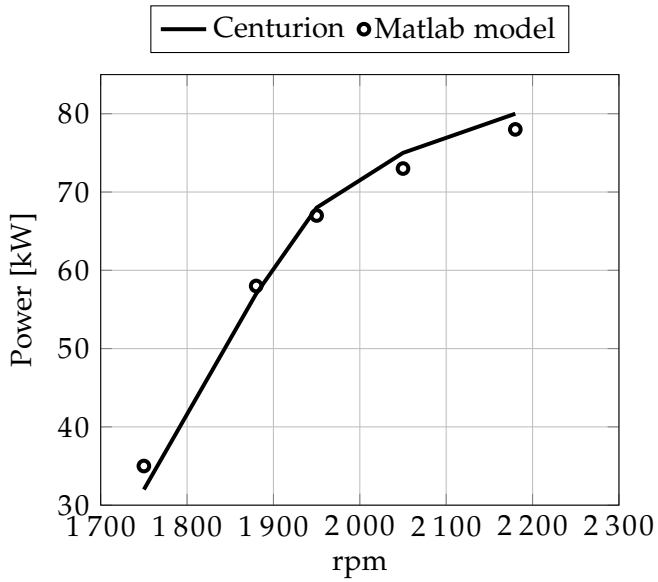

Figure 35: Shaft Power vs. rpm for the 4-stroke turbocharged Diesel model and the Thielert Centurion 2.0. Altitude=4600 m.; pressure compression ratio $\pi_c = 1.8$ @1750 rpm, $\pi_c = 3$ @2300 rpm.

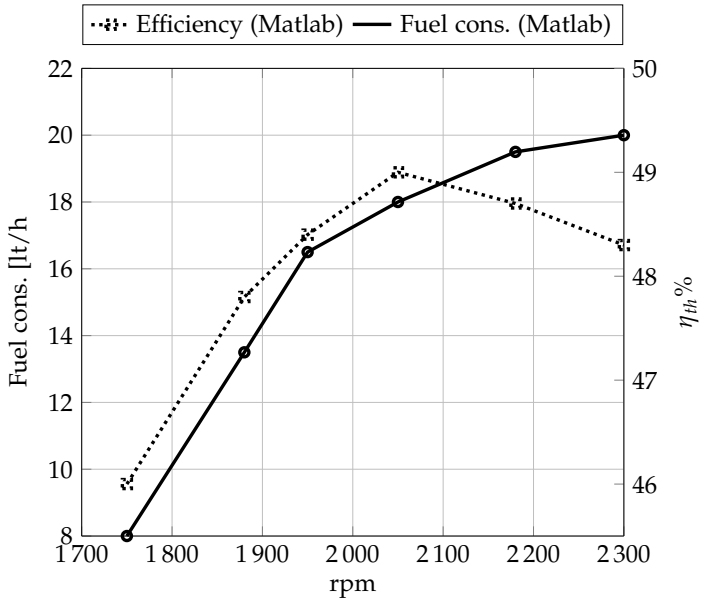

Figure 36: Thermal efficiency and fuel consumption for the 4-stroke turbocharged Diesel model. Altitude=4600 m.; pressure compression ratio $\pi_c = 1.8$ @1750 rpm, $\pi_c = 3$ @2300 rpm.

Table 24: Rotax 914UL specifications.

Cylinder diameter	79.5 mm (3.13 in)
Piston stroke	61 mm (2.4 in)
Compression	9:1
Weight (empty)	64 kg (140.8 lbs)
Maximum Power output	84.5 kW
Maximum Torque output	144 Nm
Max revolutions	5800 rpm

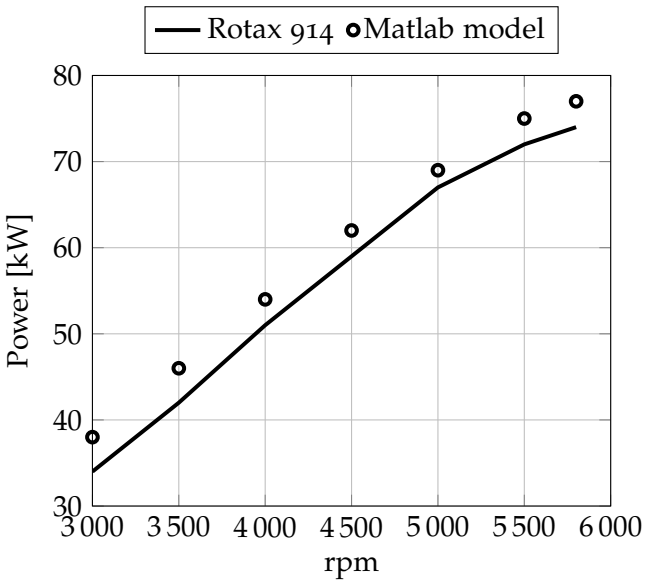

Figure 37: Shaft Power vs. rpm for the 4-stroke turbocharged spark-ignition model and the Rotax 914. Altitude=2000 m.

order to test its accuracy. The engine chosen for the analysis is the Rotax 914UL, whose specifications are reported in Table 24. For this comparison both the power curve (Fig. 37) and the fuel consumption curve (Fig. 38) are available. Hence, a more accurate comparison is possible between the numerical code and the experimental data from the maker. Although with no direct comparison, the efficiency curve in Fig. 38 follows the typical non-monotonic shape.

C.3 2-STROKE TURBOCHARGED SPARK-IGNITION ENGINE

The engine chosen for the comparison is the *Hirth 3003*. The reason of this choice is the availability of its datasheet and its power-rpm,

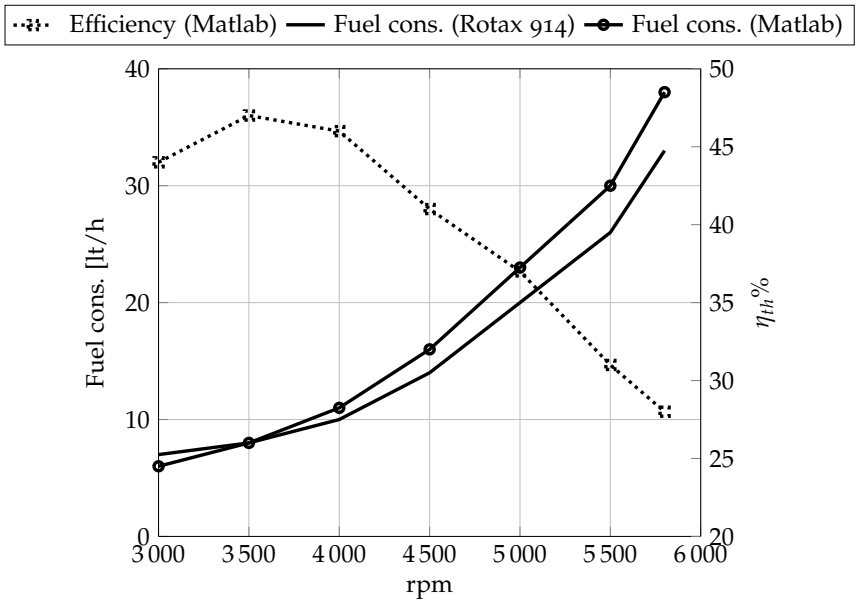

Figure 38: Thermal Efficiency and Fuel Consumption for the 4-stroke turbocharged spark-ignition model and the Rotax 914. Altitude=2000 m.

Table 25: Hirth 3003 100 hp specifications.

Cylinder bore	72 mm (2.83 in)
Piston stroke	64 mm (2.52 in)
Compression	9.5:1
Weight (empty)	57 kg (129 lbs) including gearbox
Maximum output	100 kW (135 hp)

torque-rpm and fuel consumption-rpm curves. Some of it specifications are reported in Table 25.

As can be seen from Fig. 39 and 40, the target of this analysis was to match the power-rpm and the fuel consumption-rpm curves. As a result, an efficiency-rpm curve is derived (Fig. 41). The match is not perfect because of the large number of unknown parameters involved, like the equivalence ratio, the spark advance, the combustion duration and efficiency, the turbocharger settings and the behavior of these parameters with rpm. Moreover, the crank case geometry, the exhaust and transfer ports opening and closing timing and their areas are unknown. Hence, this comparison has to be considered very carefully and only for a *qualitative* understanding of the phenomena. The values of fuel consumption and efficiency, however, are in the typical range of two-stroke spark ignition engines of this size.

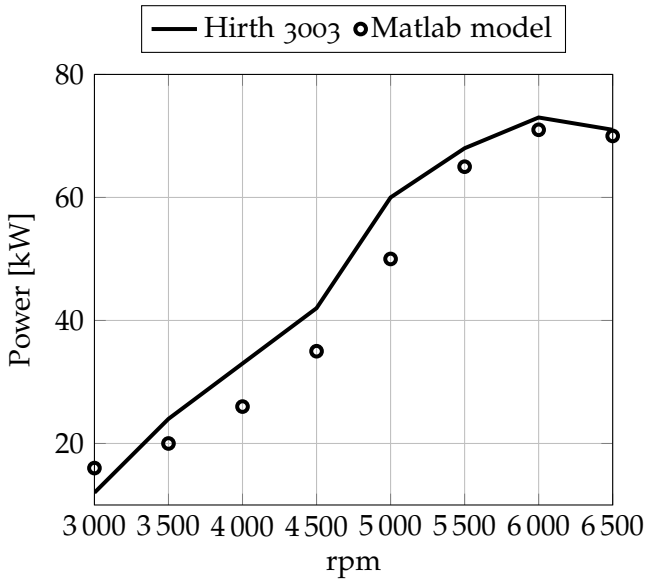

Figure 39: Shaft Power vs. rpm for the 2-stroke turbocharged spark-ignition model and the Hirth 3003. Altitude=sea level; pressure compression ratio $\pi_c = 1$ @3000 rpm, $\pi_c = 1.9$ @6500 rpm.

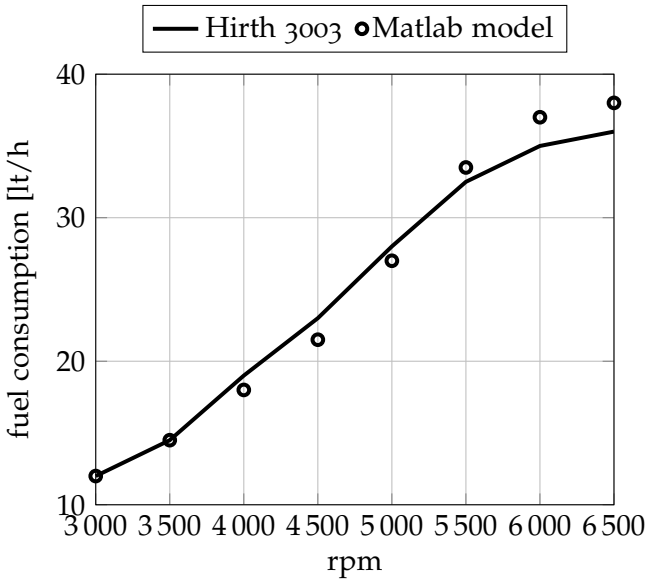

Figure 40: Fuel Consumption vs. rpm for the 2-stroke turbocharged spark-ignition model and the Hirth 3003. Altitude=sea level; pressure compression ratio $\pi_c = 1$ @3000 rpm, $\pi_c = 1.9$ @6500 rpm.

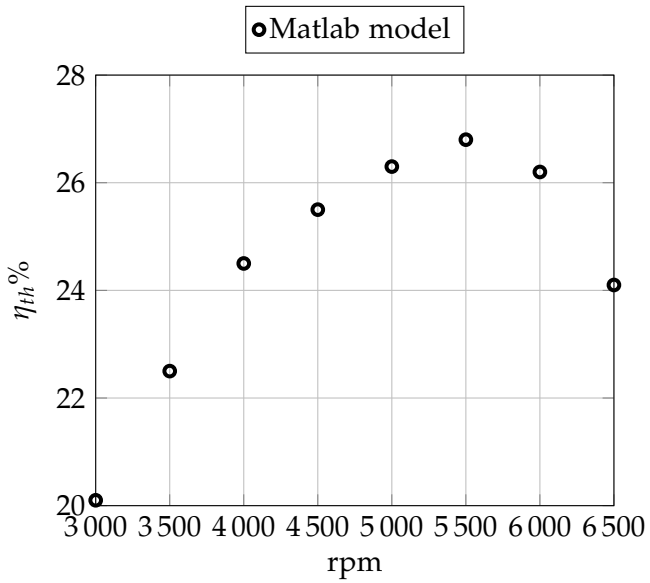

Figure 41: Thermal Efficiency vs. rpm for the 2-stroke turbocharged spark-ignition model and the Hirth 3003. Altitude=sea level; pressure compression ratio $\pi_c = 1$ @3000 rpm, $\pi_c = 1.9$ @6500 rpm.

C.4 2-STROKE TURBOCHARGED COMPRESSION-IGNITION ENGINE

2-stroke turbocharged Diesel engines are nowadays very rare in aeronautical applications. They are more often used in large ships, linked to a propeller with or without a gearbox. On the other hand, the small power requirement of motorbikes often matches the 2-stroke spark-ignition engine capabilities, as compactness, lightweight, quick response to a change of regime.
In the middle-range of 100-200 kW of power output, 2-stroke Diesels are quite uncommon. This is the reason why no engines could be found so far for this comparison.

COLOPHON

This document was typeset using the typographical look-and-feel `classicthesis` developed by André Miede. The style was inspired by Robert Bringhurst's seminal book on typography "*The Elements of Typographic Style*". `classicthesis` is available for both LaTeX and LyX.

Final Version as of March 20, 2017 (`classicthesis`).